

AFOSR-TR- 82 - 0963

12

Austin Research Associates

1901 Rutland Drive - Austin, Texas 78758 - Phone (512) 837-6623

AD A 121 673

I-ARA-82-U-89 (ARA-467)

ANNUAL TECHNICAL REPORT FOR THEORETICAL
STUDIES ON FREE ELECTRON LASERS

for Period 1 August 1981 - 31 July 1982

M. N. Rosenbluth, H. Vernon Wong and B. N. Moore

August 1982

Sponsored by
Advanced Research Projects Agency (DoD)
ARPA Order No. 3923-5
Monitored by NP
Under Contract No. F49620-81-C-0077

DTIC
ELECTE
NOV 22 1982
E

DTIC FILE COPY

The views and conclusions contained in this document are those of the authors and should not be interpreted as necessarily representing the official policies, either expressed or implied, of the Defense Advanced Research Projects Agency or the U.S. Government.

Approved for public release;
distribution unlimited.

82 11 22 066

Austin Research Associates

1901 Rutland Drive - Austin, Texas 78758 - Phone (512) 837-6623

I-ARA-82-U-89 (ARA-467)

ANNUAL TECHNICAL REPORT FOR THEORETICAL STUDIES ON FREE ELECTRON LASERS

for Period 1 August 1981 - 31 July 1982

M. N. Rosenbluth, H. Vernon Wong and B. N. Moore

August 1982

Sponsored by
Advanced Research Projects Agency (DoD)
ARPA Order No. 3923-5
Monitored by NP
Under Contract No. F49620-81-C-0077

The views and conclusions contained in this document are those of the authors and should not be interpreted as necessarily representing the official policies, either expressed or implied, of the Defense Advanced Research Projects Agency or the U.S. Government.

AIR FORCE OFFICE OF SCIENTIFIC RESEARCH (AFSC)
NOTICE OF TRANSMITTAL TO DTIC
This technical report has been reviewed and is
approved for public release IAW AFR 190-12.
Distribution is unlimited.
MATTHEW I. KREBER

UNCLASSIFIED

SECURITY CLASSIFICATION OF THIS PAGE (When Data Entered)

REPORT DOCUMENTATION PAGE		READ INSTRUCTIONS BEFORE COMPLETING FORM
1. FORM TR-82-0963 I-ARA-82-U-89 (ARA-467)	2. GOVT ACCESSION NO. ADA12167	3. RECIPIENT'S CATALOG NUMBER 3
4. TITLE (and Subtitle) Annual Technical Report for Theoretical Studies on Free Electron Lasers	5. TYPE OF REPORT & PERIOD COVERED Annual Technical Report 1 August 1981 - 31 July 1982	
	6. PERFORMING ORG. REPORT NUMBER I-ARA-82-U-89 (ARA-467)	
7. AUTHOR(s) M. N. Rosenbluth, H. Vernon Wong and B. N. Moore	8. CONTRACT OR GRANT NUMBER(s) F49620-81-C-0077	
9. PERFORMING ORGANIZATION NAME AND ADDRESS Austin Research Associates 1901 Rutland Drive Austin, Texas 78758	10. PROGRAM ELEMENT, PROJECT, TASK AREA & WORK UNIT NUMBERS Program Code 1E20 Program Element 62301E	
11. CONTROLLING OFFICE NAME AND ADDRESS Director, Advanced Research Projects Agency ARPA Order No. 3923-5 1400 Wilson Blvd., Arlington, Virginia 22209	12. REPORT DATE August 1982	
	13. NUMBER OF PAGES 200	
14. MONITORING AGENCY NAME & ADDRESS (if different from Controlling Office) NP, Air Force Office of Scientific Research Bolling Air Force Base Washington, D. C. 20332	15. SECURITY CLASS. (of this report) Unclassified	
	15a. DECLASSIFICATION/DOWNGRADING SCHEDULE n/a	
16. DISTRIBUTION STATEMENT (of this Report) Approved for public release; distribution unlimited.		
17. DISTRIBUTION STATEMENT (of the abstract entered in Block 20, if different from Report)		
18. SUPPLEMENTARY NOTES		
19. KEY WORDS (Continue on reverse side if necessary and identify by block number) Free Electron Laser (FEL) constant parameter wiggler variable parameter wiggler gain-expanded FEL		
20. ABSTRACT (Continue on reverse side if necessary and identify by block number) A summary of the Theoretical Studies on Free Electron Lasers and details of the progress to date for the period 1 August 1981 - 31 July 1982 are presented.		

DD FORM 1 JAN 73 1473

EDITION OF 1 NOV 65 IS OBSOLETE

UNCLASSIFIED

SECURITY CLASSIFICATION OF THIS PAGE (When Data Entered)

TABLE OF CONTENTS

SECTION		PAGE
I	SUMMARY	1
APPENDIX		
A	MANLEY-ROWE RELATIONS FOR THE THIN LENS GAIN EXPANDER	18
B	THEORY OF LINEAR GAIN: FREE ELECTRON LASERS OPERATED IN OSCILLATOR MODE PART I: ULTRA-SHORT ELECTRON PULSES . . .	43
C	SIMULATION OF SHORT ELECTRON PULSE FREE ELECTRON LASERS WITH VARIABLE PARAMETER WIGGLERS	132

Accession For	
NTIS GRA&I	<input checked="" type="checkbox"/>
DTIC TAB	<input type="checkbox"/>
Unannounced	<input type="checkbox"/>
Justification	
By _____	
Distribution/ _____	
Availability Codes	
Dist	Avail and/or Special
A	



THEORETICAL STUDIES ON FREE ELECTRON LASERS

I. SUMMARY

At the beginning of the contract year (August 1, 1981 to August 1, 1982) we undertook an analytic and computational study ^{with consideration} of certain theoretical questions relating to Free Electron Lasers (FEL's). ~~As originally~~ conceived, the study was divided into five tasks:

(1.) A proper Hamiltonian formulation of the nonlinear equations for gain-expanded FEL's will be made and Liouville's theorem applied to these systems.

(2.) The analytic theory for gain-expanded FEL's will be extended to include variable property gain expanders as proposed for storage rings.

3. The results of Tasks 1 and 2 will be applied, numerically if necessary, to the determination of whether a steady state gain-expanded FEL is compatible with storage ring operation.

4. The gain of a variable pitch wiggler (as a function of signal amplitude and frequency) will be studied using a single particle simulation code.

5. A fully self-consistent particle and EM wave (1-D) code, with provisions for treating micro bunches and providing frequency discrimination in order to consider Raman instability effects, will be developed to

treat the startup and pulse formation problem for variable pitch wigglers.

The first three concerned gain-expanded FEL's and the last two, FEL's with variable parameter wigglers.

Tasks 1 and 2 have essentially been completed. A Hamiltonian formulation of the electron equation of motion for the "thin lens" gain-expanded FEL has been derived (Appendix A). This leads to two fundamental limitations on gain expansion schemes: (a) The Manley Rowe relations, and (b) generalized gain-spread theorems. Having established these limits, Task 3 remains to be completed. The implications of these limits with respect to the overall efficiency of gain-expanded FELs in storage rings appear to be somewhat pessimistic.

Considerably more time and effort were devoted to Task 4 and Task 5 than had been planned. Consequently, it was possible to carry these tasks much further than anticipated. The linear eigenmode analysis leading to a calculation of the linear gain as a function of the FEL parameters has been completed. The results for the limit of very short electron pulses are discussed in Appendix B. By very short electron pulses is meant pulses with pulse length ℓ much shorter than the slippage distance $k_w L / k_s > \Gamma^{1/2} \ell$, where $\Gamma = 2k_w L \Delta\gamma_r / \gamma_r$ and $\Delta\gamma_r / \gamma_r$ is the fractional change in the resonant energy γ_r down

the wiggler. A discussion of the results for long electron pulses is under preparation and will be available in the very near future. A one-dimensional self-consistent particle and electromagnetic wave code to simulate the operation of an FEL with variable parameter wigglers and with frequency filtering of the electromagnetic pulse has been written. The details of this simulation code are described in Appendix C. This code enabled us to study not only the startup and pulse formation problem, but also the stability of the saturated state. The results are discussed in Appendix C.

Our principal results are:

1. We have derived analytic results for linear pass to pass growth of the pulse at low amplitude. For very short pulses, these are given in Appendix B. These results have been numerically verified in Appendix C.
2. We find that for high saturation systems optical discrimination is required in order to prevent nonlinear signal breakup. Qualitative agreement with the theory of sideband instabilities is obtained for the width of the required frequency filter.
3. The further requirement that the linear phase of growth saturate at a high enough level to ensure trapping seems to be satisfied except for systems which

seek to enhance linear gain by use of a long constant parameter section.

4. With proper choice of frequency discrimination (and for an ultra-short electron pulse) we have demonstrated very high extraction systems (30% efficiency at 1μ) which grow from noise to a stable steady state. We derive and numerically verify a criterion

$$\langle I \rangle > 1.28 \times 10^6 \frac{(1-r) \Delta \gamma_r}{\gamma_r^2} \text{ Amps}$$

for the minimum current required for a system with reflection coefficient r .

5. The limitation on beam thermal energy spread $\bar{\gamma}_{th}$ is determined more by the need for good linear gain ($\bar{\gamma}_{th}/\Gamma^{1/2} < 1$) than by that for effective electron trapping, ($\bar{\gamma}_{th}/\Gamma^{1/2} < 2$).

The ultra-short pulse was modeled by a δ -function in the simulation. Due to computer time limitations, this limit is easier to simulate since the number of particle orbits which must be followed is far fewer for a single electron beamlet than for the many beamlets required to represent a long continuous electron pulse. This limit is also analytically tractable. However, the basic physics of the electron-photon interaction is

expected to be qualitatively the same for long electron pulses. Preliminary simulations of long electron pulses have indeed exhibited a behavior qualitatively similar to that of short pulses. The corresponding criterion for the minimum current, however, may be slightly more severe.

Gain-Expanded FEL's

In constant parameter FEL's, electrons initially lose energy to the radiation field, but in so doing experience a gradual shift in relative phase which eventually reverses the direction of energy flow and impairs gain of the FEL. To overcome this limitation, Smith, et al.¹ have outlined a scheme for a gain-expanded FEL in which the sensitivity of gain to variations in the energy of the exciting electrons is reduced. This scheme uses a periodic magnet with transverse gradients such that the electrons which lose energy move to different transverse positions and continue to remain in phase with the transverse electric field of the electromagnetic radiation. The reduced sensitivity to energy enhances the prospects for operation of a gain-expanded FEL in conjunction with a storage ring, since many passes of the circulating electrons through the FEL would occur before gain is significantly affected by energy spread.

However, transverse betatron oscillations of the electron trajectories are simultaneously excited and may negate the effectiveness of gain expansion unless the oscillation amplitudes are kept small. For steady state operation in a storage ring, it is desirable to maximize the gain while minimizing the level of betatron oscillations. In this mode, a steady state is conceivable in which the growth in betatron oscillations in the FEL is damped by incoherent synchrotron radiation in the storage ring. The important issue to be resolved is whether a steady state can be established with a reasonable ratio of energy gain in the laser to energy loss in synchrotron radiation ($\Delta\mathcal{E}_{\text{laser}}/\Delta\mathcal{E}_{\text{sync}}$).

Madey, et al.² have considered the feasibility of cancelling transverse betatron oscillations by a careful design of the FEL magnet. Their results on the gain characteristics of gain-expanded FEL's with excitation cancellation were obtained from numerical integration of the equations of motion. In our view, this procedure did not provide a satisfactory theoretical understanding of the effect of excitation cancellation on gain. Excitation cancellation seemed to involve detailed cancellation of "big" terms in the equations, and it was not clear what residual effects were responsible for gain.

In order to gain some insight regarding the gain characteristics of gain-expanded FEL's, we have investigated the "thin lens" gain expander as recently proposed by Madey, et al.³ using a Hamiltonian formulation of the electron equations of motion. The thin lens Hamiltonian was transformed by a series of canonical transformations to an action-angle Hamiltonian of the form

$$K = k_{\beta} J + \epsilon e^{i\omega_s (\tau + (1/\beta_{\parallel} - 1) z)} \sum_{n,m} \bar{h}_{n,m}(J, \gamma) e^{i(nk_w z + m\phi)}$$

where J is the phase area for betatron oscillations and ϕ its conjugate angle, γ is the electron energy and $\tau - z$ its conjugate "momentum". z is the independent variable and ϵ is proportional to the laser field.

The Liouville equation for the electron distribution function may now be written down, solutions obtained by expanding in powers of ϵ , and the changes $\langle \delta J \rangle$ and $\langle \delta \gamma \rangle$ after passage through the thin lens wiggler determined. The details of the analysis are discussed in Appendix A.

In the usual mode of FEL operation where one resonance is of importance (which is practical, necessary and desirable to get cancellation of excitation at a definite z value) the Manley-Rowe relation holds

$$\langle \delta J \rangle = - m \frac{\langle \delta \gamma \rangle}{\omega_s}$$

where $m \neq 0$. Thus, gain is proportional to betatron excitation.

The $m = 0$ resonance does not produce betatron excitations, but since this depends on energy derivatives, presumably large energy spread results.

A generalization of the Madey theorem relating gain to spread (without making the resonant approximation; that is, keeping all m values) can readily be derived

$$\langle \delta J \rangle = \frac{1}{2} \frac{\partial}{\partial J} \langle (\delta J)^2 \rangle + \frac{1}{2} \frac{\partial}{\partial \gamma} \langle \delta J \delta \gamma \rangle$$

$$\langle \delta \gamma \rangle = \frac{1}{2} \frac{\partial}{\partial \gamma} \langle (\delta \gamma)^2 \rangle + \frac{1}{2} \frac{\partial}{\partial J} \langle \delta J \delta \gamma \rangle .$$

These relations impose severe restrictions on gain expander operation

$$\frac{\Delta \mathcal{E}_{\text{laser}}}{\Delta \mathcal{E}_{\text{sync}}} \sim \frac{\Delta \mathcal{E}}{\mathcal{E}} ,$$

where δc is the maximum beam spread allowed in the storage ring. At the present time, the existing proposals for operating a gain-expanded FEL in a storage ring do not seem capable of yielding overall efficiencies of more than a few percent.

Variable Parameter FEL'S

An alternative scheme for overcoming some of the limitations of constant parameter FEL's is the variable parameter wiggler discussed by Kroll, et al.⁴ In this scheme, a significant fraction of electrons in the beam is trapped in the ponderomotive potential well produced by the combined wiggler and radiation fields. The resonant energy of the FEL is reduced by suitable variations of the wiggler parameters and this in turn results in the extraction of energy from the trapped electrons. This reduction in energy can be much larger than the energy which can be transferred in constant parameter wigglers. Thus, the use of variable parameter wigglers to produce high power radiation is a promising prospect. The primary objectives of our investigation of FEL's with variable parameter wigglers are to define the area in parameter space where

1. The operation of the FEL can be initiated by growth of the electromagnetic pulse from noise levels.

2. The nonlinear saturation of pulse growth occurs with the trapping of a significant fraction of beam electrons.

3. The finite amplitude saturated pulse propagates without deterioration due to trapped particle sideband instabilities.

4. The energy extraction from the electron beam is optimized, consistent with reasonable growth rates, effective trapping, and stable propagation.

To achieve these objectives, we have investigated in detail the operation of an FEL configuration in which a combination of constant and variable parameter wigglers is positioned between mirrors. An electromagnetic pulse generated in the wiggler is reflected repeatedly by the mirrors, and multiple passes of the pulse through the wiggler are obtained. Relativistic electron beamlets are injected into the wiggler at periodic intervals so that on each forward pass of the pulse through the wiggler, there is overlap of the pulse and beamlets. The pulse grows on each forward pass. Eventually, the amplitude of the pulse becomes large enough to trap a fraction of the beam electrons. At this stage, the pulse is vulnerable to distortions due to the onset of trapped electron sideband instabilities. In order to avoid breakup of the pulse, the pulse is subjected to frequency

discrimination (outside the wiggler) which suppresses growth of sidebands. The frequency discriminator effectively acts as a band pass filter which attenuates frequencies above and below the pulse frequency. With stable pulse propagation, a stationary state is reached when the energy extraction from the electron beam balances the energy losses in the frequency discriminator and at the mirrors.

The electron equations of motion are derived from an approximate relativistic Hamiltonian in which the transverse motion is taken to be nonrelativistic and transverse spatial variations and beam self-fields are neglected. The electron current driving the radiation field is obtained by summing over all the single particle currents. These equations, together with Maxwell's equations, determine the temporal and spatial evolution of the electromagnetic pulse in the wiggler.

The set of equations governing the operation of the FEL as an oscillator have been formulated and they were studied both analytically and by the use of a simulation code.

The linear eigenmode analysis leading to a calculation of the linear gain as a function of the FEL parameters is described in Appendix B. Therein is discussed the limit of ultra-short electron beamlets in

which the electron pulse length ℓ is very short compared to the slippage distance $k_{wL}/k_s > \Gamma^{1/2} \ell$.

The linear gain per pass has been calculated for constant parameter wigglers, variable parameter wigglers, and a combination of constant and variable parameter wigglers. The analysis included the effects of frequency discrimination as well as a finite energy spread (modeled by a Lorentzian distribution function).

It is found that the gain depends on only two combinations of FEL parameters and graphs of the linear gain as a function of these FEL parameters have been plotted and the areas of good linear gain located. A notable feature of the linear gain is its dependence on the time delay Δt_{rel} of the electron pulse with respect to the time of entry of the EM pulse into the wiggler. The linear gain is zero when Δt_{rel} is zero, reaches a maximum when $\Delta t_{rel} > 0$ is finite, and finally decreases with increasing Δt_{rel} . These graphs have been used to select appropriate parameters for input into the simulation code.

A one-dimensional code has been written to simulate operation of the FEL in which the electromagnetic pulse is grown from noise levels all the way to saturation. The details of the code are described in

Appendix C. This code enables us to study both pulse formation and the stability of the saturated state.

Due to computer time limitations, most of the simulations have been done using δ -function electron beams. The results of the simulations are presented and discussed in Appendix C.

In a typical run in which the EM pulse grows from noise levels to saturation, the early phase of the evolution is characterised by growth of the linear eigenmode with the pulse amplitude peaked at the back. As the evolution enters the nonlinear phase, the maximum in the pulse amplitude moves to the front which then continues to grow at approximately the linear rate. Growth continues until the peak amplitude at the front of the pulse is large enough to begin to trap the beam electrons. At saturation, without frequency discrimination, the pulse remains peaked at the front and never broadens towards the back. The electrons are not effectively trapped throughout the length of the wiggler and energy extracted from the electrons is only a small fraction of that which is theoretically possible.

The failure of the EM pulse to broaden towards the back is due to the growth of unstable sidebands (of the order of the electron bounce frequency in the ponderomotive potential well), which leads to a loss of coherence and eventual detrapping of the electrons.

When frequency discrimination is introduced by passing the EM pulse through a bandpass filter, the final phase of the evolution depends critically on the bandwidth ω_F of the filter. If ω_F is small so that the growth of unstable sidebands are suppressed, the pulse broadens into a square pulse and the electrons trapped in the ponderomotive potential well remain trapped during its passage through the wiggler. The saturated pulse propagates coherently and electron trapping is very efficient.

The presence of frequency discrimination by a band pass filter has an effect (proportional to $1/\omega_F$) which tends to retard the advance of the EM pulse relative to the electron beam, that is, it tends to reduce the effective EM pulse advance produced by a finite $\Delta t_{rel} > 0$. To avoid the EM pulse running either ahead of or lagging behind the electron beamlets, it is indicated that a choice $\Delta t_{rel} \omega_F = 1$ is desirable. This was confirmed by the numerical simulation. Thus to obtain finite linear gain, ω_F cannot be altered independently of Δt_{rel} .

A small value of ω_F is desirable to suppress the sidebands and guarantee a stable saturated state. However, small values of ω_F typically implies small linear gain since $\Delta t_{rel} = 1/\omega_F$ is then large.

In order to insure that a value of ω_F may be found which allows both for linear gain and stable propagation, it has been deduced that the following minimum current criterion must be satisfied:

$$\langle I \rangle > \frac{1.42 \times 10^5}{k_w^2 r_0^2} \frac{(1-r)\Delta\gamma_r}{\gamma_r^2} \text{ Amps}$$

where $\langle I \rangle$ is the beam current averaged over the slippage distance, r is the mirror reflection coefficient, r_0 is the beam radius, the wiggler length $L_w = k_s r_0^2$ is set equal to the diffraction distance, and $e^2 B_w^2 / m^2 k_w^2 c^4 = 1$.

Linear gain can be enhanced somewhat, particularly for large Δt_{rel} , by adding a constant parameter section to the front of the variable parameter wiggler. The constant parameter section cannot be too long since electron trapping may be adversely affected. The linear growth phase in the constant parameter section will tend to saturate at an amplitude inversely proportional to the square of the length of the constant parameter section, and this amplitude may not be large enough to trap the beam electrons efficiently.

In view of the above considerations, we have simulated an FEL with the following physical parameters

Electron Energy	50 MeV
Electron Beam Current averaged over slippage distance	50 Amps
Wiggler Wavelength	1.25 cm
Number of Wiggler Wavelengths	400
Signal Wavelength $\lambda = 2\pi\omega_s/c$	1 μ
Wiggler Field Amplitude	7.0 kG
Nominal Trapped Electron Energy Loss	20 MeV
Constant Parameter Length	7.5 cm

Stable propagation of the saturated state was observed with a filter band width of $0.1 \omega_s$. An effective trapping of ~80% of the beam electrons occurred, resulting in an energy transfer efficiency of ~30%. Without frequency discrimination, the energy transfer efficiency is only 0.8%.

REFERENCES

1. T. I. Smith, J. M. J. Madey, L. R. Elias, and D. A. G. Deacon, J. Appl. Phys. 50 (1979), 4580.
2. J. M. Madey, "Cancellation of Transverse Excitation in Gain-Expanded Free Electron Lasers," HEPL Report 853, Stanford University, 1980.

J. M. J. Madey and Robert C. Taber, "Gain and Saturation in Excitation Cancelling Gain-Expanded Free Electron Lasers," HEPL Report 855, Stanford University, 1980.
3. J. M. J. Madey and J. N. Eckstein, "Realization of Gain in Constant Period Excitation Cancelling Magnets," Stanford University, June 1981.
4. N. M. Kroll, P. Morton and M. N. Rosenbluth, "Free Electron Lasers with Variable Parameter Wigglers," IEEE Journal of Quantum Electronics, Vol. QE-17, pp. 1436-1468 (1981).

A P P E N D I X A

MANLEY-ROWE RELATIONS FOR THE
THIN LENS GAIN EXPANDER

Austin Research Associates
1901 Rutland Drive - Austin, Texas 78758 - Phone (512) 837-6623

MANLEY-ROWE RELATIONS FOR THE
THIN LENS GAIN EXPANDER

by

M. Rosenbluth

and

V. Wong

July 1982

MANLEY-ROWE RELATIONS FOR THE THIN LENS GAIN EXPANDER

BY

M. ROSENBLUTH AND V. WONG

I. INTRODUCTION

In this note we argue that two-dimensional free electron lasers such as gain expanders may be described by an action-angle Hamiltonian of the form

$$K = k_{\beta} J + \epsilon e^{i\omega_s (\tau + (1/\beta_{||} - 1)z)} \sum_{n,m} h_{n,m}(J, \gamma) e^{i(nk_w z + m\phi)}$$

where J is the phase space area for betatron oscillations, ϕ its conjugate angle, γ the electron energy, i.e., $E = \gamma mc^2$ and $\tau = t - z$, its conjugate momentum. z is the independent variable and ϵ is proportional to the laser field.

In Section II, we demonstrate a series of canonical transformations which explicitly and exactly reduces the "thin lens" expander as recently proposed by Madey, et al.¹ to the above form. The details are algebraically messy but the procedure is straightforward. In Section III, we show that this Hamiltonian implies, to order ϵ^2 , the Manley-Rowe

relations, and generalized Madey theorems. These may impose severe restrictions on gain expander operation. We also display in terms of the $h_{n,m}$'s the equations for the energy transfer. In Section IV, we evaluate these for the thin lens system at low excitation amplitude. The casual reader should restrict himself to Section III.

II. REDUCTION OF THE THIN LENS GAIN
EXPANDER TO NORMAL FORM

We use as a Hamiltonian for the thin lens model the z momentum, and represent the wiggler by a vector potential A_z . So for $\gamma \gg 1$ we have

$$K_1 = \frac{(p-A)^2 + 1}{2\gamma} + xF_1(z) + \frac{x^2}{2} F_2(z) \quad . \quad (1)$$

z is the independent variable. γ may be regarded as a canonical variable and $\tau = t - z$ as its momentum.

For the thin lens, which consists of a wiggler composed of pairs of very thin magnets with transverse gradients, we have:

$$F_1(z) = \left[\alpha_+ + \alpha_- (-)^n \right] \delta(z - n\lambda_0) \quad (2)$$

$$F_2(z) = \left[\beta_+ + \beta_- (-)^n \right] \delta(z - n\lambda_0) \quad .$$

A is the vector potential of the laser $A \equiv eA_s/c$. Since electrons with no transverse excitation pass through

the magnets at a fixed x value, the coefficients in equation (2) are determined by expansion around these points. Analytic solutions are known both for the average (nominal) motion $x_0(z, \gamma); p_0(z, \gamma)$ and for the betatron deviations from average (when the laser is not present). We take advantage of this to perform a series of canonical transformations, which reduces the Hamiltonian to the standard form.

The first transformation involves a generating function

$$G_1(p', x, \tau', \gamma) = p'x - x_0 p' + x p_0 + \tau' \gamma \quad .$$

The usual canonical transformation equations are

$$x' = \partial G / \partial p'$$

$$p = \partial G / \partial x$$

$$\gamma' = \partial G / \partial \tau'$$

$$\tau = \partial G / \partial \gamma$$

$$K_2 = K_1 + \partial G / \partial z$$

so that

$$\begin{aligned}
 x' &= x - x_0 \\
 p' &= p - p_0 \\
 \tau' &= \tau + p' \frac{\partial x_0}{\partial \gamma} - (x' + x_0) \frac{\partial p_0}{\partial \gamma} \\
 \gamma' &= \gamma
 \end{aligned} \tag{3}$$

and the new Hamiltonian is

$$K_2 = \frac{p'^2 + 1}{2\gamma} + \frac{1}{2} x'^2 F_2 + \frac{p_0^2}{2\gamma} - \frac{x_0^2}{2} F_2 - \frac{pA}{\gamma} + \frac{A^2}{2\gamma} .$$

Note that for $p' = x' \equiv 0$, (no betatron oscillations) we find

$$\frac{d\tau}{dz} = \frac{p_0^2 + 1}{2\gamma^2} = \frac{1}{\beta_{||0}} - 1 .$$

Proper choice of α and β makes the system isochronous, i.e., $\partial/\partial\gamma (d\tau_0/dz) = 0$. We assume this hereafter. Next we introduce a second transformation

$$G_2 = p''x' + \tau''\gamma - \int d\gamma x_0 \frac{dp_0}{d\gamma} + \left(\frac{1}{\beta_{11}} - 1\right) \gamma z$$

which simplifies the Hamiltonian to

$$K_3 = \frac{p'^2}{2\gamma} + \frac{1}{2} x'^2 F_2 - \frac{pA}{\gamma} + \frac{A^2}{2\gamma} \quad (4)$$

with

$$\tau'' = \tau - \left(\frac{1}{\beta_{110}} - 1\right) z + p' \frac{dx_0}{d\gamma} - x' \frac{dp_0}{d\gamma} \quad (5)$$

The next transformation reduces the Hamiltonian to harmonic oscillator form. Here we take advantage of the fact that the harmonic oscillator coordinates P, Q must be linear functions of the coordinates p', x' . Hence we choose a generating function

$$G_3 = \frac{P^2 g_1(z)}{2} + \frac{x'^2}{2} g_2(z) + P x' g_3(z) + \tau''' \gamma \quad (6)$$

yielding

$$\begin{aligned}
 Q &= P g_1 + x' g_3 \\
 p' &= g_2 x' + P g_3
 \end{aligned}
 \tag{7}$$

The functions $g_{1,2,3}(z)$ may now be determined by requiring that the above equations are satisfied for the desired harmonic oscillator form, i.e., $P = -\sin k_\beta z$, $Q = \cos k_\beta z$ and where x', p' are a known thin lens solution as derived previously:

$$\begin{aligned}
 x' &= \alpha \left[1 + (-)^\eta \right] \cos nk_\beta \lambda_o + \frac{p'}{\gamma} (z - n\lambda_o) \\
 p' &= \frac{\alpha \gamma}{\lambda_o} \left[\cos(n+1)k_\beta \lambda_o \left[1 - (-)^\eta \right] \right. \\
 &\quad \left. - \left[1 + (-)^\eta \right] \cos nk_\beta \lambda_o \right]
 \end{aligned}
 \tag{8}$$

These may easily be checked from the equations of motion. Here α is a normalization coefficient, and we are at position $(n+1)\lambda_o > z > n\lambda_o$.

In terms of the magnet parameters, we have defined:

$$\eta = \frac{1 - \beta_+ \lambda_o / 2\gamma}{\beta_- \lambda_o / 2\gamma} - \sqrt{\left(\frac{1 - \beta_+ \lambda_o / 2\gamma}{\beta_- \lambda_o / 2\gamma} \right)^2 - 1}
 \tag{9a}$$

with $\beta_- > 0$, and the betatron frequency satisfies

$$\cos k_{\beta} \lambda_0 = \sqrt{\left(1 - \frac{\beta \lambda_0}{2\gamma}\right)^2 - \left(\frac{\beta - \lambda_0}{2\gamma}\right)^2} \quad (9b)$$

By substituting (8) into (7) and laboriously matching coefficients of $\cos k_{\beta} z$, $\sin k_{\beta} z$, we find:

$$g_1 = A(z)/B(z)$$

$$g_2 = C(z)/B(z)$$

$$g_3 = 1/B(z)$$

where

$$A = \sqrt{\frac{\lambda_0}{(\sin k_{\beta} \lambda_0)(1-\eta^2)\gamma}} \left\{ \left[1 + (-)^n \eta\right] \sin k_{\beta} \tilde{z} + \frac{\tilde{z}}{\lambda_0} \left[(1 - (-)^n \eta) \sin k_{\beta} (\tilde{z} - \lambda_0) - \left[1 + (-)^n \eta\right] \sin k_{\beta} \tilde{z} \right] \right\}$$

$$B = \sqrt{\frac{\lambda_0}{(\sin k_{\beta} \lambda_0)(1-\eta^2)\gamma}} \left\{ \left[1 + (-)^n \eta\right] \cos k_{\beta} \tilde{z} + \frac{\tilde{z}}{\lambda_0} \left[(1 - (-)^n \eta) \cos k_{\beta} (\tilde{z} - \lambda_0) - (1 + (-)^n \eta) \cos k_{\beta} \tilde{z} \right] \right\}$$

$$C = \sqrt{\frac{\gamma}{\lambda_0 \sin k_{\beta} \lambda_0 (1-\eta^2)}} \left\{ (1 - (-)^n \eta) \cos k_{\beta} (\tilde{z} - \lambda_0) - (1 + (-)^n \eta) \cos k_{\beta} \tilde{z} \right\} \quad (10)$$

Here $\tilde{z} = z - n\lambda_0$ and the f 's are hence proper periodic (period $2\lambda_0$) functions of z .

A detailed calculation of the new Hamiltonian may now be made using the equations of motion and after vast algebra we find as we knew must happen:

$$K_4 = \frac{k_\beta}{2} (P^2 + Q^2) - \frac{pA}{\gamma} + \frac{A^2}{2\gamma} .$$

A final transformation to action angle variables is performed involving a generating function:

$$G = \tau''' \gamma + J \left[\sin^{-1} \frac{Q}{\sqrt{2J}} + \frac{Q}{\sqrt{2J}} \sqrt{1 - Q^2/2J} \right] .$$

III. GENERAL THEOREMS FOR STANDARD HAMILTONIAN

Thus our final Hamiltonian is

$$K = k_{\beta} J - \frac{pA}{\gamma} + \frac{A^2}{2\gamma} \quad (11)$$

with $J = (P^2 + Q^2)/2$.

A price has been paid for this simple form. The canonical variables are J , its conjugate angle ϕ , γ , and a transformed time $\tau''' \equiv \tau$. The added complication in the time variable arises from the implicit dependence of the f 's since the timelike variable

$$\hat{\tau} = \frac{\partial G_3}{\partial \gamma} \quad (12)$$

Note that γ has survived as the canonical coordinate.

Before proceeding further it is worthwhile to determine the physical significance of $J = (P^2 + Q^2)/2$. By using (7), (9) and (10) we can compute J as a bilinear form in the p' , x' 's. Thus the constant J surface is a tilted ellipse in the original betatron coordinates. We find as expected from the area preserving properties of the canonical transformations that $2\pi J$ is simply the area of that ellipse. This is consistent with the observation that

the Hamiltonian (11) would, if k_β were a slowly varying function of z , have J as an adiabatic invariant.

Let us now turn our attention to the laser field. We may write the Hamiltonian (11) in the form (expanding in laser amplitude)

$$K = H_0 + H_1$$

$$H_0 \equiv k_\beta J$$

where for a plane wave laser propagating in the z direction with vector potential

$$A = a_s \cos \omega_s (t-z/c) \quad (13)$$

we find

$$H_1 = -\epsilon \frac{p' + p_0(z)}{\gamma} e^{i\omega_s \tau} + \text{complex conjugate.} \quad (14)$$

Here $\epsilon = as/2$.

The quadratic term (A^2) is irrelevant to our purposes. τ , p' , and x' must of course be expressed in terms of the canonical coordinates.

Using the redefinition of variables we have introduced along the way we see that H_1 may be written as:

$$H_1 = \frac{\varepsilon}{\gamma} \left[p_0(z) + \sqrt{J} \alpha(z) \cos \phi + \beta(z) \right] x$$

$$e^{i\omega_s \left[\hat{\tau} + \left(\frac{1}{\beta_{11}} - 1 \right) z + \psi(z) \sqrt{J} \cos(\phi + \delta(z)) \right.}$$

$$\left. + \rho(z) J \cos(2\phi + \Delta(z)) + \zeta(z) J \right]} .$$

Here all the functions of z may also depend on γ , are periodic with period $2\lambda_0$, and could be determined from the foregoing arithmetic with some effort. However in order to see the nature of the solutions it is necessary only to note that we may write our Hamiltonian in the general form

$$K = k_\beta J + \varepsilon e^{i\omega_s \left(\hat{\tau} + \left(\frac{1}{\beta_{11}} - 1 \right) z \right)} \sum h_{n,m}(J, \gamma) e^{ink_w z + m\phi}$$

+ complex conjugate. (15)

While we have derived this only for the special thin lens case it should be generally applicable for different magnets. Note that any x dependence of the laser field would not affect the form of this Hamiltonian.

The point of all this maneuvering is that we may write the Liouville equation for the distribution function $f(J, \gamma, \hat{\tau}, \phi)$:

$$\begin{aligned} \frac{\partial f}{\partial z} - \frac{\partial}{\partial J} \left[\left(\frac{\partial K}{\partial \phi} \right) f \right] + \frac{\partial}{\partial \gamma} \left[\left(\frac{\partial K}{\partial \hat{\tau}} \right) f \right] \\ + \frac{\partial}{\partial \phi} \left[\frac{\partial K}{\partial J} f \right] - \frac{\partial}{\partial \hat{\tau}} \left[\frac{\partial K}{\partial \gamma} f \right] = 0 \end{aligned} \quad (16)$$

Expanding in powers of ϵ we have $\partial K_0 / \partial \hat{\tau} = \partial K_0 / \partial \phi = 0$. We assume that f_0 is independent of τ (optical phase) and ϕ (betatron phase). The latter assumption (certainly applying to a case with no initial excitation) could probably be relaxed for our purposes. Then

$$\begin{aligned} \frac{\partial f_1}{\partial z} - \frac{\partial K_1}{\partial \phi} \frac{\partial f_0}{\partial J} + \frac{\partial K_1}{\partial \hat{\tau}} \frac{\partial f_0}{\partial \gamma} \\ + \frac{\partial K_0}{\partial J} \frac{\partial f_1}{\partial \phi} - \frac{\partial K_0}{\partial \gamma} \frac{\partial f_1}{\partial \hat{\tau}} = 0 \end{aligned} \quad (17)$$

and if we write

$$f_1 = e^{i\omega_s \left(\hat{\tau} + \left(\frac{1}{\beta_{11}} \right) - 1 \right) z} \sum_m f_{1m}(z) e^{im\phi} \\ + \text{complex conjugate,}$$

we have

$$\begin{aligned} & \frac{\partial f_{1m}}{\partial z} + i\omega_s \left(\frac{1}{\beta_{||}} - 1 \right) f_m + imk_\beta f_1 - i\omega_s \frac{\partial k_\beta}{\partial \gamma} J f_1 \\ & = \epsilon \sum_n h_{n,m} e^{ink_w z} \left[im \frac{\partial f_o}{\partial J} - i\omega_s \frac{\partial f_o}{\partial \gamma} \right] \end{aligned}$$

Assuming $f_1 = 0$ at $z = 0$, then

$$f_1 = \epsilon \sum_{n,m} h_{n,m} \left\{ \frac{m \frac{\partial f_o}{\partial J} - \omega_s \frac{\partial f_o}{\partial \gamma}}{nk_w + \omega_s \left(\frac{1}{\beta_{||}} - 1 \right) + mk_\beta - \omega_s \frac{\partial k_\beta}{\partial \gamma} J} \times \right. \quad (18)$$

$$\left. \left[e^{ink_w z} - e^{-i \left[\omega_s \left(\frac{1}{\beta_{||}} - 1 \right) + nk_\beta - \omega_s \frac{\partial k_\beta}{\partial \gamma} \right] z} \right] \right\}$$

+ complex conjugate.

Finally we look for that part of f_2 which is independent of $\hat{\tau}$ and ϕ given by:

$$\frac{\partial f_2}{\partial z} = \frac{\partial}{\partial J} \left[\left(\frac{\partial K_1}{\partial \phi} \right) f_1 \right] - \frac{\partial}{\partial \gamma} \left[\left(\frac{\partial K_1}{\partial \hat{\tau}} \right) f_1 \right]$$

We further keep only terms which are not oscillating rapidly on the scale of k_w to find:

$$\frac{\partial f_2}{\partial z} = \epsilon^2 \sum_{n,m} \left\{ \left(-im \frac{\partial}{\partial J} + i\omega_s \frac{\partial}{\partial \gamma} \right) |h_{n,m}|^2 \right. \\ \left. \frac{1 - e^{-i\Lambda_{n,m} z}}{\Lambda_{n,m}} \left[m \frac{\partial f_0}{\partial J} - \omega_s \frac{\partial f_0}{\partial \gamma} \right] \right\} \\ + \text{complex conjugate}$$

where

$$\Lambda_{n,m} = nk_w + \omega_s \left(\frac{1}{\beta_{||}} - 1 \right) + mk_\beta - \omega_s \frac{\partial k_\beta}{\partial \gamma} J \quad (19)$$

so

$$f_2(z) = \epsilon^2 \sum_{n,m} \left\{ \left[m \frac{\partial}{\partial J} - \omega_s \frac{\partial}{\partial \gamma} \right] |h_{n,m}|^2 \right. \\ \left. \frac{\sin^2 \Lambda_{m,n} z/2}{(\Lambda_{n,m}/2)^2} \left[m \frac{\partial f_0}{\partial J} - \omega_s \frac{\partial f_0}{\partial \gamma} \right] \right\} . \quad (20)$$

We see immediately, by multiplying by J and integrating by parts over $d\gamma$ dJ , that the mean action change is given by:

$$\langle \delta J \rangle = \epsilon^2 \sum_{n,m} \left\{ \int f_0 dJ d\gamma m \left[m \frac{\partial}{\partial J} - \omega_s \frac{\partial}{\partial \gamma} \right] |h_{n,m}|^2 \right. \quad (21)$$

$$\left. \frac{\sin^2 \Lambda_{m,n} z/2}{\left(\frac{\Lambda_{n,m}}{2} \right)^2} \right\}$$

and the energy change by:

$$\langle \delta \gamma \rangle = -\omega_s \epsilon^2 \sum_{n,m} \left\{ \int f_0 dJ d\gamma \left[m \frac{\partial}{\partial J} - \omega_s \frac{\partial}{\partial \gamma} \right] |h_{n,m}|^2 \right. \quad (22)$$

$$\left. \frac{\sin^2 \Lambda_{m,n} z/2}{\left(\frac{\Lambda_{n,m}}{2} \right)^2} \right\}$$

In the usual case where only one resonance is of importance (which is practically necessary and desirable to get cancellation of excitation at a definite z value) the Manley-Rowe relation follows directly:

$$\langle \delta J \rangle = -m \frac{\langle \delta \gamma \rangle}{\omega_s} \quad . \quad (23)$$

We have already remarked that $2\pi J$ is just the phase space area, hence can not be changed by moving from one magnet to another. Only going from one m to another seems to offer the possibility of excitation cancellation with gain but we haven't yet been able to implement a viable scheme.

The $m = 0$ resonance does not produce excitation but since the whole effect depends on energy derivatives, presumably large energy spread results. It should also be noted that only $m = 1$ is operative for small J , hence only $h_{1,1}$ need be calculated which is doable in spite of the complications (see Section IV).

By taking the second moments of equation (20) it is also easily possible to generalize the Madey Theorem relating gain to spread without making the resonant approximation, i.e., keeping all m values:

$$\begin{aligned} \langle \delta J \rangle &= \frac{1}{2} \frac{\partial}{\partial J} \langle (\delta J)^2 \rangle + \frac{1}{2} \frac{\partial}{\partial \gamma} \langle \delta J \delta \gamma \rangle \\ \langle \delta \gamma \rangle &= \frac{1}{2} \frac{\partial}{\partial \gamma} \langle (\delta \gamma)^2 \rangle + \frac{1}{2} \frac{\partial}{\partial J} \langle \delta J \delta \gamma \rangle \quad . \end{aligned} \quad (24)$$

IV. ENERGY GAIN FOR THE THIN LENS EXPANDER

In order to calculate energy gain at small excitation, J , coming from the resonance $m = n = -1$, it is necessary only to keep the terms in H_1 proportional to $e^{-i\phi}$ and to \sqrt{J} . From equations (13) and (5) with $\epsilon = a_s/2$, we have:

$$H_1 = -\epsilon \left\{ \frac{p'}{\gamma} - \frac{i\omega_s p_o}{\gamma} \left[p' \frac{dx_o}{d\gamma} - x' \frac{dp_o}{d\gamma} \right] \right\} . \quad (25)$$

Recalling that $P = -\sqrt{2J} \sin \phi$, $Q = \sqrt{2J} \cos \phi$ and using equations (7) and (8), we find readily that the terms in p' , x' which are proportional to $e^{-i\phi}$ are:

$$\begin{aligned} p' &= \sqrt{J/2} [C + iD] \\ x' &= \sqrt{J/2} [B + iA] \end{aligned} \quad (26)$$

where A, B, C are defined in equation (10) and

$$D = \sqrt{\frac{\gamma}{\lambda_0 \sin k_\beta \lambda_0 (1-\eta^2)}} \left[\left[1 - (-)^n \eta \right] \sin k_\beta (\tilde{z} - \lambda_0) - \left[1 + (-)^n \eta \right] \sin k_\beta \tilde{z} \right] .$$

We further need the properties of the nominal isochronous trajectories

$$p_0 \frac{dp_0}{d\gamma} = 2 \left(\frac{1}{\beta_{||}} - 1 \right) \gamma \quad (27)$$

$$p_0 \frac{dx_0}{d\gamma} = \frac{1}{2} \frac{\beta_-}{\beta_+} \frac{\lambda_0}{\gamma^2} (-)^n + \left[p_0 \frac{dp_0}{d\gamma} - \frac{p_0^2}{\gamma^2} \right] \left[\tilde{z} - \frac{\lambda}{2} \right] \quad (28)$$

where the β 's specify the magnet gradients as given in equation (2).

Equations (26) - (28) may now be substituted into equation (25). We must still perform a Fourier Transform in z . Note that the desired resonant Fourier component is:

$$h_{-1,-1} = \frac{1}{2\lambda_0} \int_{-\lambda_0}^{\lambda_0} e^{+i\pi z/\lambda_0} H_1(z) dz \quad (29)$$

and that the integrand consists of functions of $\tilde{z} \equiv z - n\lambda_0$ times constant factors and factors proportional to $(-)^n$. Only the latter contribute to (29). It is thus useful to write down the parts of equation (26) which are constant and those which go like $(-)^n$

$$C_- + iD_- = -\eta e^{ik_\beta \tilde{z}} \left[1 + e^{-ik_\beta \lambda_0} \right] \sqrt{\frac{\gamma}{\lambda_0 \sin k_\beta \lambda_0 (1-\eta^2)}}$$

$$C_+ + iD_+ = e^{ik_\beta \tilde{z}} \left[e^{-ik_\beta \lambda_0} - 1 \right] \sqrt{\frac{\gamma}{\lambda_0 \sin k_\beta \lambda_0 (1-\eta^2)}}$$

$$iA_- + B_- = -\eta/2 e^{ik_\beta \tilde{z}} \left[\left(1 - e^{-ik_\beta \lambda_0} \right) + \left(1 - 2\tilde{z}/\lambda_0 \right) \left(1 + e^{-ik_\beta \lambda_0} \right) \right] \frac{\lambda_0}{\gamma} \sqrt{\frac{\gamma}{\lambda_0 \sin k_\beta \lambda_0 (1-\eta^2)}}$$

Here the subscript - denotes the terms proportional to $(-)^n$.
The integrals are now all elementary so that we find

$$h_1 = \sqrt{\frac{J}{2}} i \chi$$

with

$$\chi = \frac{1}{(\pi + k_\beta \lambda_0)} \left\{ 2\eta(1 + \cos k_\beta \lambda_0) + \frac{\omega_s}{\gamma^2} \lambda_0 \left[-2(1 + \cos k_\beta \lambda_0) \frac{p_0^2 \eta}{(\pi + k_\beta \lambda_0)} \right] \right. \\ \left. + \sin k_\beta \lambda_0 \left[\eta + \frac{\beta_-}{\beta_+} \right] \right\} \left\{ (\sin |k_\beta| \lambda_0) (1 - \eta^2) \gamma \lambda_0 \right\}^{-\frac{1}{2}} .$$

We may simplify this somewhat if we evaluate at resonance where $\omega_s \lambda_0 (p_0^2 + 1)/2\gamma^2 = \pi + k_\beta \lambda_0$ to obtain finally:

$$\chi = \frac{2\eta}{(1+p_0^2)} \left\{ \frac{(1 + \cos k_\beta \lambda_0)}{\pi + k_\beta \lambda_0} (1 - p_0^2) + \sin k_\beta \lambda_0 \left[1 + \frac{\beta_-}{\beta_+ \eta} \right] \right\} \\ \cdot \left[(\sin |k_\beta| \lambda_0) (1 - \eta^2) \gamma \lambda_0 \right]^{-\frac{1}{2}} \quad (30)$$

and finally from equation (22)

$$\langle \delta\gamma \rangle = \frac{\omega_s}{8} a_s^2 \chi^2 \frac{\sin^2 \Lambda_{-1,-1} z/2}{(\Lambda_{-1,-1}/2)^2} \quad (31)$$

with $a_s = eA_s/m$ the dimensionless vector potential of the laser as defined in equation (13), and Λ defined in equation (9).

The term proportional to β_-/β_{+n} is usually the largest in equation (30) and yields the same result as Kroll, et al. The $m = +1$ resonance result is obtained by changing the sign of k_β in equation (30).

Those results are in agreement with numerical simulations by John Madey.³

REFERENCES

1. J. Madey and J. N. Eckstein, Stanford University, HEPL Report No. 902.
2. Kroll, Morton, Rosenbluth, Eckstein and Madey, Journal of Quantum Electronics 17, 1436 (1981).
3. J. Madey, Stanford University, private communication.

A P P E N D I X B

THEORY OF LINEAR GAIN: FREE ELECTRON

LASERS OPERATED IN OSCILLATOR MODE

PART I: ULTRA-SHORT ELECTRON PULSES

Austin Research Associates
1901 Rutland Drive - Austin, Texas 78758 - Phone (512) 837-6623

THEORY OF LINEAR GAIN: FREE ELECTRON
LASERS OPERATED IN OSCILLATOR MODE

PART I: ULTRA-SHORT ELECTRON PULSES

M. N. Rosenbluth
and
H. Vernon Wong

July 1982

I. INTRODUCTION

In the free electron laser (FEL), a relativistic electron beam is propagated through a transverse periodic (wave number k_w) magnetic field wiggler where the electrons acquire transverse oscillatory motion (amplitude $p_{0\perp}$) which enables them to couple to the transverse electric field of an electromagnetic wave (frequency ω_s and wave number k_s). For low density beams (where collective effects may be neglected) the coupling may be viewed in terms of the interaction of electrons with a ponderomotive potential well (produced by the combined wiggler and radiation field) moving with velocity $v_{res} = \omega_s / (k_w + k_s)$. Electrons with velocity close to v_{res} , or equivalently with energy close to

$$\gamma_{res} = \left[\frac{k_s}{2k_w} \left(1 + \frac{p_{0\perp}^2}{m^2 c^2} \right) \right]^{1/2},$$

are in resonance, and net energy transfer can occur between the electrons and the radiation field. Those with energy slightly larger (smaller) than γ_{res} lose (gain) energy to (from) the radiation field.

In constant parameter wigglers where γ_{res} is constant throughout the wiggler, the energy extraction from

the electrons terminates when their energy is reduced to γ_{res} . This puts severe limitations on the gain and efficiency of the constant parameter FEL. To overcome this limitation, variable parameter wigglers¹ have been proposed in which electrons are trapped in the ponderomotive potential well and γ_{res} gradually reduced by adiabatic variations of the wave number (k_w) and amplitude (p_{o_1}) of the wiggler. The energy loss of the trapped electrons translates into energy gain of the radiation field. In this way, the energy extraction in a variable parameter wiggler can be made to be much larger than that in a constant parameter wiggler. In principle, a DC electric field may be applied to keep electrons of fixed γ in resonance with a constant parameter wiggler.

While a variable parameter FEL may be operated as an amplifier by passing a finite amplitude electromagnetic pulse through the wiggler, it is desirable to initiate operation of the FEL by growing the pulse from noise levels. This necessitates that the pulse be reflected and passed repeatedly through the wiggler, and its amplitude increased on each pass. However, the successful operation of the FEL in this mode (as an oscillator) will require that:

1. The linear gain per pass be sufficient to overcome reflection losses and grow the electromagnetic pulse to a large amplitude in a finite number of passes;

2. The saturation of linear gain occurs at amplitudes large enough to trap a significant fraction of the beam electrons in the ponderomotive well;

3. The finite amplitude saturated pulse propagates without deterioration due to the onset of trapped electron sideband instabilities.¹

An investigation has been undertaken to determine the extent to which these requirements can be optimized and integrated into an efficiently functioning variable parameter FEL. The investigation will involve not only theoretical analysis of the FEL equations, but also numerical simulations, particularly when studying the nonlinear saturation of linear gain, electron trapping, and the effects of trapped electron sideband instabilities. This paper is primarily an analytic study of linear gain. In a subsequent paper, the numerical simulations will be described, and the formation and stable propagation of the finite amplitude pulse discussed. Our numerical simulations are similar to those in the pioneering work of Colson² on optical pulse formation, although we extend his techniques in order to treat the case of interest to us, the high extraction variable parameter wiggler.

In Section II, the set of equations governing the operation of the FEL are briefly formulated. A fuller

discussion may be found in Reference 1. The electron equations of motion are derived from an approximate relativistic Hamiltonian in which the transverse motion is taken to be nonrelativistic, and transverse spatial variations and beam self-fields are neglected. Thus our analysis is one-dimensional. While rough estimates show that two-dimensional effects such as diffraction and radially dependent ponderomotive wells are not crucial, much further work is required in this connection.

These equations, together with Maxwell's equations, determine the temporal and spatial evolution of the electromagnetic pulse in the wiggler. In order to suppress the growth of sideband instabilities and ensure stable propagation of the finite amplitude pulse, the formulation includes frequency discrimination of the pulse outside the wiggler, the effect of which is to attenuate frequencies above and below the desired pulse frequency ω_s . As we will see in this paper, while frequency discrimination is necessary to suppress the sideband instability, it may have a detrimental effect on linear gain. In a similar fashion, a long constant wiggler section will be found to be desirable for linear gain, but to lead to saturation at too low a level for trapping. Thus, careful design is required for a successful high extraction FEL.

The FEL equations are linearized and the linear eigenmode analysis leading to a calculation of the linear gain as a function of the FEL parameters is described in Sections III and IV.

The special case of ultra-short electron beams is considered in this paper. By an ultra-short pulse, which we approximate in the paper by $\delta(z-vt)$, we mean one such that the difference in electron and photon velocity is large enough that a photon is able to slip through the entire electron beam while traversing the wiggler. The motivation (aside from the intrinsic interest of short pulses) for considering this case are: (a) Analytic tractability and, more important, (b) the number of particle orbits which must be followed in numerical simulation is obviously far fewer for a single electron beamlet than for the many beamlets which would be required to simulate a long continuous pulse.

The basic physics of electron-photon interaction should be qualitatively the same for a long pulse whose current times slippage length equals the number of electrons in our δ function pulse. The linear gain for long electron pulses will be considered in a companion paper.

The analysis encompasses constant parameter wigglers, variable parameter wigglers, and a combination of constant

and variable parameter wigglers, with and without frequency discrimination.

In Section V, we summarize our results for linear gain and present a semiquantitative discussion of nonlinear propagation and sideband suppression.

II. BASIC EQUATIONS

A. Electron Equation of Motion

The electron equations of motion can be derived from the Hamiltonian¹

$$\begin{aligned} H &= H[x, p_x, y, p_y, (-\mathcal{E}), t, z] \\ &= - \left[\frac{(\mathcal{E} - e\phi_0)^2}{c^2} - m^2 c^2 - \left(p_x - \frac{e}{c} A_x \right)^2 - \left(p_y - \frac{e}{c} A_y \right)^2 \right]^{\frac{1}{2}} \\ &\quad - \frac{e}{c} A_z \end{aligned} \tag{1}$$

where the electron energy $(-\mathcal{E})$ plays the role of the momentum conjugate to t , and z is the independent variable.

ϕ_0 is the electrostatic potential of an accelerating electric field $-\frac{\partial \phi_0}{\partial z}$. The beam density is assumed small so that the electrostatic self-fields of the beam may be neglected.

The vector potential \underline{A} is the sum of a circularly polarized, periodic magnetic field wiggler A_w :

$$\frac{e}{mc^2} \underline{A}_w = \underline{a}_w$$

$$= - a_w(z) \left[\hat{x} \cos \int_0^z k_w dz + \hat{y} \sin \int_0^z k_w dz \right]$$

and a circularly polarized electromagnetic plane wave \underline{A}_s

$$\frac{e}{mc^2} \underline{A}_s = \underline{a}_s$$

$$= a_s(z, t) \left[\hat{x} \cos(k_s z - \omega_s t + \zeta[z, t]) \right. \\ \left. - \hat{y} \sin(k_s z - \omega_s t + \zeta[z, t]) \right]$$

where a_w , k_w , a_s , and ζ are slowly varying functions of z and t . As has been shown elsewhere a linearly polarized wiggler gives only slightly modified equations.

The assumption that \underline{A} is independent of transverse coordinates (x and y) implies that the canonical perpendicular momenta P_x , P_y are constants of the motion. We will assume $P_x = 0$, $P_y = 0$, an assumption corresponding to the neglect of transverse velocities in the incoming beam before it enters the wiggler.

If we introduce as new variables the energy parameter

$$\gamma = \frac{(\mathcal{E} - e\phi_0)}{mc^2}$$

and the relative phase

$$\zeta = \int_0^z k_w dz + k_s z - \omega_s t$$

the Hamiltonian H takes the form:

$$H = H(-\mathcal{E}, t, z)$$

$$= -mc[\gamma^2 - \mu^2 + 2a_w a_s \cos(\psi + \zeta)]^{1/2}$$

(2)

$$\approx -mc\gamma + \frac{mc}{2\gamma} \left\{ \mu^2 - 2a_w a_s \cos(\psi + \zeta) \right\} + \dots$$

where $\mu^2 = 1 + a_w^2 + a_s^2$, $a_w \gg a_s$, and $\gamma^2 \gg \mu^2 \gg 2a_w a_s$.

The electron equations of motion in terms of γ and ψ , derivable from $H(-\mathcal{E}, t, z)$, are then given by:

$$\frac{d\gamma}{dz} = -\frac{e}{mc^2} \frac{d\phi_0}{dz} + \frac{1}{mc^2} \frac{\partial H}{\partial t}$$

(3)

$$= -\frac{e}{mc^2} \frac{d\phi_0}{dz} - \frac{k_s a_w a_s}{\gamma} \sin(\psi + \zeta)$$

$$\frac{d\psi}{dz} = k_w + k_s + \omega_s \frac{\partial \zeta}{\partial t}$$

(4)

$$\approx k_w - \frac{k_s \mu^2}{2\gamma^2}$$

where $\omega_s = k_s c$, and terms of order $\frac{1}{\omega_s} \frac{\partial \zeta}{\partial t} \ll 1$, $\frac{1}{\omega_s} \frac{\partial \omega_s}{\partial t} \ll 1$, $2a_w a_s / \mu^2 \ll 1$, have been deleted.

The relative phase ψ varies slowly for electrons with values of γ close to γ_r (the resonant energy) defined by:

$$\gamma_r = \left(\frac{k_s}{2k_w} \right)^{1/2} \mu$$

These electrons interact strongly with the radiation field and will exchange net energy with it. Electrons with values

of γ far from γ_r have negligible effects on the radiation field.

It is therefore convenient to describe the electron motion in terms of the variables $\tilde{\gamma} = \gamma - \gamma_r$ and ψ .

In the limit of $\tilde{\gamma} \ll \gamma_r$, the electron equations of motion may finally be approximated by

$$\frac{d\tilde{\gamma}}{dz} = - \frac{d\gamma_r}{dz} - \frac{e}{mc^2} \frac{d\phi_0}{dz} - \frac{k_s a_s a}{\gamma_r} \sin(\psi + \zeta) \quad (5)$$

$$\frac{d\psi}{dz} = \frac{2 k_w \tilde{\gamma}}{\gamma_r} \quad (6)$$

and are derivable from the approximate Hamiltonian

$H_1(\tilde{\gamma}, \psi, z)$:

$$H_1 = \frac{k_w}{\gamma_r} \tilde{\gamma}^2 + \left\{ \frac{d\gamma_r}{dz} + \frac{e}{mc^2} \frac{d\phi_0}{dz} \right\} \psi - \frac{k_s a_s a}{\gamma_r} \cos(\psi + \zeta) \quad (7)$$

We define a constant parameter wiggler by $\frac{d\gamma_r}{dz} = 0$
 and $\frac{d\phi_0}{dz} = 0$.

In a variable parameter wiggler, γ_r is allowed to vary spatially, $\frac{d\gamma_r}{dz} \neq 0$. The presence of an accelerating electric field $d\phi_0/dz$ affects the electron phase space $(\tilde{\gamma}, \psi)$ trajectories in a manner similar to spatial variations of γ_r , as may be seen from Equation (7). In subsequent sections, it will be assumed that γ_r is constant, $\frac{d\gamma_r}{dz} = 0$. A constant or variable parameter wiggler is then modeled by

$$\frac{d\phi_0}{dz} = 0 \quad \text{or} \quad \frac{d\phi_0}{dz} \neq 0$$

B. Electromagnetic Field Equations

The transverse electron beam current density \underline{J}_\perp determines the time and spatial evolution of \underline{A}_s through Maxwell's equation:

$$\frac{\partial^2}{\partial z^2} \underline{A}_s - \frac{1}{c^2} \frac{\partial^2}{\partial t^2} \underline{A}_s = - \frac{4\pi}{c} \underline{J}_\perp$$

Substitution of the assumed form of \underline{A}_s yield:

$$\frac{\partial a_s}{\partial t} + c \frac{\partial a_s}{\partial z} = - \frac{2\pi e}{k_s mc^2} J_2 \quad (8)$$

$$a_s \left(\frac{\partial \zeta}{\partial t} + c \frac{\partial \zeta}{\partial z} \right) = \frac{2\pi e}{k_s mc^2} J_1 \quad (9)$$

where

$$J_j = \underline{J}_1 \cdot \hat{e}_j, \quad j = 1, 2$$

$$\begin{aligned} \hat{e}_1 &= \hat{x} \cos(k_s z - \omega_s t + \zeta) \\ &\quad - \hat{y} \sin(k_s z - \omega_s t + \zeta) \end{aligned}$$

$$\begin{aligned} \hat{e}_2 &= -\hat{x} \sin(k_s z - \omega_s t + \zeta) \\ &\quad - \hat{y} \cos(k_s z - \omega_s t + \zeta) \end{aligned}$$

The assumption that a_s and ζ vary slowly in space and time has again been invoked to delete higher order terms.

If $F_0(\tilde{\gamma}_0, \psi_0)$ is the distribution function of the electron beam on entry at $z = 0$ into the wiggler at time $t_0 = -\frac{\psi_0}{\omega_s}$, the beam density $n(z, t)$ and transverse beam current density $J_j(z, t)$ are:

$$n(z, t) = \int F_0(\tilde{\gamma}_0, \psi_0) \delta[t - t(\tilde{\gamma}_0, \psi_0, z)] d\tilde{\gamma}_0 d\psi_0 \quad (10)$$

$$J_j(z, t) = e \int F_0(\tilde{\gamma}_0, \psi_0) \underline{v}_\perp \cdot \hat{e}_j \delta[t - t(\tilde{\gamma}_0, \psi_0, z)] d\tilde{\gamma}_0 d\psi_0 \quad (11)$$

where the transverse electron velocity \underline{v}_\perp is ($\underline{p}_\perp = 0$):

$$\begin{aligned} \underline{v}_\perp \cdot \hat{e}_1 &= -\frac{c}{\gamma} a_w \cdot \hat{e}_1 \\ &\approx \frac{c}{\gamma_r} a_w(z) \cos \left\{ \psi(\tilde{\gamma}_0, \psi_0, z) + \zeta[z, t(\tilde{\gamma}_0, \psi_0, z)] \right\} \\ \underline{v}_\perp \cdot \hat{e}_2 &\approx -\frac{c}{\gamma_r} a_w \sin \{ \psi + \zeta \} \end{aligned}$$

$\tilde{\gamma}(\tilde{\gamma}_0, \psi_0, z)$ and $\psi(\tilde{\gamma}_0, \psi_0, z)$ are the phase space coordinates of the electron trajectory with initial values $\tilde{\gamma}_0$ and ψ_0 at $z = 0$. $t(\tilde{\gamma}_0, \psi_0, z)$ is the time of arrival of the electron at z and is given approximately by

$$t(\tilde{\gamma}_0, \psi_0, z) \approx t_0 + \frac{z}{v} = -\frac{\psi_0}{\omega_s} + \frac{z}{v}$$

where

$$v = \frac{c}{\left(1 + \frac{\mu^2}{2\gamma_r^2}\right)} \approx c\left(1 - \frac{\mu^2}{2\gamma_r^2}\right)$$

Let $F_0(\tilde{\gamma}_0, \psi_0) = 1/\omega_s H(\psi_0/\omega_s) f(\tilde{\gamma}_0)$, where $f(\tilde{\gamma}_0)$ determines the energy distribution and $\int d\tilde{\gamma}_0 f(\tilde{\gamma}_0) = 1$.

Then, from Equation (10):

$$n(z, t) = H\left(\frac{z}{v} - t\right)$$

and from Equation (11):

$$J_1(z, t) = \frac{ec}{\gamma_r} a_w(z) H\left(\frac{z}{v} - t\right)$$

$$\int d\hat{\gamma}_0 f(\hat{\gamma}_0) \cos\{\psi(\hat{\gamma}_0, \psi_0, z) + \zeta(z, t)\} \Big|_{\psi_0 = \omega_s \left(\frac{z}{v} - t\right)}$$

When t changes by $\Delta t = \frac{2\pi}{\omega_s}$ or z by $\Delta z = \frac{2\pi v}{\omega_s} = \frac{2\pi}{k_s}$, the argument ψ_0 of $\psi(\hat{\gamma}_0, \psi_0, z)$ changes by 2π . Assuming that the beam density $H\left(\frac{z}{v} - t\right)$ varies slowly over these small changes in t or z , it is appropriate to average $\cos\{\psi + \zeta\}$ over ψ_0 . Thus

$$J_1(z, t) \approx \frac{ec}{\gamma_r} a_w(z) H\left(\frac{z}{v} - t\right)$$

$$\frac{1}{2\pi} \int d\hat{\gamma}_0 d\psi_0 f(\hat{\gamma}_0) \cos\{\psi + \zeta\}$$

$$\equiv \frac{eca_w(z)}{\gamma_r} H\left(\frac{z}{v} - t\right) \langle \cos\{\psi + \zeta\} \rangle$$

Similarly

$$J_2(z, t) = - \frac{eca_w(z)}{\gamma_r} H \left(\frac{z}{v} - t \right) \langle \sin \{ \psi + \zeta \} \rangle$$

The field equations for a_s and ζ are then given by

$$\frac{\partial a_s}{\partial t} + c \frac{\partial a_s}{\partial z} \tag{12}$$

$$= \frac{2\pi e^2 a_w}{k_s c m \gamma_r} H \langle \sin \{ \psi + \zeta \} \rangle$$

$$a_s \left(\frac{\partial \zeta}{\partial t} + c \frac{\partial \zeta}{\partial z} \right) \tag{13}$$

$$= \frac{2\pi e^2 a_w}{k_s c m \gamma_r} H \langle \cos \{ \psi + \zeta \} \rangle$$

C. FEL Equations

In the FEL configuration which will be analyzed, a combination of constant and variable parameter magnetic field wigglers is positioned between mirrors so that an electromagnetic pulse can be reflected repeatedly and multiple passes of the pulse through the wiggler achieved (see Fig. 1).

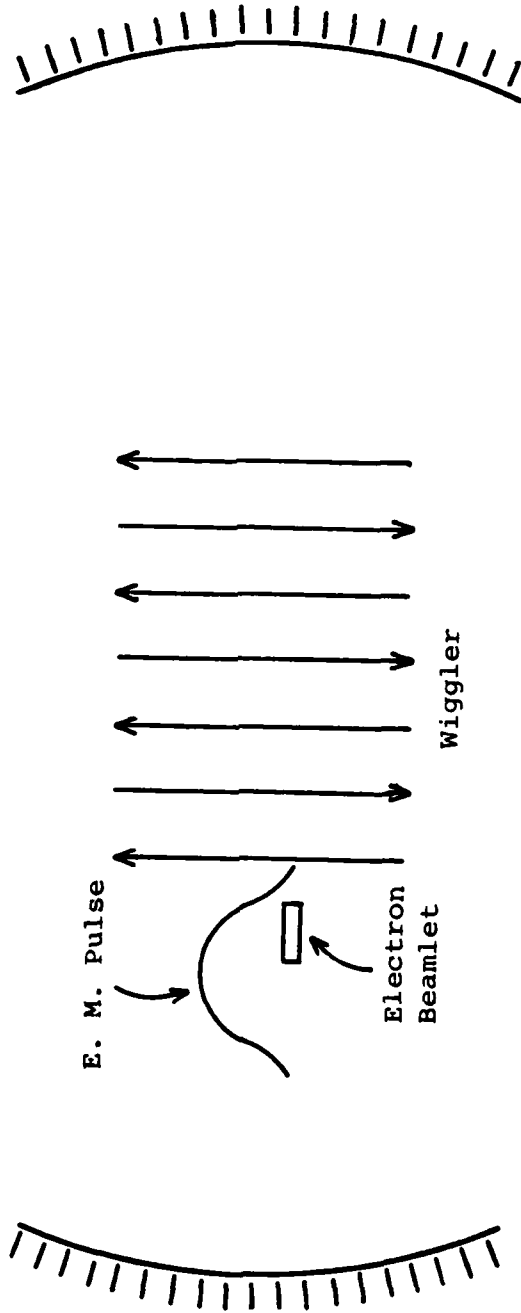


Figure 1. FEL Configuration

Relativistic electron beamlets of finite length are injected into the wiggler at periodic intervals so that on each forward pass of the pulse through the wiggler, there is overlap of the pulse and beamlet. The pulse grows on each forward pass. Eventually, the amplitude of the pulse becomes large enough to trap a fraction of the beam electrons. At this stage, the pulse is susceptible to detrimental spatial distortions due to the onset of trapped electron sideband instabilities. To avoid breakup of the pulse, it will be necessary to suppress the growth of the sideband instabilities. This may be accomplished by passing the pulse through a frequency discriminator which effectively acts as a band pass filter, attenuating frequencies above and below the desired pulse frequency. With stable pulse propagation, a stationary state is reached when the energy extraction from the electron beam is balanced by the energy losses in the frequency discriminator and at the mirrors.

To facilitate formulation of the equations which describe the operation of the FEL, it is advantageous to transform the variables z and t to the variables u and v :

$$u = \frac{c}{L \left(\frac{c}{v} - 1 \right)} \left(\frac{z}{v} - t \right)$$

$$v = \frac{c}{L \left(\frac{c}{v} - 1 \right)} \left(t - \frac{z}{c} \right)$$

where L is the length of the wiggler.

The line $z = 0$ in $z - t$ space maps into the line $v = -u$ in $u - v$ space and $z = L$ into $v = -u + 1$ (see Fig. 2).

In $u - v$ space, the beam electrons, entering the wiggler at $z = 0$ and exiting at $z = L$, move on lines of constant u . The photons of the electromagnetic pulse, propagating in the beam direction, move on lines of constant v . During the n^{th} pass of the pulse through the wiggler, the pulse interacts with the electrons when the values of u and v lie in the area defined by $u_{2n} > u > u_{1n}$, $1 - u > v > -u$, where the difference $u_{2n} - u_{1n} \equiv u_0$ is determined by the length of the injected electron beam.

In terms of the $u - v$ variables, the coupled set of equations, (5), (6), (12), and (13), which describe the evolution of the electromagnetic pulse passing through the wiggler together with the electron beam, can be rewritten as follows:

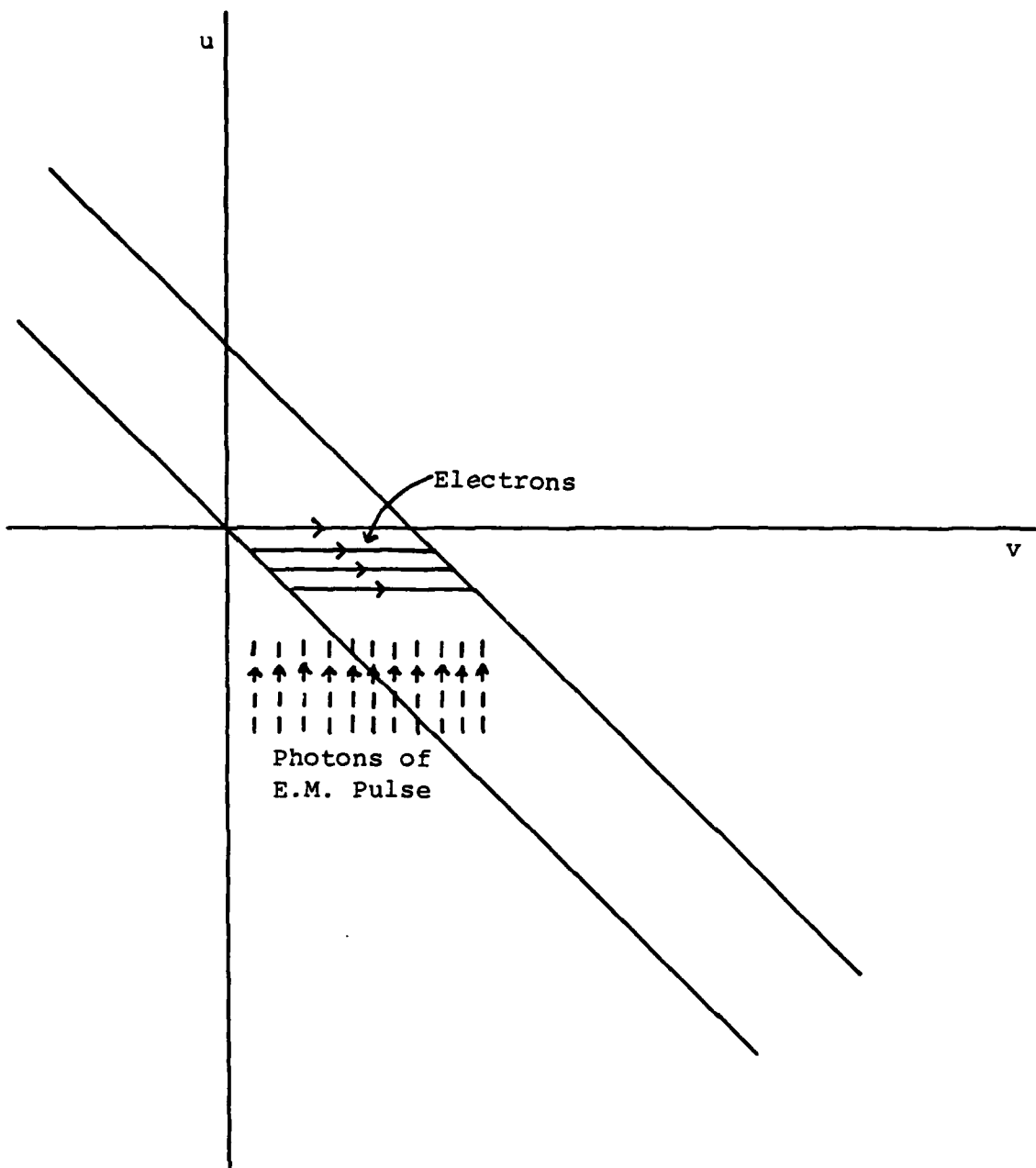


Figure 2. Electron and Photon Trajectories in $u - v$ plane

$$\frac{\partial \psi}{\partial v} = \hat{\gamma} \quad (14)$$

$$\frac{\partial \hat{\gamma}}{\partial v} = \Gamma + \frac{1}{2} \left[i \hat{a} e^{i\psi} - i \hat{a}^* e^{-i\psi} \right] \quad (15)$$

$$\frac{\partial \hat{a}}{\partial u} = i \eta h(u) \left\langle e^{-i\psi} \right\rangle \quad (16)$$

where \hat{a}^* is the complex conjugate of \hat{a} , and

$$\hat{a} = \hat{a}_s e^{i\zeta}$$

$$\hat{a}_s = \frac{2 k_w L}{\gamma_r} \frac{k_s L a_w}{\gamma_r} a_s$$

$$\hat{\gamma} = \frac{2 k_w L}{\gamma_r} \tilde{\gamma}$$

$$\Gamma = - \frac{2 k_w L}{\gamma_r} \frac{e}{mc^2} \frac{\partial \phi_0}{\partial v}$$

$$\equiv \frac{2 k_w L}{\gamma_r} \Delta \gamma_r$$

with $\Delta\gamma_r$ the change in γ which would be experienced by an electron freely accelerating under the potential ϕ_0 . $h(u)$ is a form factor which determines the beam density profile and is defined by:

$$n(z,t) = H\left(\frac{z}{v} - t\right) \tag{17}$$

$$\equiv \frac{c}{vL} \frac{1}{\left(\frac{c}{v} - 1\right)} N_T h(u)$$

where $\int_{u_{1n}}^{u_{2n}} h(u) du = 1$ and N_T is the total number of electrons in the beam per unit area, $N_T = \int dz n(z, t)$. The dimensionless parameter η is given by:

$$\eta \equiv \frac{8\pi e^2 N_T k_w L^2 a_w^2}{\gamma_r mc v \mu^2} \tag{18}$$

Thus, for the n^{th} pass of the electromagnetic pulse through the wiggler, the electron phase space $(\hat{\gamma}, \psi)$ trajectories are determined by the solutions of equations (14) and (15), with initial conditions $\hat{\gamma} = \gamma_0, \psi = \psi_0$ at $v = -u$. The phase of electrons entering the wiggler is uncorrelated with that of the electromagnetic pulse. Thus, ψ_0 is distributed uniformly between 0 and 2π . The average over ψ_0 is indicated by $\langle \rangle$. The pulse amplitude after interaction with the beam electrons is given by:

$$\hat{a}^n(v, 0) = \hat{a}^n(v, -u_0) + \Delta \hat{a}^n(v) \quad (19)$$

where

$$\Delta \hat{a}^n(v) = i n \int_{-u_0}^0 du h(u) \langle e^{-i\psi(v,u)} \rangle g(v,u)$$

$$g(v,u) = \begin{cases} 1 & \begin{array}{l} 1 - u > v > -u \\ 0 > u > -u_0 \end{array} \\ 0 & \text{otherwise} \end{cases} \quad (20)$$

In deriving equation (20), the u, v coordinates were transformed so that the interaction of pulse and electrons during the n^{th} pass occur for u and v in the range $0 > u > -u_0, 1 - u > v > -u$. It will be assumed that there is no overlap of the electromagnetic pulse from pass to pass, and consequently, this transformation can be carried out in deriving corresponding equations for the $(n + 1)^{\text{th}}$ pass, etc.

The electromagnetic pulse is reflected backwards and then forwards for the $(n + 1)^{\text{th}}$ pass through the wiggler. Without optical filtering, the pulse amplitude $\hat{a}^{n+1}(v, -u_0)$ before the $(n + 1)^{\text{th}}$ pass may be related to the pulse amplitude $\hat{a}^n(v, 0)$ after the n^{th} pass by

$$\begin{aligned} \hat{a}^{n+1}(v - \beta, -u_0) &= r \hat{a}^n(v, 0) \\ &= r \left[\hat{a}^n(v, -u_0) + \Delta \hat{a}^n(v) \right] \end{aligned} \tag{21}$$

where $r < 1$ accounts for the reduction in amplitude due to energy losses on reflection at the mirrors, and β represents the tunable pass to pass shift in the position of the

pulse relative to the front of the electron beam at the moment of entry into the wiggler. As we will see the linear growth rate depends sensitively on β which is physically determined by the distance between mirrors and the interpulse spacing of the e-beam.

If identical electron beams are injected into the wiggler on each pass with fixed periodicity, the pass to pass change in pulse amplitude is determined by equations (19) and (21), independent of the value of n .

To suppress the growth of sideband instabilities when the pulse amplitude is large enough to trap electrons, the pulse can be filtered to attenuate sideband frequencies above and below the desired pulse frequency ω_s . This filtering may be accomplished by a band pass filter, modeled by the equation:

$$\frac{\partial}{\partial v} \hat{a}^n(v,0) + v \hat{a}^n(v,0) = v \hat{a}^n(v,0) \quad (22)$$

where \hat{a}^n is the filtered pulse amplitude, and the frequency half width $\Delta\omega$ of the band pass filter is

$$\Delta\omega = \frac{vc}{L\left(\frac{c}{v} - 1\right)}$$

Since $\hat{a}^{n+1}(v - \beta, -u_0) = r\hat{a}^n(v, 0)$, the pass to pass change in pulse amplitude after interaction with the beam electrons, filtering, and reflection at the mirrors, is given by

$$\begin{aligned} \frac{1}{v} \frac{\partial}{\partial v} \hat{a}^{n+1}(v - \beta, -u_0) + \hat{a}^{n+1}(v - \beta, -u_0) \\ (23) \\ = r \left[\hat{a}^n(v, -u_0) + \Delta a^n(v) \right] \end{aligned}$$

Equations (14), (15), (21), and (23) govern the operation of the FEL.

III. LINEAR THEORY--WITHOUT FREQUENCY DISCRIMINATION

For small pulse amplitudes, the FEL equations are linearized to obtain the linear eigenmode equations. In the limit of short electron beams ($u_0 \ll 1$) where

$$h(u) = \begin{cases} \frac{1}{u_0} & 0 \geq u \geq -u_0 \\ 0 & \end{cases}$$

equations (14), (15), and (21) yield:

$$\begin{aligned} \langle e^{-i\psi(v,u)} \rangle &= \frac{1}{2} \int_0^v dv' (v-v') I(v-v') \\ &\times \left[\hat{a}^n(v', -u_0) + i \frac{n}{u_0} \int_{-u_0}^u du' \langle e^{-i\psi(v',u')} \rangle \right] e^{i \frac{\Gamma}{2} (v'^2 - v^2)} \end{aligned}$$

$$1 > v > 0$$

(24)

$$\begin{aligned} & \hat{a}^{n+1}(v-\beta, -u_0) - r \hat{a}^n(v, -u_0) \\ &= \left(1 - \beta \frac{\partial}{\partial v} \right) \hat{a}^{n+1}(v, -u_0) \\ & \quad - r \hat{a}^n(v, -u_0) \end{aligned}$$

$$= \begin{cases} i r \frac{\eta}{u_0} \int_{-u_0}^0 du \langle e^{-i\psi(v, u)} \rangle \\ 0 \end{cases}$$

$$1 > v > 0$$

otherwise

(25)

where

$$I(v-v') = \int d\hat{\gamma}_0 f(\hat{\gamma}_0) e^{i\hat{\gamma}_0(v'-v)}$$

and the relative pass to pass shift β of the pulse is assumed to be small permitting the indicated Taylor series expansion. Γ is considered to be independent of u and v .

Let

$$\begin{aligned} \hat{a}^{n+1}(v, -u_0) &= e^{\delta} \hat{a}^n(v, -u_0) \\ &\approx (1 + \delta) \hat{a}^n(v, -u_0), \\ &|\delta| \ll 1 \end{aligned}$$

where δ is the linear gain and phase shift per pass.

Equation (25) may therefore be approximated by:

$$\begin{aligned} (1 - r + \delta) \hat{a}^n - \beta \frac{\partial}{\partial v} \hat{a}^n \\ = \frac{i\eta}{u_0} \int_{-u_0}^0 du \langle e^{-i\psi(v,u)} \rangle \\ 1 > v > 0 \end{aligned} \tag{26}$$

where r is assumed to be close to unity.

The boundary condition on \hat{a}^n at $v = 1$ is

$$\hat{a}^n(v=1, -u_0) = 0$$

since photons with $v > 1$ have never interacted with the driving electron beam.

Equations (24) and (26) are valid only in the interval $1 > v > 0$. However, the upper limit may be extended to infinity since the solution of these equations in the interval $1 > v > 0$ are unaffected by the solutions in the interval $v > 1$. With this extension of the interval to $\infty > v > 0$, the solution of these equations may be obtained by Laplace transformation.

Define the Laplace transforms

$$\Theta_p(u) = \int_0^{\infty} dv e^{-pv} \langle e^{-i\psi(v,u)} \rangle e^{i \frac{\Gamma v^2}{2}}$$

$$A(p) = \int_0^{\infty} dv e^{-pv} \hat{a}(v, -u_0) e^{i \frac{\Gamma v^2}{2}}$$

$$I_p = \int_0^{\infty} dv e^{-pv} I(v)$$

The superscript on \hat{a} will be deleted except when it is necessary to differentiate variables referring to different passes through the wiggler.

Equations (24) and (26) are Laplace transformed:

$$\Theta_p(u) = -\frac{1}{2} \left[A + \frac{i\eta}{u_0} \int_{-u_0}^u du' \Theta_p(u') \right] \frac{\partial I_p}{\partial p} \quad (27)$$

$$i\Gamma\beta \frac{\partial}{\partial p} A + \beta p A - (1 + \delta - r) A$$

$$+ \frac{i\eta}{u_0} \int_{-u_0}^0 du \Theta_p(u)$$

$$= \beta \hat{a}(0, -u_0) \equiv a_0 \quad (28)$$

Equation (27) is solved to obtain

$$\theta_p(u) = -\frac{A}{2} \frac{\partial I_p}{\partial p} e^{-i \frac{\eta}{2} \frac{\partial I_p}{\partial p} \left(\frac{u}{u_0} + 1 \right)} \quad (29)$$

and substitution of $\theta_p(u)$ in equation (28) yields:

$$i\Gamma\beta \frac{\partial}{\partial p} A + \beta p A - (1 + \delta - r) A + A \left[e^{-i \frac{\eta}{2} \frac{\partial I_p}{\partial p}} - 1 \right] = a_0 \quad (30)$$

The function I_p is determined by the initial energy distribution $f(\hat{\gamma}_0)$ of the beam electrons. If

$$f(\hat{\gamma}_0) = \frac{1}{\sqrt{\pi} \bar{\gamma}_{th}} e^{-\frac{(\hat{\gamma}_0 - \bar{\gamma})^2}{\bar{\gamma}_{th}^2}}$$

is Maxwellian, or

$$f(\hat{\gamma}_0) = \frac{1}{\pi \bar{\gamma}_{th}} \left[\frac{1}{1 + \frac{(\hat{\gamma}_0 - \bar{\gamma})^2}{\bar{\gamma}_{th}^2}} \right]$$

Lorentzian:

$$I_p = \begin{cases} \frac{2}{\bar{\gamma}_{th}} e^{\frac{(p + i\bar{\gamma})^2}{\bar{\gamma}_{th}^2}} \int_{(p + i\bar{\gamma})/\bar{\gamma}_{th}}^{\infty} d\xi e^{-\xi^2} & \text{Maxwellian} \\ \frac{1}{p + \bar{\gamma}_{th} + i\bar{\gamma}} & \text{Lorentzian} \end{cases} \quad \begin{matrix} (31a) \\ (31b) \end{matrix}$$

$\bar{\gamma}_{th}$ is a measure of the energy spread. I_p is comparatively

simple when $f(\hat{\gamma}_0)$ is Lorentzian, and consequently, the Lorentzian form of I_p is used in the subsequent analysis unless otherwise stated.

Equation (30) is solved to obtain the solution $A(p)$ which vanished at ∞ in the right half p -plane. The pulse amplitude $\hat{a}(v, -u_0)$ is then evaluated from $A(p)$ by the inverse Laplace transform

$$\hat{a}(v, -u_0) = \frac{e^{\frac{-i\Gamma v^2}{2}}}{2\pi i} \int_C dp e^{pv} A(p), \quad 1 > v > 0 \quad (32)$$

where C denotes the contour of the inverse Laplace transform.

The eigenvalue equation is obtained from the boundary condition

$$\hat{a}(v=1, -u_0) = 0$$

which in terms of $A(p)$ may be written

$$e^{-\frac{i\Gamma}{2}} \int_c dpe^p A(p) = 0 \quad (33)$$

A. Constant Parameter Wiggler

In a constant parameter FEL, Γ is zero. Thus, from equations (30) and (33):

$$\int_{C_\xi} d\xi \frac{e^{i\left(\frac{\eta}{2\beta}\right)^{1/3} \xi}}{\left[\xi - \delta_1 - i\left(\frac{2}{\eta\beta^2}\right)^{1/3} \left\{ e^{-i\left(\frac{\eta\beta^2}{2}\right)^{1/3} \frac{1}{\xi^2} - 1} \right\} \right]} \quad (34)$$

where

$$(1 - r + \delta) + \beta(\bar{\gamma}_{th} + i\bar{\gamma}) = i\left(\frac{\eta\beta^2}{2}\right)^{1/3} \delta_1 \quad (35)$$

$$p + \bar{\gamma}_{th} + i\bar{\gamma} = i\left(\frac{\eta}{2\beta}\right)^{1/3} \xi \quad (36)$$

and C_ξ is obtained from C through the transformation from p to ξ .

If $(\eta\beta^2)^{1/3} \ll 1$, and the exponential is approximated by

$$e^{-i\left(\frac{\eta\beta^2}{2}\right)^{1/3} \frac{1}{\xi^2} - 1} \approx -i\left(\frac{\eta\beta^2}{2}\right)^{1/3} \frac{1}{\xi^2}$$

[which corresponds to neglecting the second term within the square bracket of equation (24)], equation (34) simplifies to

$$\sum_{j=1,2,3} \frac{\xi_j e^{i\left(\frac{\eta}{2\beta}\right)^{1/3} \xi_j}}{(3\xi_j - 2\delta_1)} = 0 \quad (37)$$

where ξ_j are the roots of the cubic equation

$$\xi^3 - \delta_1 \xi^2 - 1 = 0 \quad (38)$$

Since δ_1 is complex, the roots ξ_j are complex. In the limit of a long wiggler where $(\eta/2\beta)^{1/3} \rightarrow \infty$ a root with negative imaginary part will contribute an exponentially large term to the sum. It may therefore be conjectured (and established a posteriori) that equation (37) can be satisfied for $(\eta/2\beta)^{1/3} \rightarrow \infty$ if two roots (ξ_1 and ξ_2) have equal and negative imaginary parts. The requirement for this to occur is

$$\delta_1 = \left(\frac{27}{4}\right)^{1/3} e^{-\frac{i\pi}{3}} - \left(\frac{27}{16}\right)^{1/3} \frac{(\xi_2 - \xi_1)^2}{4} e^{\frac{i\pi}{3}} \quad (39)$$

where $\xi_2 - \xi_1 = (2\beta/\eta)^{1/3} C_0 \pi$ is small and real.

Equation (37) is solved numerically, and in Figure 3, the variable $\text{Re}[(1 - r + \delta + \beta \bar{\gamma}_{th})(2/\eta\beta^2)^{1/3}]$ is plotted as a function of β/η . For small β/η , the curve follows equation (39) with $C_0 \sim 1.9$ and decreases to zero at $\beta/\eta \approx 0.065$.

B. Variable Parameter Wiggler

In a variable parameter FEL, Γ is nonzero.

It is convenient to define the new independent variable

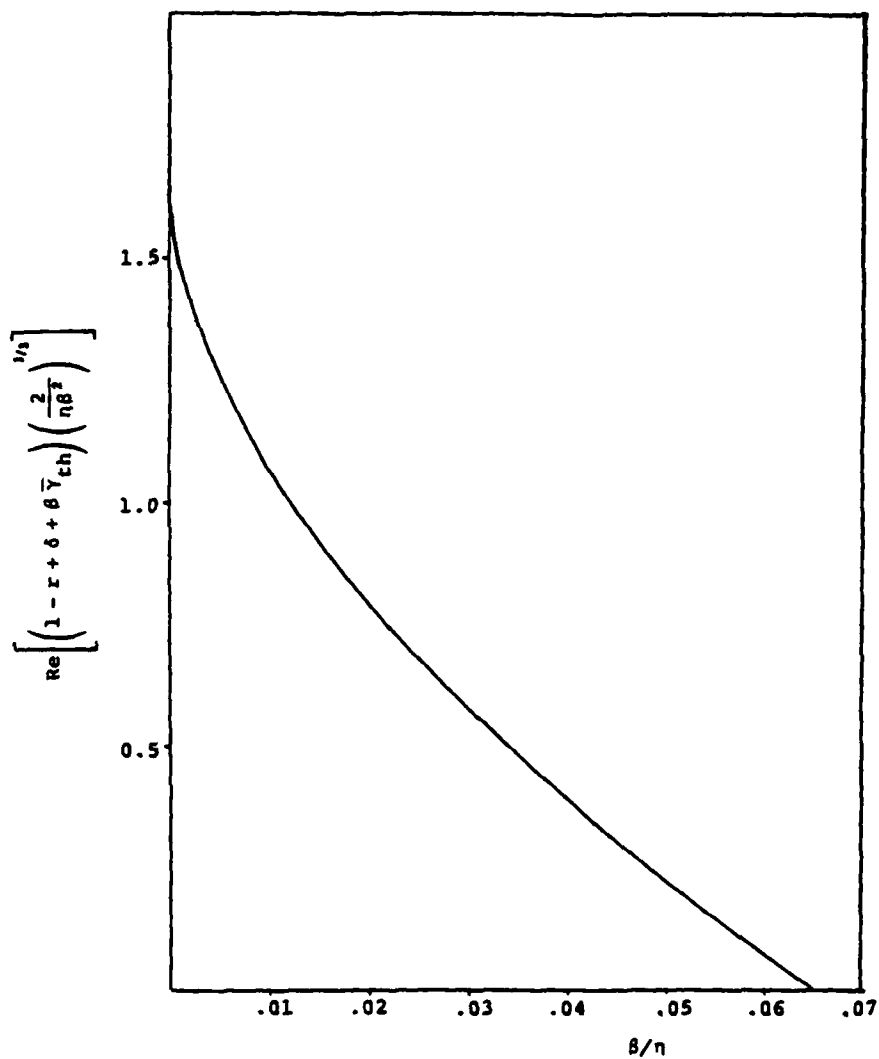


Figure 3. Constant Parameter Wiggler without Frequency Discrimination - $\text{Re}(i \delta_1)$ vs β/n

$$q = \frac{(p + \bar{\gamma}_{th} + i\bar{\gamma})}{\Gamma^{1/2}}$$

and to rewrite equation (30) as follows:

$$\frac{\partial A}{\partial q} - i q A + i \Lambda A - \frac{i}{\beta \Gamma^{1/2}} \left\{ e^{\frac{i\eta}{2\Gamma q^2}} - 1 \right\} A = \frac{a_0}{i \beta \Gamma^{1/2}} \quad (40)$$

where

$$\Lambda = \frac{(1 - r + \delta) + \beta(\bar{\gamma}_{th} + i\bar{\gamma})}{\beta \Gamma^{1/2}}$$

The solution of equation (40) which vanishes when p tends to infinity in the right half p -plane is

$$A = \frac{ia_0}{3\Gamma^{1/2}} e^{S_1(q)} \int_q^{\infty(1-i)} dq' e^{-S_1(q')}$$

where

$$S_1(q) = \frac{iq^2}{2} - i\Lambda q + \frac{i}{3\Gamma^{1/2}} \int_{\infty(1-i)}^q dq' \left\{ e^{\frac{i\eta}{2\Gamma q'^2}} - 1 \right\}$$

The eigenvalue equation is therefore given by

$$e^{-\frac{i\Gamma}{2}} \int_c^q dq e^{\Gamma^{1/2} q + S_1(q)} \int_q^{\infty(1-i)} dq' e^{-S_1(q')} = 0 \quad (41)$$

In the limit of an infinitely long wiggler where $\Gamma \rightarrow \infty$, the integral in equation (41) may be evaluated by

deforming the contour C_q towards the $\text{Im } q$ axis. The contour approaches a saddle point at $q \sim \Lambda + i \Gamma^{1/2}$, and if $\text{Re } \Lambda > 0$, the contribution of this saddle point is exponentially $\sim e^{\Lambda \Gamma^{1/2}}$ large. This implies that equation (41) can be satisfied only if

$$\int_{-\infty(1-i)}^{\infty(1-i)} dq e^{-S_1(q)} = 0 \quad (42)$$

where the contour passes above the origin. Equation (42) determines the eigenvalue δ in the limit $\Lambda \Gamma^{1/2} \rightarrow \infty$.

If the exponential in $S_1(q)$ is again approximated by

$$e^{\frac{i\eta}{2\Gamma q^2}} - 1 \approx \frac{i\eta}{2\Gamma q^2} + \dots$$

equation (42) reduces to:

$$\int_{-\infty(1-i)}^{\infty(1-i)} dq e^{-\frac{iq^2}{2} + i\Lambda q - \frac{\alpha}{q}} = 0 \quad (43)$$

where

$$\alpha = \frac{\eta}{2\beta\Gamma^{3/2}}$$

For $\alpha \rightarrow 0$, equation (43) may be approximated by

$$e^{i\left(\frac{\Lambda^2}{2} + \frac{\pi}{4}\right)} \approx \sqrt{2\pi} \alpha, \quad \text{Im}\left(-\frac{e^{\frac{i\pi}{4}}\Lambda}{\sqrt{2}}\right) > 0$$

Equation (43) determines Λ as a function of α and it is readily verified that $\Lambda(\alpha)$ is a solution of the differential equation

$$\frac{d^2\Lambda}{d\alpha^2} + i\left(\frac{d\Lambda}{d\alpha}\right)^2 \left\{ \Lambda + \alpha \frac{d\Lambda}{d\alpha} \right\} + \frac{1}{\alpha} = 0 \quad (44)$$

For $\alpha \gg 1$, a solution of equation (44) is given approximately by

$$\Lambda \approx \left(\frac{27}{4}\right)^{1/3} e^{i\frac{\pi}{6}} \alpha^{1/3} + C_1 \alpha^{-1/9} + i\left(\frac{4}{27}\right)^{1/3} e^{-i\frac{\pi}{6}} \alpha^{-1/3} \quad (45)$$

where C_1 is a constant to be determined.

Equation (43) is solved numerically, and in Figure 4, the variable $\text{Re}[(1 - r + \delta + \beta \bar{\gamma}_{\text{th}})(2/\eta\beta^2)^{1/3}]$ is plotted as a function of $28\Gamma^{3/2}/\eta = 1/\alpha$. For small $1/\alpha$, the curve follows equation (45) with $C_1 \approx -1.61 - i 1.94$ and decreases to zero at $\frac{1}{\alpha} \approx 1.42$.

C. Combination of Constant and Variable Parameter Wiggler

In the case of a magnetic wiggler with a constant parameter section at $v_1 > v > 0$ and a variable parameter section at $1 > v > v_1$, the eigenmode equation may be obtained by an extension of the analysis previously described.

Thus, in the constant parameter section $v_1 > v > 0$, the pulse amplitude is [equation (32)]:

$$\hat{a}(v, -u_0) = a(0, -u_0) \sum_{j=1,2,3} \frac{q_j e^{(q_j - \epsilon) \Gamma^{1/2} v}}{(3q_j - 2\Lambda)}$$

$$v_1 > v > 0$$

(46)

where $\epsilon = (\bar{\gamma}_{th} + i \bar{\gamma}) / \Gamma^{1/2}$

and q_j are the roots of the cubic $q^3 - q^2 \Lambda + i \alpha = 0$.

In the variable parameter section $1 > v > v_1$, the relevant equation for $\langle e^{-i \psi(v,u)} \rangle$ is:

$$\begin{aligned} \langle e^{-i \psi(v,u)} \rangle &= e^{i \Gamma \frac{(v - v_1)^2}{2}} \\ &= \frac{1}{2} \int_0^{v_1} dv' (v_1 - v') I(v - v') \hat{a}(v', u) \\ &+ \frac{1}{2} (v - v_1) \int_0^{v_1} dv' I(v - v') \hat{a}(v', u) \\ &+ \frac{1}{2} \int_{v_1}^v dv' (v - v') I(v - v') \hat{a}(v', u) e^{i \Gamma \frac{(v' - v_1)^2}{2}} \end{aligned} \quad (47)$$

The corresponding equation for A is:

$$\begin{aligned}
 \frac{\partial A}{\partial q} - iqA + i\Lambda A & \\
 - \frac{i}{\beta\Gamma^{1/2}} \left(e^{i\eta/2\Gamma q^2} - 1 \right) A & \\
 = - \frac{i\hat{a}(v_1, -u_0)}{\Gamma^{1/2}} + \frac{2iq^2}{\beta\Gamma} \left(e^{i\eta/2\Gamma q^2} - 1 \right) \left(\frac{b_1(v_1)}{q} + \frac{b_2(v_1)}{q^2} \right) &
 \end{aligned}
 \tag{48}$$

where

$$b_1(v_1) = \frac{\Gamma}{2} \int_0^{v_1} dv' (v_1 - v') \hat{a}(v', -u_0) e^{-(\bar{\gamma}_{th} + i\bar{\gamma})(v_1 - v')}
 \tag{49a}$$

$$b_2(v_1) = \frac{\Gamma^{1/2}}{2} \int_0^{v_1} dv' \hat{a}(v', -u_0) e^{-(\bar{\gamma}_{th} + i\bar{\gamma})(v_1 - v')}
 \tag{49b}$$

The eigenvalue equation analogous to equation (43)

is:

$$\int_{-\infty(1-i)}^{\infty(1-i)} dq e^{-iq^2/2 + i\Lambda q - \alpha/q}$$

$$\left[\hat{a}(v_1, -u_0) - 2i\alpha \left\{ \frac{b_1(v_1)}{q} + \frac{b_2(v_1)}{q^2} \right\} \right]$$

$$= 0 \quad (50)$$

This equation determines Λ as a function of α and $\Gamma^{1/2} v_1$. Equation (50) is solved numerically, and in Figure 4 the variable $\text{Re} \left[(1-r+\delta+\beta \bar{v}_{th}) (2/\eta\beta^2)^{1/3} \right]$ is plotted as a function of $2\beta\Gamma^{3/2}/\eta = 1/\alpha$ for different values of $\Gamma^{1/2} v_1$.

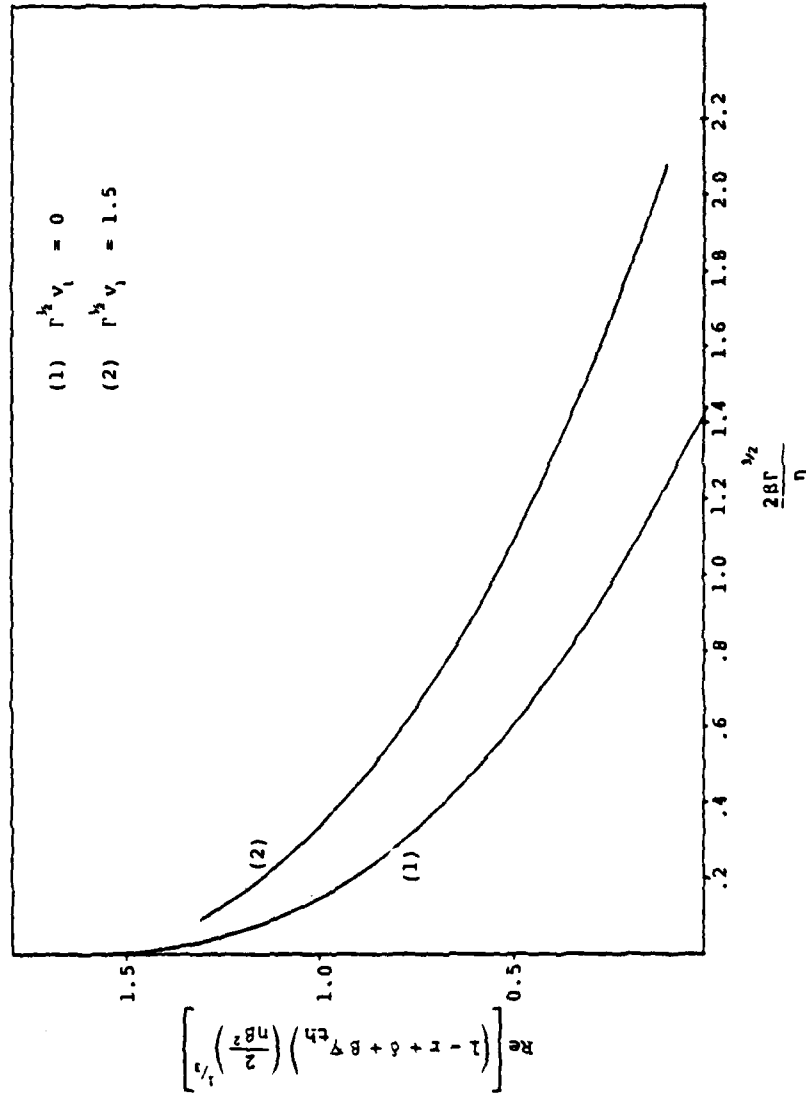


Figure 4. Constant and Variable Parameter Wiggler without Frequency Discrimination - $\text{Re}(i\delta_1)$ vs $2B\Gamma^{3/2}/\eta$

IV. LINEAR THEORY - WITH FREQUENCY DISCRIMINATION

With frequency discrimination, the pulse amplitude equation (eg. 23) is

$$\begin{aligned}
 & (1 + \delta + \dots) \left[\frac{1}{v} \frac{\partial}{\partial v} + 1 \right] \left\{ \hat{a} - \beta \frac{\partial \hat{a}}{\partial v} \right. \\
 & \qquad \qquad \qquad \left. + \frac{\beta^2}{2} \frac{\partial^2}{\partial v^2} \hat{a} + \dots \right\} \\
 & = r \left[\hat{a} + \Delta a \right]
 \end{aligned} \tag{51}$$

where δ is defined in Section III and $\beta \ll 1$.

The analysis will be restricted to the case of $v = \frac{1}{\beta}$. This choice is motivated by the consideration that Equation (22) indicates that the filtered pulse is effectively an average of the preceding $\Delta v = \frac{1}{v}$, i.e., it corresponds to an effective retardation of the light pulse by $\frac{1}{v}$ relative to the electron beam, while β represents a forward shift of the light pulse. Unless the two are nearly equal, the electron pulse and photon will separate after many passes. Numerical work has verified that this choice is approximately optimal.

Equation (51) then simplifies to

$$(1 - r + \delta) \hat{a} - \frac{\beta^2}{2} \frac{\partial^2}{\partial v^2} \hat{a} \approx \frac{i\eta}{u_0} \int_{-u_0}^0 du \langle e^{-i\psi(v,u)} \rangle \quad (52)$$

$1 > v > 0$.

When $v < 0$ or $v > 1$,

$$(1 - r + \delta) \hat{a} - \frac{\beta^2}{2} \frac{\partial^2 \hat{a}}{\partial v^2} = 0 .$$

The solution satisfying the boundary conditions $\hat{a} \rightarrow 0, v \rightarrow \pm\infty$ are:

$$\hat{a} = \begin{cases} e^{\frac{\{2(1-r+\delta)\}^{\frac{1}{2}} v}{\beta}} & v < 0 \\ e^{-\frac{\{2(1-r+\delta)\}^{\frac{1}{2}} v}{\beta}} & v > 1 \end{cases}$$

where $\text{Re}(1 - r + \delta) > 0$. At $v = 0$ and $v = 1$, \hat{a} and $\partial\hat{a}/\partial v$ are continuous.

The procedure of Section III may now be followed to obtain the eigenvalue equation. Thus, Equation (52) is Laplace transformed, and the equation for $A(p)$ in the limit of short electron beams is:

$$\begin{aligned}
 & - \left[p^2 - i\Gamma + 2i\Gamma \frac{\partial}{\partial p} p - \Gamma^2 \frac{\partial^2}{\partial p^2} \right] A \\
 & + \frac{2(1-r+\delta)}{\beta^2} A - \frac{2}{\beta^2} A \left\{ e^{-\frac{i\eta}{2} \frac{\partial I}{\partial p}} - 1 \right\} \\
 & = - \left\{ \frac{\partial \hat{a}}{\partial v} + p \hat{a} \right\}_{v=0} \quad (53) \\
 & = - \left\{ p + \frac{\{2(1-r+\delta)\}^{\frac{1}{2}}}{\beta} \right\} \hat{a}(0, -u_0) .
 \end{aligned}$$

Equation (53) is solved to obtain the solution $A(p)$ which vanishes in the right half p -plane. The pulse amplitude $a(v, -u_0)$ is then evaluated from $A(p)$ by the inverse Laplace transform

$$\hat{a} = \frac{e^{-i\Gamma_0 v^2/2}}{2\pi i} \int_C dp e^{pv} A(p), \quad 1 > v > 0$$

and the eigenvalue equation is determined by the boundary condition at $v = 1$.

A. Constant Parameter Wiggler

For a constant parameter FEL where $\Gamma = 0$, the pulse amplitude $\hat{a}(v, -u_0)$ is:

$$\hat{a}(v, -u_0) = \frac{\hat{a}(0, -u_0)}{2\pi i} \int_{C_\xi} d\xi e^{\frac{(n/\beta^2)^{1/2} (\xi - \delta_3) v}{(\xi - \delta_3 + \delta_2^{1/2})}} \left[\frac{2}{(\xi - \delta_3)^2 - \delta_2 + (n\beta^2)^{1/2}} \left(e^{i(n\beta^2)^{1/2}/2\xi^2} - 1 \right) \right]$$

(54)

where

$$p + \bar{\gamma}_{th} + i\bar{\gamma} = \left(\frac{n}{\beta^2} \right)^{1/2} \xi$$

$$\delta_2 = \frac{2(1-r+\delta)}{(n\beta^2)^{1/2}}$$

$$\delta_3 = \left(\frac{\beta^2}{n} \right)^{1/2} (\bar{\gamma}_{th} + i\bar{\gamma})$$

If $(n\beta^2)^{1/2} \ll 1$ and the exponential is approximated by

$$e^{i(n\beta^2)^{1/2}/2\xi^2} - 1 \approx i(n\beta^2)^{1/2}/2\xi^2 \quad ,$$

Equation (54) simplifies to

$$\hat{a}(v, -u_0) = \frac{\hat{a}(0, -u_0)}{2} \sum_{j=1,2,3,4} e^{\frac{(n/\beta^2)^{1/2} (\xi_j - \delta_3) v}{\xi_j (\xi_j - \delta_3 + \delta_2^{1/2})}} \frac{1}{[(\xi_j - \delta_3) (2\xi_j - \delta_3) - \delta_2]} \quad (55)$$

where ξ_j are the roots of the quartic

$$\xi^2 (\xi - \delta_3)^2 - \xi^2 \delta_2 + i = 0 \quad . \quad (56)$$

The continuity of \hat{a} and $\partial\hat{a}/\partial v$ at $v = 1$ is satisfied if

$$\sum \frac{e^{\frac{(n/\beta^2)^{1/2} \xi_j (\xi_j - \delta_3 + \delta_2^{1/2})}{\xi_j (\xi_j - \delta_3 + \delta_2^{1/2})}}}{[(\xi_j - \delta_3) (2\xi_j - \delta_3) - \delta_2]} = 0 \quad . \quad (57)$$

Equation (57) is the eigenvalue equation.

If $\delta_3 = 0$ (no thermal spread), the roots of the quartic are

$$\xi^2 = \frac{1}{2} \left[\delta_2 \pm \sqrt{\delta_2^2 - 4i} \right]$$

As in Section III, it may be conjectured that in the limit $(\eta/\beta^2)^{1/2} \rightarrow \infty$, Equation (57) can be satisfied if two roots (ξ_1 and ξ_2) of the quartic have equal positive real parts. The requirement for this to occur is

$$\delta_2 = 2e^{i\pi/4} + (\xi_2 - \xi_1)^2$$

$$\xi_2 - \xi_1 = iC_2\pi \left(\frac{\beta^2}{\eta} \right)^{1/2} \quad (58)$$

where $\xi_2 - \xi_1 = iC_2\pi(\beta^2/\eta)^{1/2}$ is small and imaginary.

Equation (57) is solved numerically and in Figure 5, the variable $\text{Re} [(1-r+\delta)(4/\eta\beta^2)^{1/2}]$ is plotted as a function of $\beta/\eta^{1/2}$ for different values of $\bar{\gamma}_{th}$ ($\bar{\gamma} = 0$). When $\bar{\gamma}_{th} = 0$, the curve follows Equation (58) for very small $\beta/\eta^{1/2}$, and decreases to zero at $\beta/\eta^{1/2} \approx .118$. As $\bar{\gamma}_{th}$ increases from zero, the curve falls more rapidly and is zero at smaller values of $\beta/\eta^{1/2}$.

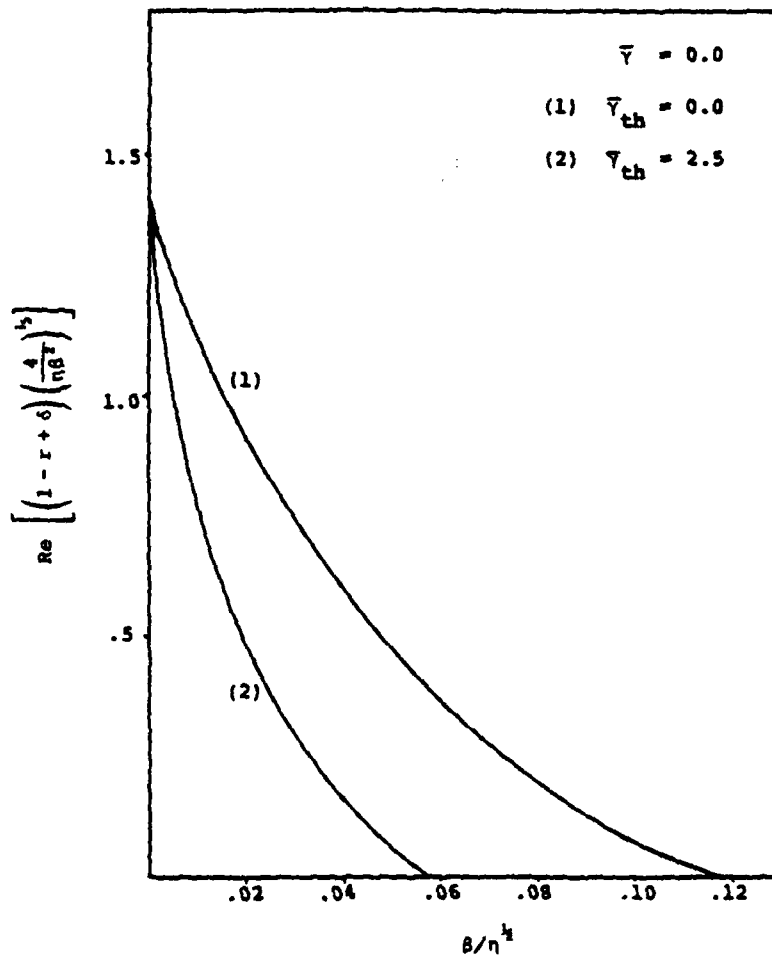


Figure 5. Constant Parameter Wiggler with Frequency Discrimination - $\text{Re}(\delta_2)$ vs $\beta/n^{1/2}$

The effect on linear gain of finite values of $\bar{\gamma}$ is shown in Figure 6.

B. Variable Parameter Wiggler

For a variable parameter FEL where $\Gamma \neq 0$, it is convenient to introduce new independent and dependent variables:

$$q = \frac{p + \bar{\gamma}_{th} + i\bar{\gamma}}{\Gamma^{\frac{1}{2}}}$$

$$B = A e^{-ip^2/2\Gamma}$$

Equation (53) can then be rewritten as follows:

$$\begin{aligned} \frac{\partial^2 B}{\partial q^2} + \Lambda_1^2 B - \frac{2}{\beta^2 \Gamma} \left\{ e^{\frac{i\eta}{2\Gamma q^2}} - 1 \right\} B \\ = - \frac{1}{\Gamma^{\frac{1}{2}}} (q - \epsilon + \Lambda_1) \hat{a}(0, -u_0) e^{-i \frac{(q - \epsilon)^2}{2}} \\ \equiv G(q) \end{aligned} \quad (59)$$

where

$$\Lambda_1^2 = \frac{2(1-r+\delta)}{\beta^2 \Gamma}$$

$$\epsilon = \frac{\bar{\gamma}_{th} + i\bar{\gamma}}{\Gamma^{\frac{1}{2}}}$$

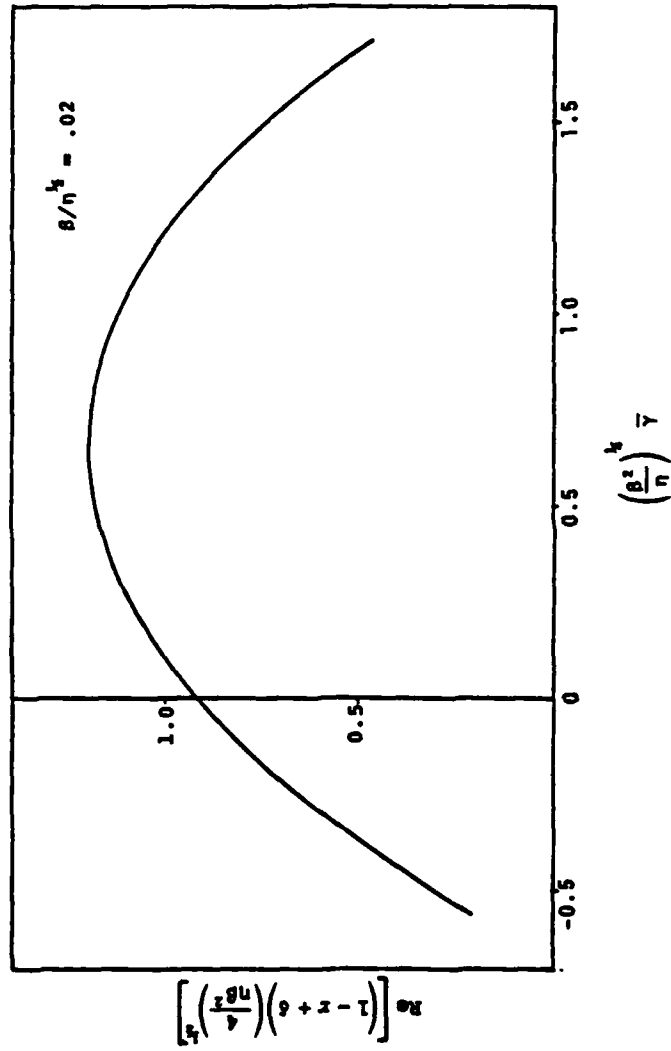


Figure 6. Constant Parameter Wiggler with Frequency Discrimination -
 $\text{Re}(\delta_2)$ vs $(\beta^2/\eta)^{1/4} \bar{\gamma}$

If the exponential is approximated by

$$e^{i\eta/2\Gamma q^2} - 1 \approx \frac{i\eta}{2\Gamma q^2} + \dots,$$

Equation (59) simplifies to:

$$\frac{\partial^2 B}{\partial q^2} + \Lambda_1^2 B - \frac{i\alpha_1}{q^2} B = G(q) \quad (60)$$

where

$$\alpha_1 = \frac{\eta}{\beta^2 \Gamma^2}.$$

Numerical integration of the equation without expansion of the exponential indicates that as expected for $\eta/2q^2\Gamma < 1$, the growth rates are not altered substantially.

The solution of Equation (60) is:

$$B = \frac{\pi q^{\frac{1}{2}}}{4i \Lambda_1^{\frac{1}{2}}} \left[H_{\mu}^{(2)}(\Lambda_1 q) \int_q^{\infty(1-i)} dq' H_{\mu}^{(1)}(\Lambda_1 q') q'^{\frac{1}{2}} G(q') - H_{\mu}^{(1)}(\Lambda_1 q) \int_q^{\infty(1-i)} dq' H_{\mu}^{(2)}(\Lambda_1 q') q'^{\frac{1}{2}} G(q') \right] \quad (61)$$

where $H_{\mu}^{(1)}$ and $H_{\mu}^{(2)}$ are Hankel functions of order

$$\mu = (\frac{1}{2} + i\alpha_1)^{\frac{1}{2}} .$$

As p tends to infinity in the right half of the p -plane, $B \rightarrow \frac{1}{p} \exp(-ip^2/2\Gamma)$, and consequently $A(p) = B \exp(ip^2/2\Gamma)$, tends to zero.

The pulse amplitude is obtained from the inverse Laplace transform

$$\hat{a}(v, -u_0) = \frac{e^{-i\Gamma v^2/2}}{2\pi i} \int_{C_q} dq e^{\Gamma^{\frac{1}{2}}(q-\epsilon)v + i \frac{(q-\epsilon)^2}{2}} B(q)$$

$$1 > v > 0 \quad . (62)$$

In the limit of an infinitely long wiggler where $\Gamma \rightarrow \infty$, the integral in Equation (62) may be evaluated by deforming the contour C_q towards the $\text{Im } q$ axis. The integrand is

$$\sim \frac{(2\pi)^{\frac{1}{2}}}{4i\Lambda_1} e^{\left\{ \Gamma^{\frac{1}{2}}v(q-\epsilon) + i\frac{(q-\epsilon)^2}{2} - i\left(\Lambda_1 q - \frac{\mu\pi}{2} - \frac{\pi}{2}\right) \right\}}$$

$$\int_q^{\infty(1-i)} dq' H_{\mu}^{(1)}(\Lambda_1 q') q'^{\frac{1}{2}} G(q')$$

$$|\Lambda_1 q| \gg 1, \text{Im}(\Lambda_1 q) > 0$$

The contour approaches a saddle point at $q-\epsilon \sim i v \Gamma^{\frac{1}{2}} + \Lambda_1$, and the contribution of this saddle point increases exponentially $\sim \exp(\Lambda_1 \Gamma^{\frac{1}{2}}v)$. However, if $\hat{a}(v, -u_0)$, ($v < 1$) has this behavior, it will not be possible to match \hat{a} to the exponentially decaying solution $\sim \exp(-\Lambda_1 \Gamma^{\frac{1}{2}}v)$, ($v > 1$) in order to satisfy the continuity of \hat{a} and $\partial\hat{a}/\partial v$ at $v = 1$. This implies that the boundary condition at $v = 1$ can be satisfied in the limit $\Lambda_1 \Gamma^{\frac{1}{2}} \rightarrow \infty$ only if

$$\int_{-\infty(1-i)}^{\infty(1-i)} dq H_{\mu}^{(1)}(\Lambda_1 q) q^{\frac{1}{2}} G(q) = 0 \quad (63)$$

where the contour passes above the origin. Equation (63) is the eigenvalue equation in the limit $\Lambda_1 \Gamma^{\frac{1}{2}} \rightarrow \infty$.

If $\epsilon = 0$, the integral can be expressed in terms of Whittaker functions, and the eigenvalue equation is then given by

$$\int_{-\infty}^{\infty} d\xi H_{\mu}^{(1)}(2\sqrt{z_0}\xi) \left[\xi^{\frac{3}{2}} + i\sqrt{z_0}\xi^{\frac{1}{2}} \right] e^{-\xi^2}$$

$$= e^{i\frac{\pi}{4} - i\frac{\mu\pi}{2} - \frac{z_0}{2}} \left[z_0^{-\frac{1}{2}} W_{\frac{3}{4}, \frac{\mu}{2}}(z_0) + W_{\frac{1}{4}, \frac{\mu}{2}}(z_0) \right] \quad (64)$$

$$= 0$$

where

$$z_0 \equiv \frac{-i\Lambda_1^2}{2}$$

and the contour passes above the origin.

In the limit $|z_0| \sim |\frac{\mu}{2}| \gg 1$,

$$\begin{aligned}
 W_{\frac{1}{4}, \frac{\mu}{2}}(z_0) &\longrightarrow \frac{z_0^{1/3}}{\pi^{1/2}} K_{\frac{\mu}{2}}(z_0/2) \\
 &\longrightarrow (2\pi)^{1/2} e^{i\pi\mu/4} (2z_0)^{1/6} \\
 &\quad \text{Ai} \left((2z_0)^{-1/3} (z_0 + i\mu) \right)
 \end{aligned}$$

where $K_{\mu/2}$ is the modified Bessel function of order $\mu/2$ and Ai is the Airy function. Thus, the solutions of Equation (64) are given approximately by the zeros of the Airy function. For the most unstable solution

$$\frac{(z_0 + i\mu)}{(2z_0)^{1/3}} \approx -2.3$$

and therefore

$$\delta_2 \approx 2 e^{i\frac{\pi}{4}} \left[1 - (2.3) \left(\frac{2}{\alpha_1} \right)^{1/3} e^{i\frac{\pi}{6}} + \dots \right] \quad (65)$$

In the limit $\{|Z_0|, \alpha_1\} \ll 1$, Equation (64) may be approximated by

$$2 + i\alpha_1 \log Z_0 + i \frac{\alpha_1 \pi^{1/2}}{2Z_0^{1/2}} \approx 0$$

and therefore

$$\delta_2 \approx \frac{2\alpha_1^{3/2} \pi}{8} \left[-i - \alpha_1 \left\{ \log \left(\frac{\pi\alpha_1^2}{16} \right) + i(2N+1)\pi \right\} \right] \quad (66)$$

Equation (64) is solved numerically, and in Figure 7, the variable $\text{Re} [(1-r+\delta) (4/\eta\beta^2)^{1/2}]$ is plotted as a function of $\beta\Gamma/\eta^{1/2}$. As $\beta\Gamma/\eta^{1/2}$ increases from zero, the curve decreases from $(2)^{1/2}$ and asymptotes to zero as $\beta\Gamma/\eta^{1/2} \rightarrow \infty$.

The effect on linear gain of finite values of $\bar{\gamma}_{th}$ and $\bar{\gamma}$ has been calculated by numerical solution of Equation (63), and the results are displayed in Figures 7, 8 and 9.

A more exact eigenvalue equation can be obtained by replacing the Hankel function $H_\mu^{(1)}$ in Equation (63) with the appropriate homogeneous solution of Equation (59), namely

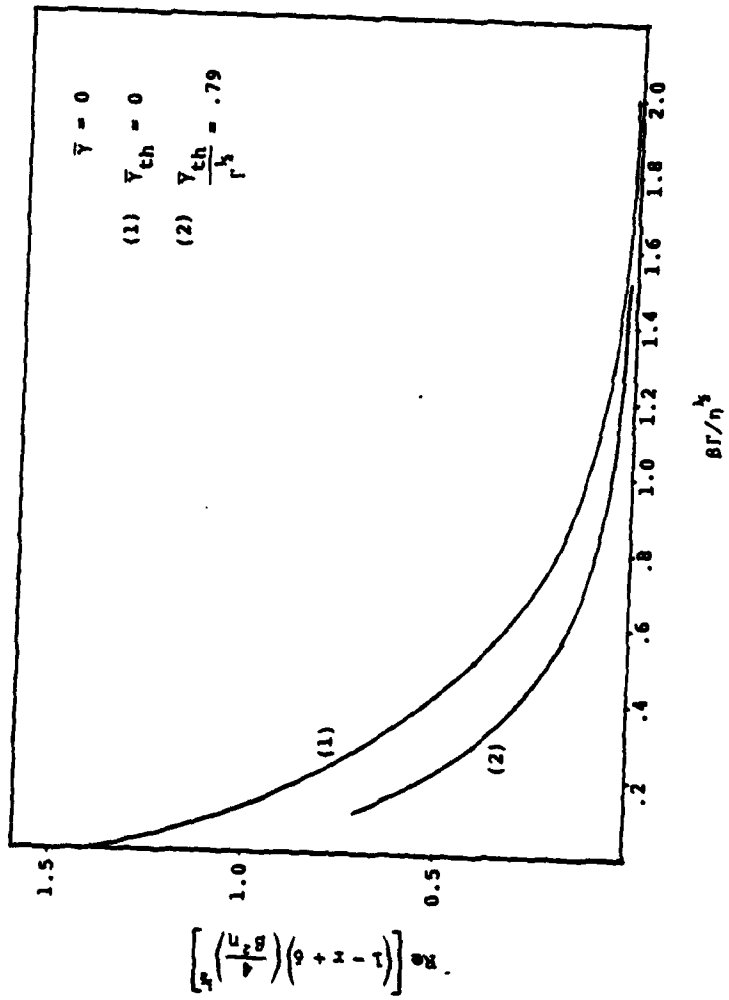


Figure 7. Variable Parameter Wiggler with Frequency Discrimination - $Re(\delta_2)$ vs $\beta\Gamma/\eta^2$

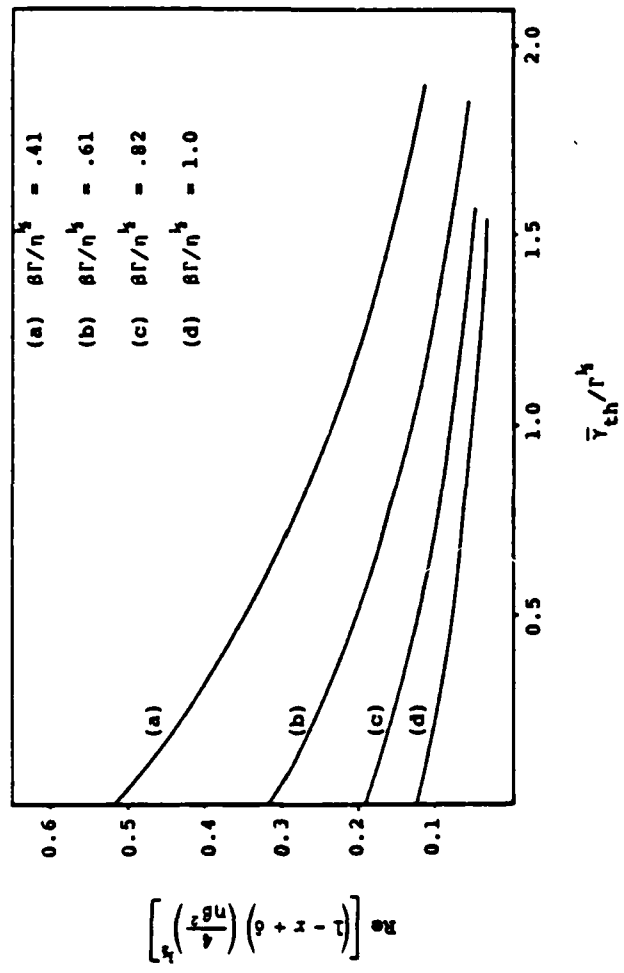


Figure 8. Variable Parameter Wiggler with Frequency Discrimination - $\text{Re}(\delta_2)$ vs $\bar{\gamma}_{th}/\Gamma^{1/2}$

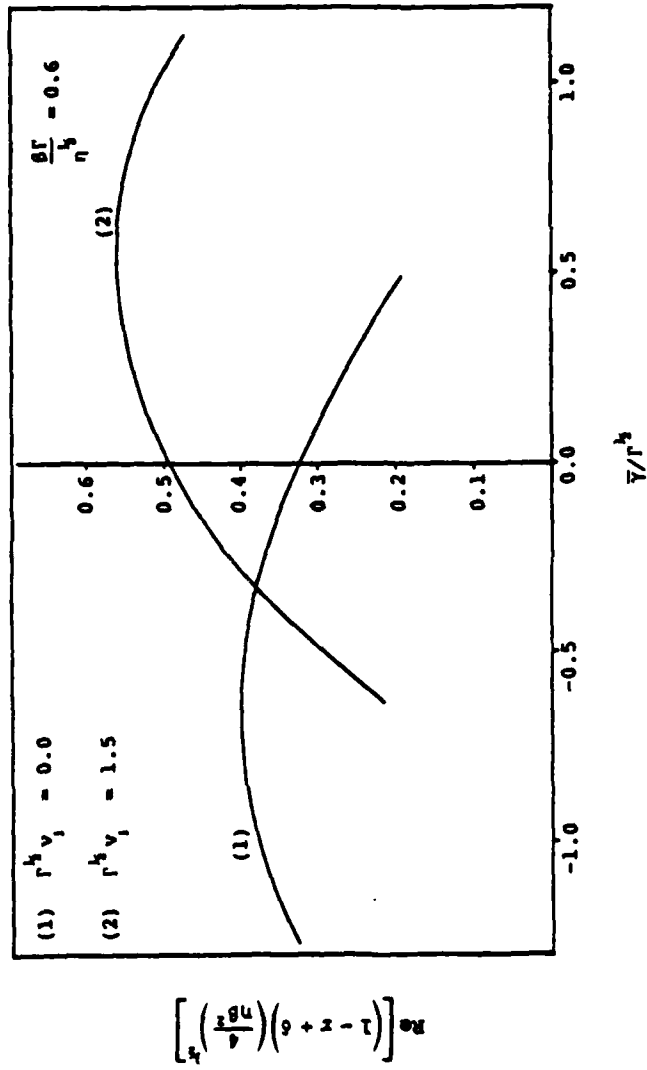


Figure 9. Variable Parameter Wiggler with Frequency Discrimination - $\text{Re}(\delta_2)$ vs $\sqrt{\Gamma^2}$

the solution B_h^+ which asymptotes to $\sim \exp(i\Lambda_1 q)$ for $|q| \gg 1$:

$$\int_{-\infty(1-i)}^{\infty(1-i)} dq B_h^+(q) G(q) = 0 \quad . \quad (67)$$

From numerical solutions of this equation, the linear gain curves relating $\text{Re} [(1-r+\delta) (4/n\beta^2)^{1/2}]$ to $\beta\Gamma/n^{1/2}$ is plotted in Figure 12 for a value of $n/\Gamma = 1$ ($\bar{\gamma}_{th} = 0$ and $\bar{\gamma} = 0$). An additional parameter n/Γ is necessary to completely describe the linear gain characteristics. However, the difference in the eigenvalue solutions between the more exact and approximate eigenvalue equations is small when $n/\Gamma \leq 1$.

C. Combination of Constant and Variable Parameter Wiggler

In the constant parameter section $v_1 > v > 0$, the pulse amplitude \hat{a} is given by Equation (55) which may be rewritten in the form:

$$\hat{a}(v, -u_0) = \frac{\hat{a}(0, -u_0)}{2} \sum_{j=1,2,3,4} e^{(q_j - \epsilon) \Gamma^{1/2} v} \frac{q_j (q_j - \epsilon + \Lambda_1)}{[(q_j - \epsilon) (2q_j - \epsilon) - \Lambda_1^2]} \quad (68)$$

where q_j are the roots of

$$q^2(q-\epsilon)^2 - \Lambda_1^2 q^2 + i\alpha_1 = 0 \quad .$$

In the variable parameter section $1 > v > v_1$, Equation (47) is applicable and the corresponding equation for B is:

$$\begin{aligned} \frac{\partial^2 B}{\partial q^2} + \Lambda_1^2 B \\ - \frac{2}{\beta^2 \Gamma} \left\{ e^{\frac{i\eta}{2\Gamma q^2}} - 1 \right\} B \\ = \frac{1}{\Gamma^{1/2}} \left[G_1(q) + G_2(q) \right] e^{-\frac{i}{2}(q-\epsilon)^2} \end{aligned} \quad (69)$$

where

$$G_1(q) = - \left[\frac{1}{\Gamma^{1/2}} \frac{\partial}{\partial v_1} \hat{a}(v_1, -u_0) + (q-\epsilon) \hat{a}(v_1, -u_0) \right]$$

$$G_2(q) = \frac{4q^2}{\beta^2 \Gamma} \left(e^{i\eta/2\Gamma q^2} - 1 \right) \left(\frac{b_1(v_1)}{q} + \frac{b_2(v_1)}{q^2} \right) \quad ,$$

$b_1(v_1)$ and $b_2(v_1)$ are defined by Equations (49a) and (49b).

Thus, the eigenvalue equation analogous to Equation (61) in the limit $\Lambda_1 \Gamma^{1/2} (1-v_1) \rightarrow \infty$ is

$$\int_{-\infty(1-i)}^{\infty(1-i)} dq H_{\mu}^{(1)}(\Lambda_1 q) q^{1/2} e^{-\frac{i}{2}(q-\epsilon)^2}$$

$$\left[G_1(q) + 2i\alpha_1 \left\{ \frac{b_1(v_1)}{q} + \frac{b_2(v_2)}{q^2} \right\} \right] = 0 \quad (70)$$

When $\epsilon = 0$, the integral can be expressed in terms of Whittaker functions.

Equation (70) determines Λ_1 as a function of α_1 , $\Gamma^{1/2} v_1$, and ϵ .

Equation (70) is solved numerically and in Figure 10, the curves relating $\text{Re}[(1-r+\delta)(4/\eta\beta^2)^{1/2}]$ to $\beta\Gamma/\eta^{1/2}$ are plotted for different values of $\Gamma^{1/2} v_1$.

V. SUMMARY AND DISCUSSION

A Summary of Linear Gain Results

In this section, the linear gain characteristics per pass of the short pulse FEL for the most unstable mode is summarized. However, before presenting this summary, the relationship between the symbols introduced in the linear eigenmode analysis and the physical variables of the FEL will be recapitulated.

δ	Gain per pass, i.e., the amplitude of the EM pulse on pass $n+1$ is e^δ times the amplitude after the n th pass
k_w	Wiggler wave number
$k_w A_w \equiv B_w$	Wiggler magnetic field amplitude
L	Wiggler length
ω_s, k_s	Design frequency and wave number of the electromagnetic pulse
r	Fractional reduction per round trip of pulse amplitude due to losses on reflection at the mirrors

$$\Omega_w = eB_w/mc$$

$$\mu^2 = 1 + \Omega_w^2/k_w^2 c^2$$

$$\gamma_r = (k_s/2k_w)^{1/2} \mu$$

$$\eta = 8\pi e^2 N_T L^2 \Omega_w^2 / \gamma_r mc^4 \mu^2 k_w$$

N_T

Resonant energy in units of mc^2

Total number of electrons, $\int n dl$, in the beam per unit area. Note that the beam is considered to be finite and uniform over a length $l \ll L/2\gamma_r^2$.

$$\beta = \frac{k_s c}{k_w L} \Delta T$$

ΔT is the pass-to-pass temporal advance of the electromagnetic pulse relative to the electron beam on entry into the wiggler

$$\Gamma = \frac{2k_w L}{r} \Delta \gamma_r$$

$\Delta \gamma_r$ is the change in γ of electrons freely accelerated by the accelerating potential

$$\nu = \frac{k_w L}{k_w c} \Delta \omega$$

$\Delta \omega$ is the frequency half width of the frequency discriminator, i.e., the effective reflection coefficient is $r(\omega) \sim r/[1+i(\omega-\omega_s)/\Delta\omega]$

$$\bar{\gamma} = \frac{2k_w L}{\gamma_r} | \langle \gamma \rangle - \gamma_r |$$

$\langle \gamma \rangle - \gamma_r$ is the difference between the mean energy of the beam and the resonant energy

$$\bar{\gamma}_{th} = \frac{2k_w L}{\gamma_r} \gamma_{th}$$

γ_{th} is the mean energy spread of the electron beam

ν_1

Fractional length of the initial constant parameter section of a variable parameter wiggler.

1. No Frequency Discrimination

For an FEL without frequency discrimination, the linear gain per pass $\text{Re } \delta$ is conveniently expressed in terms of the dimensionless variable

$$\text{Re}(i\delta_1) = \text{Re} \left[\left(1 - r + \delta + \beta \bar{\gamma}_{\text{th}} \right) \left(\frac{2}{\eta \beta^2} \right)^{1/3} \right] .$$

Figure 3 displays a plot of $\text{Re}(i\delta_1)$ as a function of the parameter β/η , obtained from a numerical solution of the eigenvalue Equation (37) for a constant parameter wiggler. $\text{Re}(i\delta_1)$ is zero at $\beta/\eta = 0.065$ and increases in magnitude as β/η decreases. In the limit of a very long wiggler where $\beta/\eta \rightarrow 0$ while $\beta^2 \eta$ remains finite, the linear gain is

$$\text{Re}(1 - r + \delta + \beta \bar{\gamma}_{\text{th}}) \rightarrow \frac{3^{3/2}}{4} (\eta \beta^2)^{1/3} . \quad (71)$$

In Figure 4, $\text{Re}(i\delta_1)$ is plotted as function of $2\beta\Gamma^{3/2}/\eta$ for a variable parameter wiggler. The graph is obtained from a numerical solution of Equation (43). $\text{Re}(i\delta_1)$ is zero at $2\beta\Gamma^{3/2}/\eta \approx 1.42$, and increases in magnitude as $2\beta\Gamma^{3/2}/\eta$ decreases. In the limit of $2\beta\Gamma^{3/2}/\eta \rightarrow 0$, the linear gain is

$$\text{Re}(1 - r + \delta + \beta \bar{\gamma}_{\text{th}}) \rightarrow \frac{3^{3/2}}{4} (\eta \beta^2)^{1/3} . \quad (72)$$

The linear gain of a variable parameter wiggler can be increased by the addition of a constant parameter wiggler section at the front. In Figure 4, the corresponding curve of $\text{Re}(i\delta_1)$ as a function of $2B\Gamma^{3/2}/\eta$ is plotted for a composite constant and variable parameter wiggler. It is obtained from a numerical solution of Equation (50), assuming that the fractional length $v_1 \ll 1$ of the constant parameter section is given by $\Gamma^{1/2}v_1 = 1.5$. The enhancement of linear gain increases with $\Gamma^{1/2}v_1$, and can be particularly significant for $2B\Gamma^{3/2}/\eta \geq 1.42$.

Deviations $\bar{\gamma}$ of the mean energy of the beam from the resonant energy do not affect linear gain. However, a finite energy spread $\bar{\gamma}_{th}$ decreases linear gain by $B\bar{\gamma}_{th}$.

2. Frequency Discrimination

For a FEL with frequency discrimination ($v \equiv 1/\beta$) the linear gain per pass $\text{Re } \delta$ is conveniently expressed in terms of the dimensionless variable $\text{Re } \delta_2 = \text{Re}[(1-r+\delta)(4/\eta\beta^2)^{1/2}]$.

In Figure 5, the constant parameter linear gain curve [obtained from a numerical solution of Equation (57)] which relates $\text{Re } \delta_2$ to the parameter $\beta/\eta^{1/2}$ is plotted for different values of the energy spread $\bar{\gamma}_{th}$ (but with $\bar{\gamma} = 0$). Linear gain is possible when $\beta/\eta^{1/2}$ is below an upper limit $(\beta/\eta^{1/2})_{max}$. For a beam with $\bar{\gamma} = 0$, $(\beta/\eta^{1/2})_{max} \approx 0.118$. In the limit $\beta/\eta^{1/2} \rightarrow 0$, the linear gain is:

$$\text{Re}(1 - r + \delta) \rightarrow \left(\frac{\beta^2 \eta}{2}\right)^{\frac{1}{2}} \quad (73)$$

As $\bar{\gamma}_{\text{th}}$ increases, $(\beta/\eta^{\frac{1}{2}})_{\text{max}}$ decreases, and the magnitude of $\text{Re } \delta_2$ is reduced.

In Figure 7, the variable parameter linear gain curve [Equation (63)] which relates $\text{Re } \delta_2$ to the parameter $\beta\Gamma/\eta^{\frac{1}{2}}$ is plotted for different values of $\bar{\gamma}_{\text{th}}/\Gamma^{\frac{1}{2}}$ (but with $\bar{\gamma} = 0$). For a beam with $\bar{\gamma}_{\text{th}} = 0$

$$\text{Re}(1 - r + \delta) \rightarrow \begin{cases} (\eta\beta^2/2)^{\frac{1}{2}} & \frac{\beta\Gamma}{\eta^{\frac{1}{2}}} \rightarrow 0 \\ 0 & \frac{\beta\Gamma}{\eta^{\frac{1}{2}}} \rightarrow \infty \end{cases} \quad (74)$$

A finite energy spread $\bar{\gamma}_{\text{th}}$ reduces the magnitude of $\text{Re } \delta_2$.

In Figure 10, the linear gain curve of a composite constant and variable parameter wiggler [Equation (70)] which relates $\text{Re } \delta_2$ to $\beta\Gamma/\eta^{\frac{1}{2}}$ is plotted for different values of $\Gamma^{\frac{1}{2}} v_1$. The addition of a constant parameter section can enhance the linear gain of a variable parameter wiggler and can be of significance for $\beta\Gamma/\eta^{\frac{1}{2}} \geq 1.0$.

For a given set of FEL parameters, the linear gain is not in general a maximum at $\bar{\gamma} = 0$. The effect on the linear gain of a variation in $\bar{\gamma}$ is shown in Figure 6 for

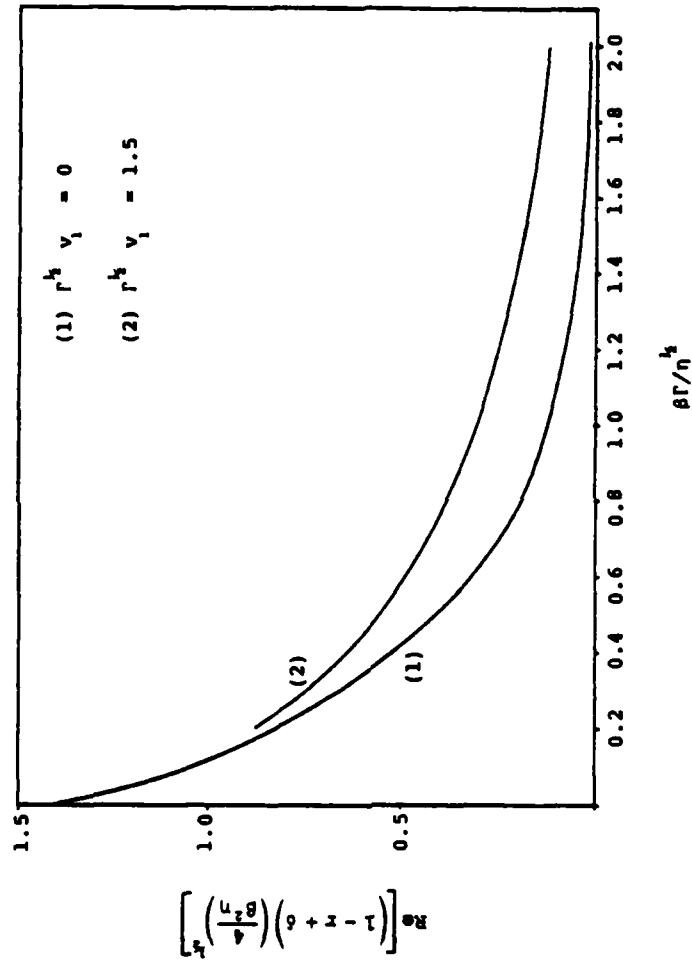


Figure 10. Constant and Variable Parameter Wiggler with Frequency Discrimination - $\text{Re}(\delta_2)$ vs $\beta \Gamma / \eta^2$

a constant parameter wiggler, and in Figure 9 for variable parameter wigglers. Some enhancement of linear gain is possible by making an appropriate non-zero choice of $\bar{\gamma}$.

These results are applicable to the special case of $\nu = 1/\beta$. The rationale for studying this case is based on the observation that frequency discrimination has an effect (proportional to $1/\nu$) which tends to retard the pulse advance, that is, it tends to reduce the effective pulse advance produced by a finite positive value of β . To avoid the EM pulse running either ahead of or lagging behind the electron pulse it is indicated that one should choose $\nu = 1/\beta$. Some numerical evidence from our simulations indicates that this choice is indeed nearly optimal.

The graphs which have so far been described are obtained from approximate eigenvalue equations derived after expansion of the exponential term

$$\left(e^{\frac{-i\eta}{2} \frac{\partial I_p}{\partial p}} - 1 \right) \approx - \frac{i\eta}{2} \frac{\partial I_p}{\partial p}$$

in Equation (30) and Equation (53).

This expansion of the exponential should be reasonable for the constant parameter wiggler when

$(\eta\beta^2)^{1/3} \ll 1$ and $(\eta\beta^2)^{1/2} \ll 1$, without and with frequency discrimination respectively. The dominant poles of the integrand in the integral of Equation (34) [Equation (54)] are then determined to a good approximation by the roots of the cubic Equation (38) [quartic Equation (56)].

In order to assess the error introduced for the variable parameter wiggler without frequency discrimination, the more exact eigenvalue Equation (42) is solved numerically, and the linear gain curve relating $\text{Re}(i\delta_1)$ to the parameter $2\beta\Gamma^{3/2}/\eta$ is plotted in Figure 11 for a value of $\eta/\Gamma = 1.0$ ($\bar{\gamma} = 0$, $\bar{\gamma}_{th} = 0$). One additional parameter, namely η/Γ , is necessary to completely describe the linear gain characteristics. Similarly, from the more exact eigenvalue Equation (67) for the variable parameter wiggler with frequency discrimination, the linear gain curve relating $\text{Re} \delta_2$ to the parameter $\beta\Gamma/\eta^{1/2}$ is plotted in Figure 12 for a value of $\eta/\Gamma = 1.0$ ($\bar{\gamma} = 0$, $\bar{\gamma}_{th} = 0$).

In both the FEL with and without frequency discrimination, the difference in eigenvalue solutions between the more exact and approximate eigenvalue equation is small when $\eta/\Gamma \leq 1$.

2. Significance of Results for FEL Design

The parameter regime of interest for variable parameter FEL's is dictated not only by the need to grow the electromagnetic pulse to a large amplitude in a finite

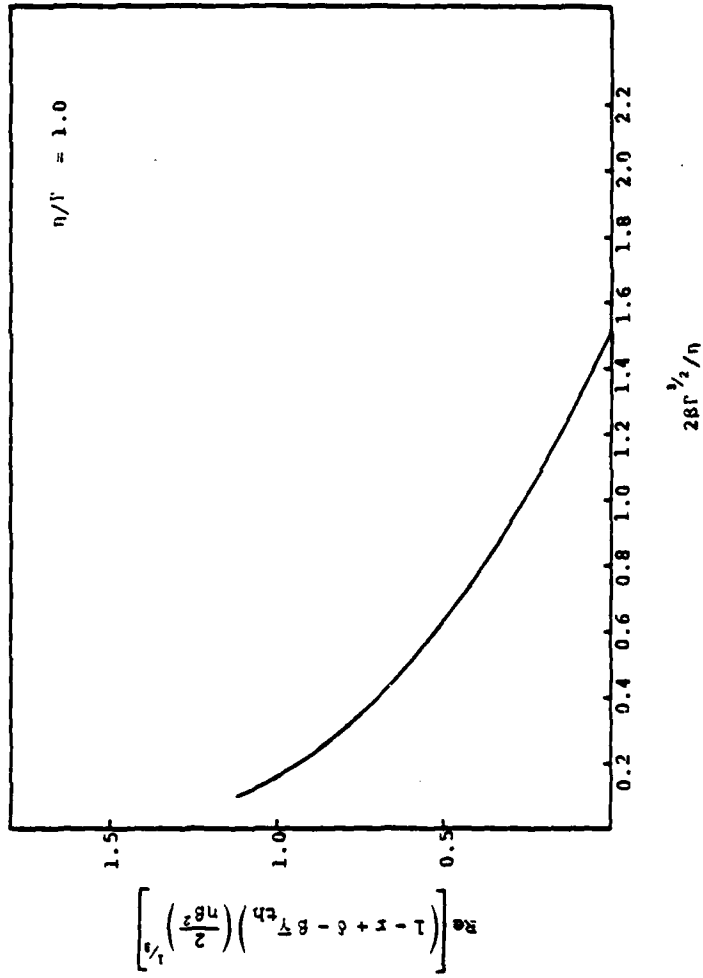


Figure 11. Variable Parameter Wiggler without Frequency Discrimination - $\text{Re}(i\delta_1)$ vs $2\delta\Gamma^{3/2}/\eta$

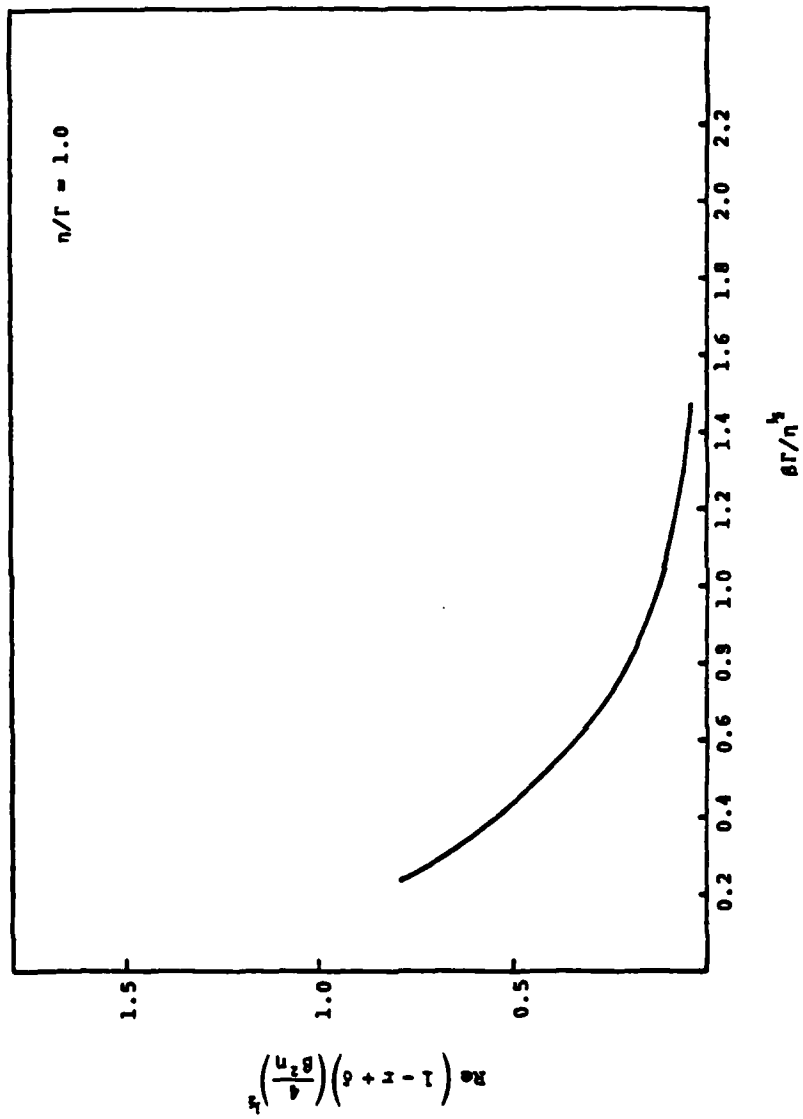


Figure 12. Variable Parameter Wiggler with Frequency Discrimination -
 $\text{Re}(\delta_2)$ vs $\beta\Gamma/\eta^{1/2}$

number of passes (i.e., linear growth characteristics), but also by the requirements of effective electron trapping and stable propagation of the finite amplitude pulse. Although the latter two requirements are not the main topics of this paper, it will be useful to briefly indicate some constraints on the choice of parameters which they impose. The comments on the constraints imposed by the requirements of non-linear propagation will be abstracted from Reference 1. They are compared to those summarized for linear gain. The electron equations of motion [Equations (14) and (15)] are derivable from the Hamiltonian \bar{H} :

$$\begin{aligned}\bar{H} &= \frac{\hat{Y}^2}{2} - \Gamma\psi - \hat{a}_s \cos(\psi + \xi) \\ &\equiv \frac{\hat{Y}^2}{2} + V(\psi) \quad .\end{aligned}$$

In a finite amplitude stationary state where \hat{a}_s and ξ are constant, electrons with small \bar{Y} are trapped in the potential well $V(\psi)$. The effective potential well depth is

$$\Delta V = 2\hat{a}_s \cos\psi_r + \left(\psi_r - \frac{\pi}{2}\right) \sin\psi_r$$

where $\psi_r < \frac{\pi}{2}$ is given by

$$\hat{a}_s \sin \psi_r = \Gamma .$$

The oscillation 'frequency' at the bottom of the potential well is

$$(\hat{a}_s \cos \psi_r)^{\frac{1}{2}} .$$

The magnitude of the stationary value of \hat{a}_s may be estimated from energy balance. Assuming \hat{a}_s independent of v , Equation (52) yields

$$(1-r) \hat{a}_s^2 \approx \eta \langle \hat{a}_s \sin (\psi + \xi) \rangle$$

$$\sim f_t \eta \Gamma$$

where f_t is the fraction of trapped electrons, which should be close to unity.

From these properties of the potential well, the following observations can be made:

- 1) To secure a finite well depth, it is desirable to have:

$$\sin \psi_r = \frac{\Gamma}{\hat{a}_s} \tag{75}$$

$$\sim \left[\frac{(1-r)\Gamma}{f_t \eta} \right]^{\frac{1}{2}} < 1 .$$

- 2) To trap a large fraction of electrons, the energy spread $\bar{\gamma}_{th}$ should satisfy

$$\frac{\bar{\gamma}_{th}}{\Gamma^{1/2}} < \left(\frac{\hat{a}_s}{\Gamma} \right)^{1/2} \sim \left[\frac{f_t \eta}{(1-r)\Gamma} \right]^{1/2} \quad (76)$$

We will discuss below how this nonlinear limitation on thermal spread compares with that determined by the limiting spread for linear gain calculated herein.

In reference 1, it is shown that the gain of sideband instabilities driven by electrons trapped in the ponderomotive potential wells which oscillate at frequency $(\hat{a}_s)^{1/2}$ is of the order of 2-3 times the gain experienced by the signal (which is by definition equal to the losses in the reflectors in steady state). Furthermore, sideband frequencies in the range $0.2(\hat{a}_s)^{1/2}$ to $(\hat{a}_s)^{1/2}$ show such gain. We can therefore make a crude estimate of the needed frequency discrimination.

To suppress sideband frequencies of the order of a quarter of the oscillation frequency $\sim \frac{1}{4} (\hat{a}_s)^{1/2}$, the reduction in power due to filtering by frequency discrimination should exceed the relative gain due to sideband instabilities:

$$\frac{1}{16} \frac{\hat{a}_s}{v^2} > 2(1-r)(\bar{G}-1) .$$

\bar{G} is the ratio of gain of the sideband instability to the gain of the pulse amplitude. Substituting for \hat{a}_s , and taking $v = \frac{1}{\beta}$:

$$\frac{\beta^2 \Gamma^2}{\eta} > \frac{32(\bar{G}-1)}{f_t^{1/2}} \left[\frac{(1-r)\Gamma}{\eta} \right]^{3/2} .$$

Such arguments are, of course, not quantitative, but the results of our numerical simulation suggest that a rough rule compatible with the above discussion is

$$\beta^2 \left[\frac{\Gamma \eta}{(1-r)^3} \right]^{1/2} \geq 70 , \quad (77)$$

where the numerical coefficient is uncertain by a factor of the order of 2.

We note, of course, that large β (i.e., high frequency discrimination) is desirable for stable propagation in the presence of the sideband instability. Comparing now with the linear theory of this paper, we note that Figure 6 gives a plot of $(1-r+\delta)(4/\eta\beta^2)^{1/2}$ vs. $\beta\Gamma/\eta^{1/2}$. Here, of course, small β is desirable for linear gain. At marginal stability ($\delta=0$) and using the lowest value of β allowable from Equation (77), i.e., $\beta=8.5(1-r)^3/\Gamma\eta^{1/2}$, we see that Figure 6 may be regarded as a transcendental equation

determining the maximum value of $(1-r)\Gamma/\eta$ for which a value of frequency discrimination may be chosen which both allows for linear gain and stable propagation. Solving this equation numerically, we find

$$(1 - r) \Gamma/\eta < .05 \quad (78)$$

as a fundamental limitation on the design of a variable parameter short pulse FEL.

Obviously to provide for reasonable positive gain, we must make $(1-r)\Gamma/\eta$ somewhat less than this critical value. The situation may be ameliorated somewhat by use of a constant wiggler section (see Figure 6) to allow linear gain at higher β . However, the use of such a section leads to saturation of the linear growth phase at an amplitude which may be too low for trapping since $(\hat{a}_{\text{sat}})^{1/2} v_1 \approx \pi$. It appears then that in practice the length of the constant wiggler should be limited by $\Gamma^{1/2} v_1 \leq 1$. With this optimization, Equation (78) appears as a reasonable design limitation. Note that from Equation (75) this limitation may also be expressed in the form

$$\sin \psi_r \leq 0.25 \quad .$$

We note also that using this value, Equation (76) for the nonlinear limitation on temperature may be expressed as:

$$\bar{\gamma}_{th}/\Gamma^{1/2} < 2 ,$$

while from Figure (8) we see that the linear gain is strongly reduced if $\bar{\gamma}_{th}/\Gamma^{1/2} > 1$. Hence, we see that good linear gain requires about twice as small an effective energy spread as would be deduced from looking at nonlinear trapping alone.

We have seen that the properties of a very short pulse FEL can be characterized by the dimensionless parameters Γ (related to the total variation of resonant energy induced by the variable parameters), η (related to the strength of electron current) and β the advance of the electromagnetic pulse compared to the next pulse in the electron train. We have also introduced a frequency discrimination ν in order to suppress sideband instabilities in the nonlinear evolution. In terms of these parameters, we have calculated the linear gain of the system and its degradation by thermal spread. We note that small thermal spread, low frequency discrimination, high current, and small variation of resonant energy are conducive to good linear gain.

In our companion paper, we will discover that large frequency discrimination is required to suppress sideband instabilities in the nonlinear region, thus determining a minimum value of n/Γ for which good operation may be expected with optimal frequency discrimination if beam energy spreads and emittance can be kept low enough.

REFERENCES

1. N. M. Kroll, P. L. Morton, and M. N. Rosenbluth, "Free Electron Lasers with Variable Parameter Wigglers," IEEE Journal of Quantum Electronics, Vol. QE-17, pp. 1436-1468 (1981).
2. W. B. Colson, Physics of Quantum Electronics, Vol. 8, p. 457 (Addison-Wesley, 1982).

A P P E N D I X C

SIMULATION OF SHORT ELECTRON PULSE FREE ELECTRON
LASERS WITH VARIABLE PARAMETER WIGGLERS

Simulation of Short Electron Pulse Free Electron
Lasers with Variable Parameter Wigglers

B. N. Moore, M. N. Rosenbluth,
and H. Vernon Wong

I. INTRODUCTION

The free electron laser (FEL) is a device for converting the directed energy of a relativistic electron beam into short wavelength electromagnetic energy. This is achieved by exploiting a resonant interaction between the beam and wave in a region where beam dynamics is dominated by a spatially varying magnetic field.^{1,2} Such devices may be operated in either an amplifier or oscillator mode and experimental lasers have been operated in each mode.¹ Analyses of constant parameter wiggler FELs have identified the major limitations on energy extraction efficiency.² The most important is that the EM pulse tends to grow to a level at which electrons just become trapped, but because additional extraction would bring electrons below the resonant energy, further growth is prevented. The saturated state then is one in which efficient energy

extraction takes place only near the end of the wiggler. The variable parameter wiggler is a modification of the FEL² which overcomes this problem by optimally adjusting the resonant energy as a function of position through the introduction of suitable wiggler amplitude and/or wavelength variation. Alternatively, one could in principle employ an electrostatic field to make up for radiative losses and keep an electron in resonance with a constant wiggler. It was anticipated that the variable parameter wiggler would have problems associated with trapped particle instabilities at sidebands offset from the resonant frequency. However, these instabilities can be suppressed by the introduction of frequency discrimination into the FEL optics. Such frequency discrimination, of course, reduces growth in the unsaturated state. One of the accomplishments of this simulation effort has been to demonstrate that efficient energy extraction may be expected in interesting parameter regimes with frequency discrimination.

The focus of this simulation study has been the FEL with variable parameter wiggler. A family of simulation codes has been written and applied to an investigation of growth and saturation of FELs with variable parameter wigglers. This report describes the codes, the results obtained to date and future plans. Some correlation of

simulation results with other analyses and experiments has been presented elsewhere.^{3,4} This report is organized into sections describing the physical and mathematical model of an FEL with discussion of the underlying assumptions and simplifications. This is followed by descriptions of the numerical algorithms including considerations of numerical stability and error estimation.

Due to computer time limitations, most of the simulations have been done using ultrashort electron pulses modeled by a δ -function. The results should apply to cases where the electron pulse is much shorter than the slippage distance; i.e., the difference in distance traveled by photons and electrons in the time taken by a photon to traverse the wiggler.

The results of the simulation of various cases are summarized in the following sections and particularly interesting simulations are presented in greater detail. In a separate report⁵ we have made extensive analytic studies of linear growth of FEL oscillators, and we will present in this report some confirmations of those studies.

II. FEL PHYSICS

The essential features of an FEL oscillator are shown schematically in Figure 1.

It consists of an EM cavity, bounded on each end by mirrors, into which are injected pulses of high energy electrons. The mirrors also serve to extract EM energy and possibly as filters. Also within the cavity is a region of spatially varying magnetic field with its major component transverse to the direction of pulse propagation. This is the wiggler, whose amplitude and wavelength may be adjusted to optimize energy extraction. The electron pulses and coherent EM pulses pass synchronously through the wiggler field. The effect of the wiggler field acting alone would be to establish the transverse motion of the electrons. In fact the EM field couples with the magnetic field of the wiggler to establish an effective ponderomotive potential for the electrons. Both fields are assumed circularly polarized.

The electron equation of motion in terms of energy γ and phase angle ψ are given below. A full derivation may be found in Reference 2.

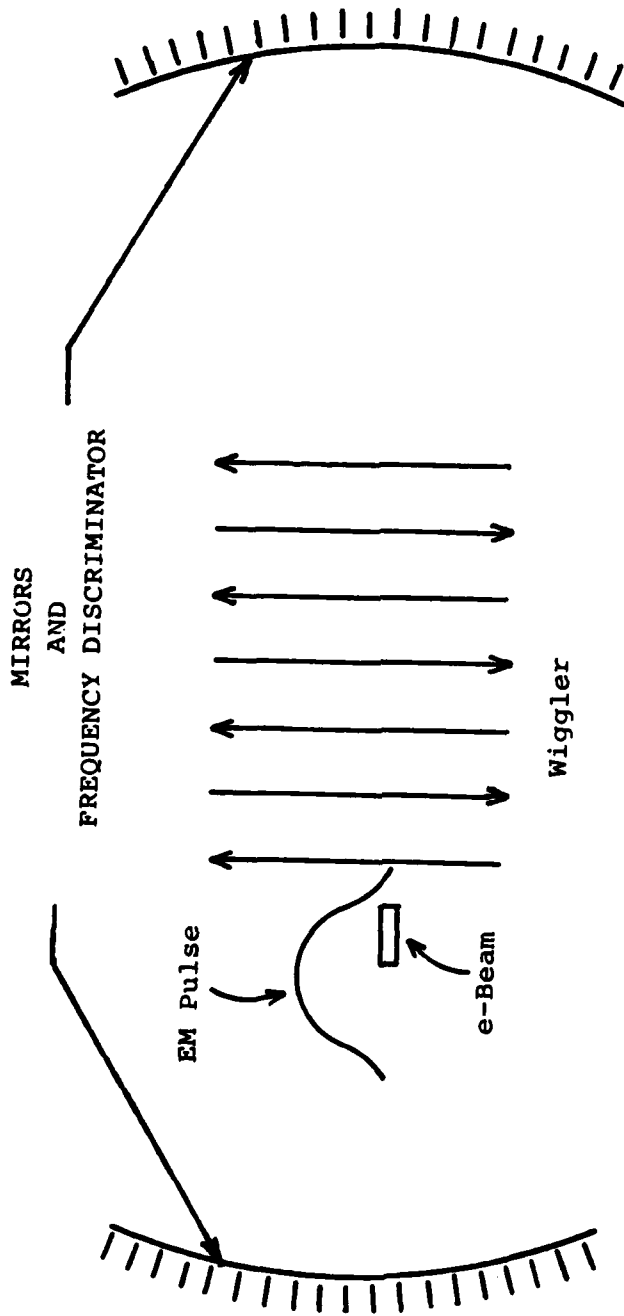


Figure 1. FEL Schematic Diagram

$$\frac{d\gamma}{dz} = -\frac{e}{mc^2} \frac{d\phi_0}{dz} - \frac{k_s a_w a_s}{\gamma} \sin(\psi + \zeta) \quad (1)$$

$$\frac{d\psi}{dz} = k_w - \frac{k_s \mu^2}{2\gamma^2} \quad (2)$$

$$a_w = \frac{eA_w}{mc^2}, \quad a_s = \frac{eA_s}{mc^2} \quad (3)$$

$$k_w = 2\pi/\lambda_w, \quad k_s = 2\pi/\lambda_s \quad (4)$$

$$\mu^2 = (1 + a_w^2 + a_s^2) \quad (5)$$

Where

ψ is particle phase

ζ is electromagnetic phase

A_s is electromagnetic vector potential amplitude

A_w is wiggler vector potential amplitude

ϕ_0 is the electrostatic potential which mocks up the wiggler parameter variation.

λ_s is the EM wave length

λ_w is the wiggler wave length

m , e and c are electron mass, electron charge and light speed. γ is the relativistic factor for the beam.

$$\gamma = \frac{\text{Electron Energy}}{mc^2} . \quad (6)$$

The transverse electron current serves as a source for the electromagnetic field of the EM pulse governed by Maxwell's equations.

$$\begin{aligned} \frac{\partial a_s}{\partial z} + \frac{1}{c} \frac{\partial a_s}{\partial t} &= \frac{2\pi e}{k_s mc^3} (J_x \sin \psi_s + J_y \cos \psi_s) \quad (7) \\ &\equiv - \frac{2\pi e}{k_s mc^3} J_2 \end{aligned}$$

$$\begin{aligned} a_s \left(\frac{\partial \zeta}{\partial z} + \frac{1}{c} \frac{\partial \zeta}{\partial t} \right) &= \frac{2\pi e}{k_s mc^3} (J_x \cos \psi_s - J_y \sin \psi_s) \quad (8) \\ &\equiv \frac{2\pi e}{k_s mc^3} J_1 \end{aligned}$$

The current densities may be calculated from the electron trajectories

$$J_1 = \frac{e c a_w(z)}{\gamma_r} n \left(\frac{z}{V} - t \right) \langle \cos(\psi + \zeta) \rangle \quad (9)$$

$$J_2 = - \frac{e c a_w(z)}{\gamma_r} n \left(\frac{z}{V} - t \right) \langle \sin(\psi + \zeta) \rangle . \quad (10)$$

Where the notation $\langle \rangle$ implies averages over the initial phase and energy distribution of the electron beam, and the function n is the number density of the electron beamlet, and γ_r is the resonant γ . Here it has been assumed that the EM field is of the form

$$\vec{E} = -\frac{1}{c} \frac{\partial \vec{A}}{\partial t} \quad (11)$$

$$\frac{e\vec{A}_s}{mc^2} = a_s(z,t) \left[\hat{x} \cos(\psi_s) - \hat{y} \sin(\psi_s) \right] \quad (12)$$

$$\frac{e\vec{A}_w}{mc^2} = -a_w \left[\hat{x} \cos k_w z + \hat{y} \sin k_w z \right] \quad (13)$$

$$\psi_s = k_s z - \omega_s t + \zeta(z,t) \quad (14)$$

$$\omega_s = k_s c \quad (15)$$

where a_s and ζ are slowly varying functions of z and t and are independent of x and y .

The EM pulse leaves the wiggler, propagates to the mirror where it is filtered and partially reflected before encountering the next electron pulse. These processes are modeled as follows.

$$a_{s \text{ into filter}} = r a_s(z=L_w, t) \quad (16)$$

(reflection)

$$\left(\frac{\partial}{\partial t} + \omega_F \right) a_{s \text{ out of filter}} = \omega_F a_{s \text{ into filter}} \quad (17)$$

(filtering)

Where

ω_F is the bandpass cutoff frequency centered
about ω_s
 r is the extraction mirror reflection coefficient
 L_w is the wiggler length.

Before entrance into the wiggler on the next pass,
a fixed time delay is introduced. The electron beam
density into the wiggler is assumed to be perfectly
periodic, with the period Δt .

The major assumptions underlying this model are:

- (1) The wiggler field has negligible axial and fringe components.
- (2) Transverse variations of all quantities are neglected.
- (3) An EM pulse is a nearly plane wave whose amplitude and phase vary negligibly over a few EM wavelengths.
- (4) The appropriate EM filter with Lorentzian line shape is assumed.
- (5) $\gamma \gg 1$.

III. SIMULATION EQUATIONS

By appropriate normalization, the FEL equations may be further simplified for the simulation code. Other simplifying assumptions will also be convenient. Additionally, finite difference algorithms must be selected which do not introduce numerical instabilities and which efficiently approximate the time and spatial derivatives involved.

Introduce the variables u and v ,

$$u = \frac{1}{L_w} \left(\frac{\frac{c}{v} z - ct}{\frac{c}{v} - 1} \right) \quad (18)$$

$$v = \frac{1}{L_w} \left(\frac{ct - z}{\frac{c}{v} - 1} \right) \quad (19)$$

$u = \text{constant}$ follows an electron, and $v = \text{constant}$ a photon. L_w is wiggler length, v the electron longitudinal velocity. The electron beam runs from $-u_0$ to zero. The wiggler interaction occurs for $1 > u + v > 0$ (See Figure 2). The equations for this region of interaction are:

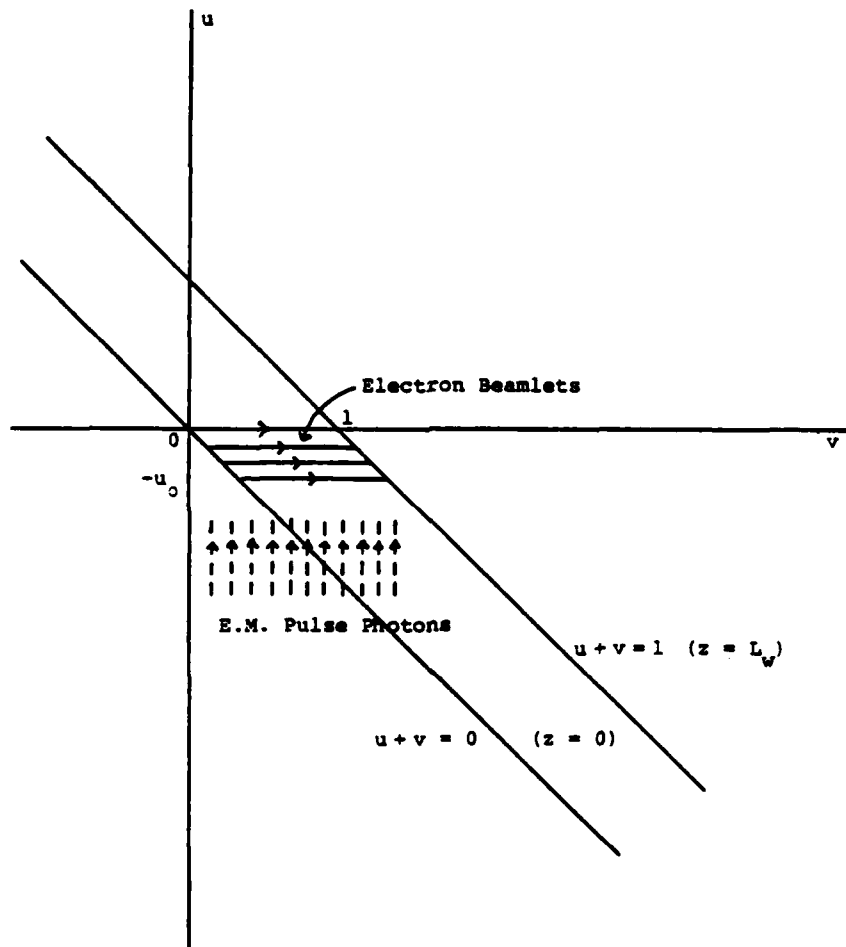


Figure 2. Simulation Coordinate System

$$\frac{\partial \hat{a}}{\partial u} = i \eta h(u) \langle e^{-i\psi} \rangle \quad (20)$$

$$\frac{\partial \hat{\gamma}}{\partial v} = \frac{1}{2} \left[i \hat{a} e^{i\psi} - i \hat{a}^* e^{-i\psi} \right] + \Gamma \quad (21)$$

$$\frac{\partial \psi}{\partial v} = \hat{\gamma} \quad (22)$$

where \hat{a} , Γ , η and $h(u)$, expressed in terms of physical parameters, are defined by

$$\hat{a} = \hat{a}_s e^{i\zeta} \quad (23)$$

$$\hat{a}_s = \frac{2k_w L_w}{\gamma_r} \frac{k_s L_w a_w}{\gamma_r} a_s \quad (24)$$

$$\hat{\gamma} = \frac{2k_w L_w}{\gamma_r} (\gamma - \gamma_r) \quad (25)$$

$$\gamma_r = \left(\frac{k_s}{2k_w} \right)^{\frac{1}{2}} \left(1 + a_w^2 + a_s^2 \right)^{\frac{1}{2}} \quad (26)$$

$$\Gamma = - \frac{2k_w L_w}{\gamma_r} \frac{d\gamma_r}{dv} = \frac{2k_w L_w}{\gamma_r} \frac{e}{mc^2} \frac{d\phi_0}{dz} \quad (27)$$

$$\eta = \frac{8(k_w L_w)^2 \frac{e \langle I \rangle}{mc^3}}{\gamma_r \left(1 + \frac{\Omega^2}{k_w^2 c^2} \right)} u_0 \left(\frac{L_w}{r_0^2 k_s} \right) \left(\frac{\Omega}{k_w c} \right)^2 \quad (28)$$

$$\Omega = \frac{eB_w}{mc}, \quad u_0 = \frac{\ell k_s}{L_w k_w} \quad (29)$$

$$h(u) = \frac{L_w \left(\frac{c}{v} - 1 \right)}{\ell \frac{c}{v}} \frac{I(z, t)}{\langle I \rangle} \quad (30)$$

$$\langle I \rangle = \frac{1}{\ell} \int I(z, t=0) dz \quad (31)$$

ℓ is nominal electron pulse length
 r_0 is electron beam radius
 I is the beam current

In terms of the normalized variables, the pass-to-pass EM processes are modeled as:

$$\frac{\partial \hat{a}_F(v)}{\partial v} + v \hat{a}_F(v) = v \hat{a}^{(n)}(u=0, v) \quad (32)$$

$$\hat{a}^{(n+1)}(u = u_0, v) = r \hat{a}_F(v + \beta) \quad (33)$$

Where

$$v = \frac{L_w}{c} \left(\frac{c}{v} - 1 \right) \omega_F = \frac{k_w L_w}{k_s c} \omega_F \quad (34)$$

r = reflection coefficient of extractor

$$\beta = \frac{c}{L_w \left(\frac{c}{v} - 1 \right)} \Delta t_{rel} = \frac{k_s c}{k_w L_w} \Delta t_{rel} \quad (35)$$

with Δt_{rel} being the time delay of the electron pulse with respect to the EM pulse at the wiggler.

Some preliminary attempts at algorithms for solving these equations met with limited success, either due to problems with numerical instabilities or lack of computational efficiency. The EM amplitude and phase (a_s, ζ) and the particle phase space variables $(\hat{\gamma}, \psi)$ are defined on a discrete grid in the $u - v$ plane. The indices i_u and i_v define the location on this grid. The index i is the particle label. The following algorithms were eventually selected.

$$u = u_0 + (i_u - 1) \Delta u \quad (36)$$

$$v = v_0 + (i_v - 1) \Delta v \quad (37)$$

$$\hat{\gamma}_{i_e}(u, v + \Delta v) = \hat{\gamma}_{i_e}(u, v) - \Delta v \left(\tilde{a}_c \sin \psi_{i_e} + \tilde{a}_s \cos \psi_{i_e} \right) \quad (38)$$

Where the centered EM field components are:

$$\tilde{a}_c \equiv |\hat{a}| \cos \zeta + \frac{\Delta u}{2} \eta h(u) \langle \sin \psi(u, v) \rangle \quad (39)$$

$$\tilde{a}_s \equiv |\hat{a}| \sin \zeta + \frac{\Delta u}{2} \eta h(u) \langle \cos \psi(u, v) \rangle \quad (40)$$

The particle phases are advanced for a fixed u value.

$$\sin \psi_{i_e}(v + \Delta v) = \beta_1 \sin \psi_{i_e}(v) + \beta_2 \cos \psi_{i_e}(v) \quad (41)$$

$$\cos \psi_{i_e}(v + \Delta v) = \beta_1 \cos \psi_{i_e}(v) - \beta_2 \sin \psi_{i_e}(v) \quad (42)$$

With β_1 and β_2 chosen to preserve $\sin^2 \psi_{i_e} + \cos^2 \psi_{i_e} = 1$.

$$\beta_1 \equiv \frac{1 - \alpha^2}{1 + \alpha^2} \quad (43)$$

$$\beta_2 \equiv \frac{2\alpha}{1 + \alpha^2} \quad (44)$$

The contribution of the wiggler parameter variation to the particle phases is isolated to the term:

$$\alpha = \left(\hat{\gamma}_{i_e}(v + \Delta v) + \sum_{i_v=N_{v_1}}^{N_v} \Gamma \Delta v \right) \frac{\Delta v}{2} \quad (45)$$

Steps (38) through (45) are repeated for each particle.

Then the particle currents are calculated and the field amplitudes at the next value of u are determined.

$$\langle \sin \psi (v + \Delta v) \rangle = \sum_{i_e=1}^{N_e} \frac{\sin \psi_{i_e}}{N_e} \quad (46)$$

$$\langle \cos \psi (v + \Delta v) \rangle = \sum_{i_e=1}^{N_e} \frac{\cos \psi_{i_e}}{N_e} \quad (47)$$

$$a_s(u + \Delta u, v) = a_s(u, v) + \Delta u \eta h(u) \langle \cos \psi(u, v) \rangle \quad (48)$$

$$a_c(u + \Delta u, v) = a_c(u, v) + \Delta u \eta h(u) \langle \sin \psi(u, v) \rangle \quad (49)$$

$$a_s \equiv |\hat{a}| \sin \zeta \quad (50)$$

$$a_c \equiv |\hat{a}| \cos \zeta \quad (51)$$

Steps (46) through (51) are repeated for each v interval in the wiggler ($0 < u + u < 1$). For other values of v these quantities propagate unchanged. Finally, the entire series, (36) through (51), is repeated for each value of u . The basic scheme is depicted in Figure 2. Specification of the EM pulse as a function of time into the wiggler is equivalent to specification vs v at $u = -u_0$.

Similarly, the electron pulse density distribution is a specified function $h(u)$ at $v = -u$. The field equations are integrated along the vertical characteristics ($v=\text{constant}$) and the equations of motion along horizontal ($u=\text{constant}$) characteristics. Note that the $\hat{\gamma}$, $\sin \psi$ and

$\cos \psi$ functions are advanced independently with an algorithm which preserves $\sin^2 \psi + \cos^2 \psi$. The particles at a given u are advanced from $v = -u$ to $v = 1-u$ with an algorithm which estimates the effects of the averaged EM field acting on the particles. Once the phase-averaged particle currents are available at a given u , the EM fields are advanced to the next u value. The process is repeated until the electron pulse and EM pulse have moved completely through the interaction region. The EM pulse then propagates undisturbed to the mirrors where energy extraction and optical discrimination are carried out. Negligible interaction on the return through the wiggler is assumed.

One group of simulation programs incorporates the additional renormalization:

$$P_{EM} = \sum_{i_V} \left[(|\hat{a}| \cos \zeta)^2 + (|\hat{a}| \sin \zeta)^2 \right] \Delta v \quad (52)$$

$$a = \frac{a_0}{\sqrt{P_{EM}}} |\hat{a}| \quad (53)$$

This renormalization involves a reduction of the output amplitude \hat{a} to a such that the input pulse energy is always at a level a_0^2 , small enough to be in the linear regime.

This keeps the EM pulse at a constant total energy before entry into the wiggler. The result of many repetitions of this algorithm will be a pulse corresponding to the fastest growing linear eigenmode, which can be compared with analytic results and used to begin the nonlinear simulation.

Three options are provided for loading the initial electron beam. These are: cold beam and Maxwellian and Lorentzian thermal distributions. The distributions are specified by $\langle \gamma \rangle$, which is the mean γ , and γ_{th} , which characterizes the thermal spread.

$$f(\hat{\gamma}) = \begin{cases} \sim \delta(\hat{\gamma} - \bar{\gamma}) & \text{Cold} & (54) \\ \sim e^{-\frac{(\hat{\gamma} - \bar{\gamma})^2}{\hat{\gamma}_{th}^2}} & \text{Maxwellian} & (55) \\ \sim \left[1 + \frac{(\hat{\gamma} - \bar{\gamma})^2}{\hat{\gamma}_{th}^2} \right]^{-1} & \text{Lorentzian} & (56) \end{cases}$$

$$\hat{\gamma} = \frac{2k_w L_w}{\gamma_r} [\gamma - \gamma_r] \quad (57)$$

$$\hat{\gamma}_{th} = \frac{2k_w L_w}{\gamma_r} \gamma_{th} \quad (58)$$

$$\bar{\gamma} = \frac{2k_w L_w}{\gamma_r} [\langle \gamma \rangle - \gamma_r] \quad (59)$$

The particles are also distributed uniformly in phase.

IV. DIAGNOSTICS

A number of diagnostics are provided in the codes, including growth rates, integrated power, phase space plots and Fourier transforms. The growth rate represents the pass to pass exponentiation as follows:

$$\text{Re } \delta = \frac{1}{2} \ln \left(\frac{P_{EM}}{a_0^2} \right) \quad (60)$$

The particle phase space corresponding to any point in the interaction region may be displayed for any pass, allowing a determination of trapping efficiency. The energy extracted per particle is monitored as a function of pass with the parameter:

$$\delta \gamma_{\text{ext}} = \sum_{i_u} \sum_{i_e=1}^{N_e} \left(\hat{\gamma} - \int_{v_1}^1 \Gamma dv \right) h(u) \frac{\Delta u}{N_e} \quad (61)$$

where N_e is the total number of simulation electrons.

The Fourier transform diagnostics and their relation to physical parameters are:

$$\hat{a}(\nu) = a_c + i a_s \quad (62)$$

$$A_\kappa = \sum_{i\nu} \hat{a}(\nu) e^{i\kappa(i\nu\Delta\nu)} \quad (63)$$

$$\kappa = \frac{k_w L}{(V/c)} \left(\frac{\frac{\omega}{\omega_s} - 1}{1 + \frac{k_w}{k_s}} \right) \quad (64)$$

Note that the diagnostic frequency (or wave vector) is expressed relative to the nominal resonant wavelength.

V. RESULTS

The major tasks accomplished to date include the verification of the code against established theory of the constant wiggler FEL, confirmation and extension of the linear theory of variable wiggler devices, including thermal effects, and investigations of the nonlinear phenomena associated with saturation of both short and long pulse FELs. These investigations have established the necessity for some frequency discrimination in order to achieve acceptable performance for both classes of devices, and the scaling laws for variable parameter wiggler FELs with frequency discrimination have been determined.

Preliminary simulations of finite length electron beams without frequency discrimination have given results similar to those of Goldstein, et al.⁶ for parameters associated with the LANL proposed experiments. In the absence of frequency discrimination, the EM pulse shape at saturation is irregular and characterized by random peaks. With frequency discrimination, much smoother pulse shapes were obtained, and the saturated pulse energy was somewhat smaller. However, the variation with pulse length indicates that with longer beam pulses such as those actually envisaged, frequency discrimination would be more

effective in producing not only smoother saturated pulse shapes, but also higher pulse energies. Further work on finite length pulse simulation will be published separately.

In the following sections, we focus exclusively on the limit of very short electron beams in which the electron pulse length ℓ is short compared to the slippage distance $k_w L_w / k_s \gg \Gamma^{1/2} \ell$ or $\Gamma^{1/2} |u_0| \ll 1$.

In the simulation, this limit is modeled as a δ -function; that is, $h(u) = \delta(u)$. Obviously this model requires minimal simulation time (only one value of u) so that long, high extraction wigglers may be studied.

As a check on the accuracy of the code, the linear gain per pass calculated from the linear eigenmode analysis⁵ was compared with that observed in the simulations for a range of FEL parameters. In the parameter regions where the theory is applicable, the agreement between theory and simulation is satisfactory (see Figures 3, 4, 8, 9 and 10) and is of the order of or better than 15%.

1. No Frequency Discrimination

In FELs without frequency discrimination, the linear gain per pass for a very long constant parameter wiggler ($\beta/\eta \rightarrow 0$) is given by

$$\operatorname{Re} \delta_1 \equiv \operatorname{Re} \left[\frac{1 - r + \delta + \beta \bar{\gamma}_{\text{th}}}{(\eta \beta^2)^{1/3}} \right] \approx \frac{3^{3/2}}{4} \quad (65)$$

If the beam and wiggler parameters are kept constant, $\operatorname{Re} \left[(\beta/\eta)^{2/3} \delta_1 \right]$ increases from zero as the phase advance β of the EM pulse is increased, reaches a maximum $\operatorname{Re} \left[(\beta/\eta)^{2/3} \delta_1 \right] = .047$ at $\beta/\eta = .022$, and finally decreases to zero at $\beta/\eta = .065$. The theoretical linear gain curve⁵ is plotted as a solid line in Figure 3, while the linear gain observed in the simulations is represented by the circled points.

If the wiggler is made variable by applying a finite accelerating electric field ($\Gamma \neq 0$), the linear gain remains close to that of the constant parameter wiggler when $2\beta\Gamma^{3/2}/\eta \ll 1$. (The accelerating electric field produces essentially the same effect as varying the wiggler parameters, i.e., keeping trapped electrons in resonance as they radiate energy). As the magnitude of the variation is further increased, $\operatorname{Re} \delta_1$ decreases. In the limit of a very long variable wiggler where $\beta/\eta \ll 1$ and $\Gamma \gg 1$, $\operatorname{Re} \delta_1 \approx 0$ when $2\beta\Gamma^{3/2}/\eta = 1.42$. In Figure 4, the theoretical linear gain curve is plotted as a solid line indicating the variation of $\operatorname{Re} \delta_1$ as a function of $2\beta\Gamma^{3/2}/\eta$. The results of the simulations are represented as circled points for values of $\beta/\eta = 3.3 \times 10^{-5}$, .01.

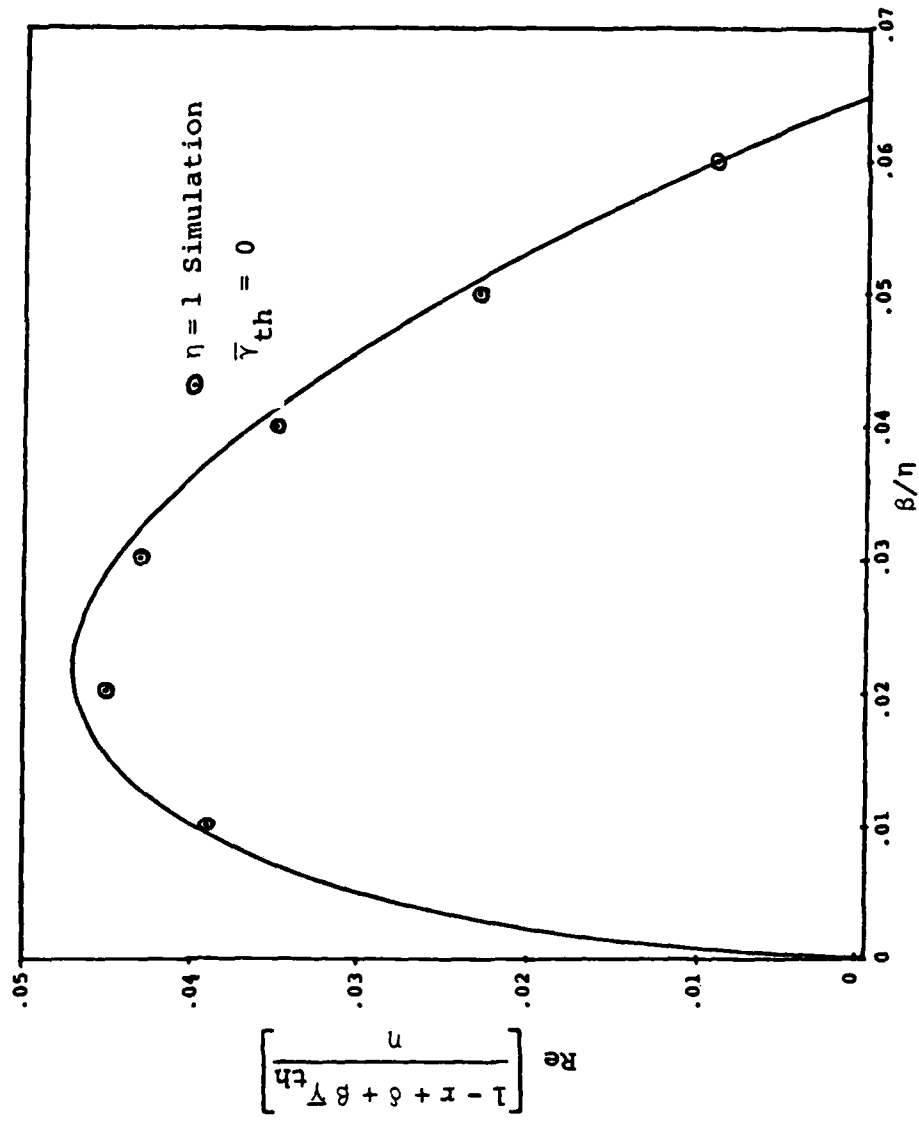


Figure 3. Linear Gain - Constant Parameter Wiggler Without Frequency Discrimination

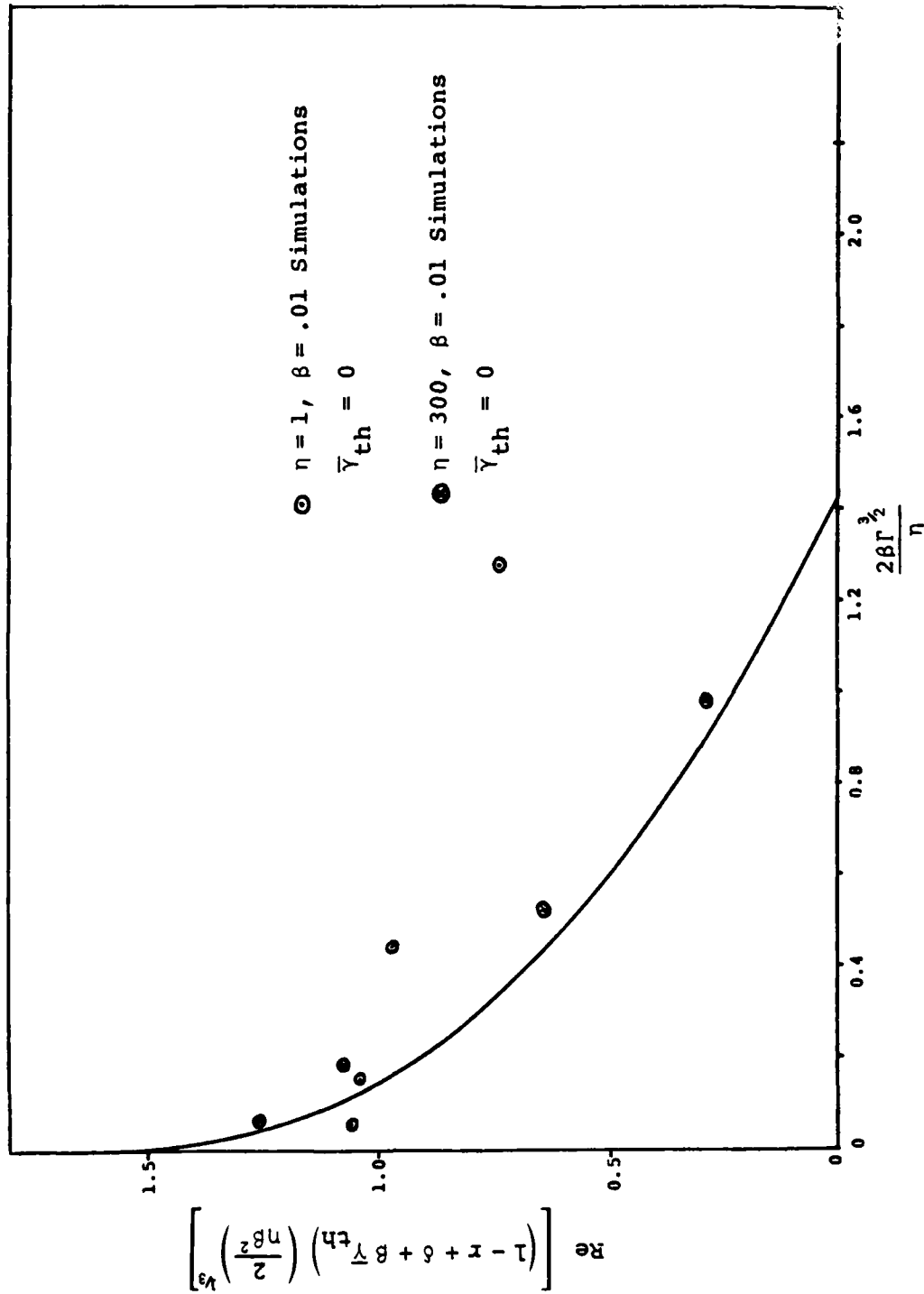


Figure 4. Linear Gain Variable Parameter Wiggler Without Frequency Discrimination

The differences between the observed linear gain and the theoretical linear gain curve for $\beta/\eta = .01$ are due to finite length effects not included in the theory. For most cases of physical interest, the criterion $\delta/\beta > 1$ for neglecting finite length effects is well satisfied.

The pulse shape of the linear eigenmodes are displayed in Figure 5. For a constant parameter wiggler, the pulse amplitude increases smoothly to a maximum and then falls to zero at the back. As the wiggler is made variable, the change in the pulse phase angle in going from the front of the pulse to the back progressively increases. At the same time, the pulse amplitude becomes more sharply peaked at the back.

In a typical run in which the EM pulse grows from noise levels to saturation, the early phase of the evaluation is characterized by growth of the linear eigenmode. Eventually, nonlinearities reduce and then saturate wave growth.

For constant parameter wigglers, the maximum pulse energy occurs for values of the pulse phase advance parameter β which are small and positive. This decreases as β increases. Similar results were previously obtained by Colson for finite length electron beams.³ The effect of $\beta > 0$ is to shift the EM pulse ahead of the electron beam on each pass through the wiggler. As β increases, the

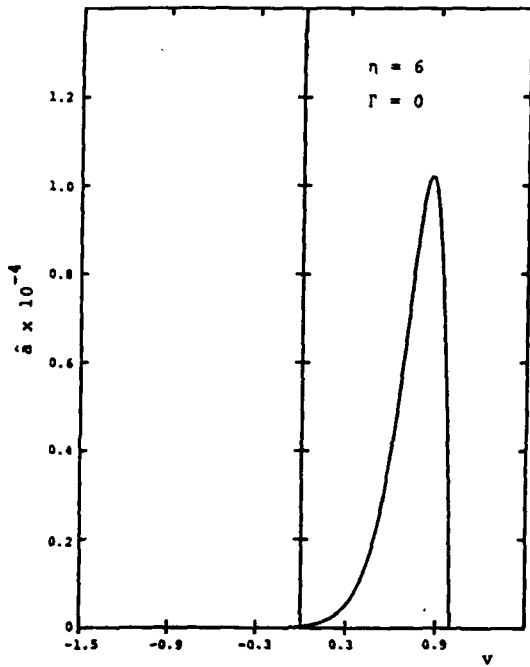


Figure 5a. Amplitude vs. v

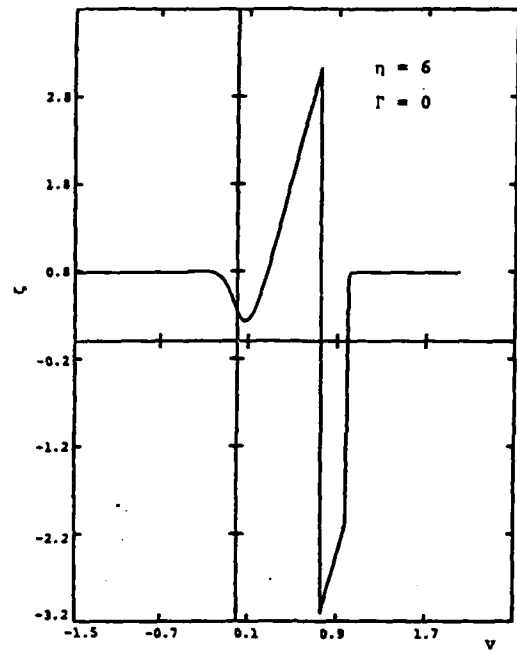


Figure 5b. EM Pulse Phase vs. v

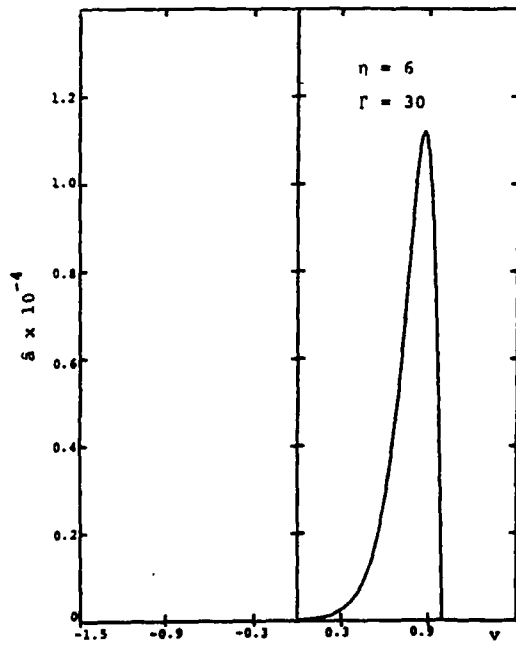


Figure 5c. Amplitude vs. v

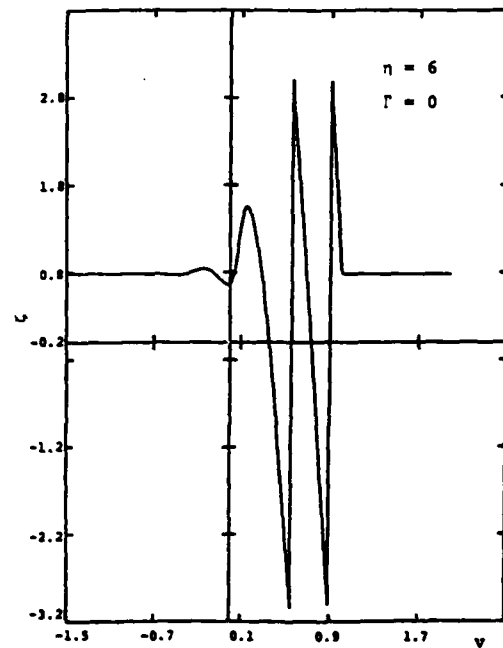


Figure 5d. EM Pulse Phase vs. v

net interaction time of each section of the pulse with the electron beam decreases and this leads to a progressive reduction of the saturated pulse energy.

For a variable parameter wiggler, the evolution enters a nonlinear phase during which the peak in the pulse amplitude moves to the front, which continues to grow at approximately the linear rate after the back has saturated. Growth continues until the peak amplitude at the front of the pulse is large enough to begin to trap the beam electrons. At saturation, without optical discrimination, the pulse remains peaked at the front and never broadens towards the back. Most of the energy resides in the front part of the pulse which no longer interacts coherently with the beam.

The pulse shape and pulse spectrum at saturation for a representative simulation run with the following FEL parameters are shown in Figure 6:

$$\begin{aligned}r &= 0.99 \\ \eta &= 600. \\ \beta &= 0.01 \\ \Gamma &= 2000. \\ v_1 &= .015 \\ v &= 1000 \\ \bar{\gamma}_{th} &= 0.\end{aligned}$$

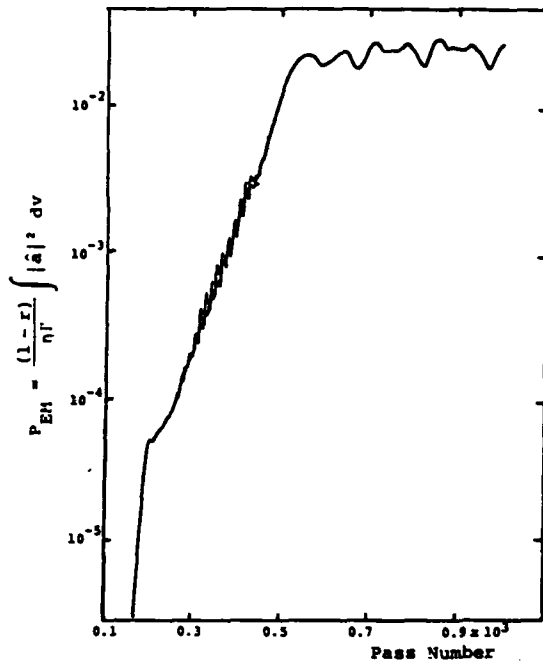


Figure 6a. Pulse Energy vs. Pass Number

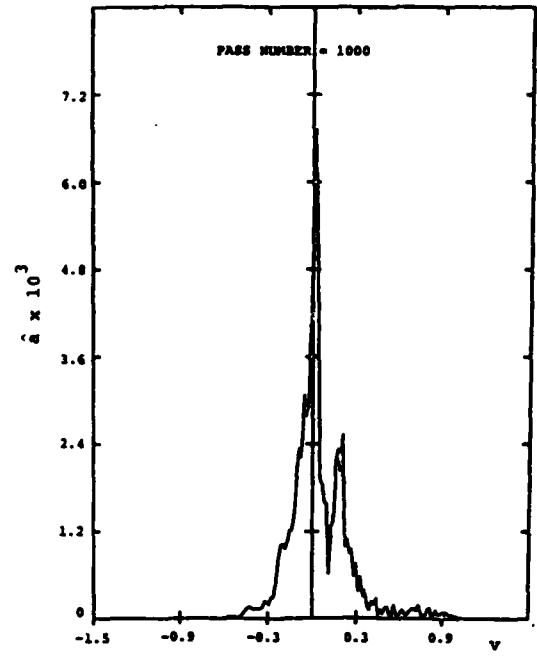


Figure 6b. Amplitude vs. v

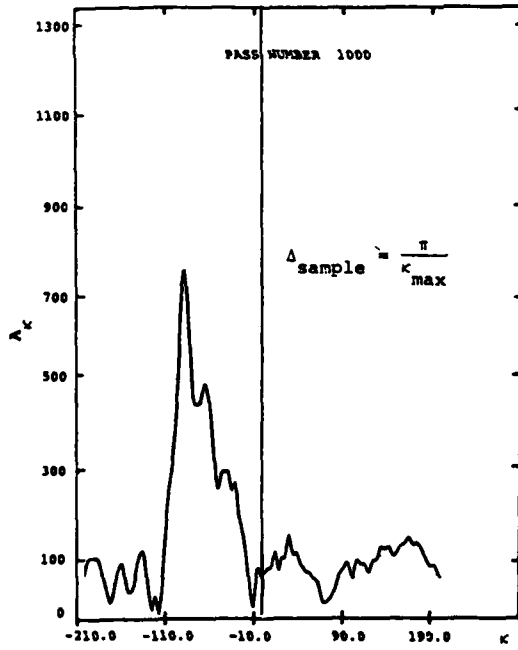


Figure 6c. Complex Amplitude vs. Frequency κ

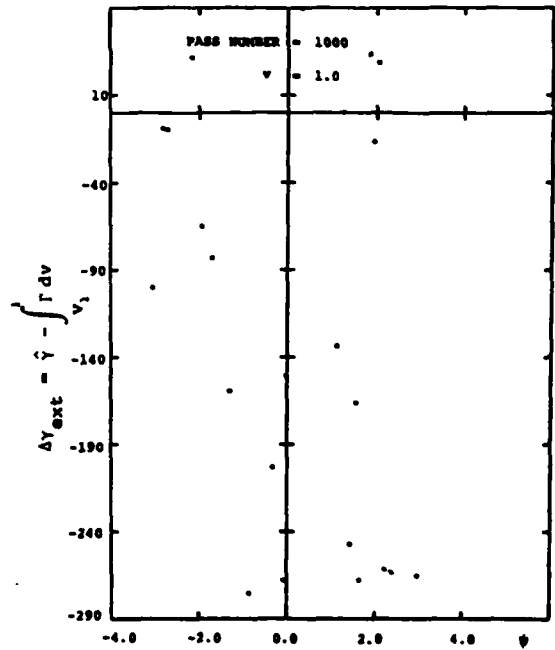


Figure 6d. Energy Extracted vs. Phase ψ

The value of $\nu = 1000$ corresponds to a filter cutoff frequency approximately ten times the largest observed electron bounce frequency in the ponderomotive potential well and thus effectively models an infinite bandwidth filter; that is, there is no frequency discrimination.

These values for the dimensionless parameters were chosen to simulate an FEL with the following physical parameters:

Electron Energy	50 MeV
Electron beam current averaged over a slippage length	50 Amps
Wiggler Wavelength	1.25 cm
Number of wiggler wavelengths	400
Signal Wavelength	1 μ
Wiggler Field Amplitude	7 kG
Nominal Trapped Electron Energy Loss	20 MeV
Constant Parameter Length	7.5 cm

A constant parameter wiggler of fractional length ν_1 was added to the front of the variable wiggler to enhance the linear gain per pass, $\text{Re } \delta = .071$ for this case.

In Figure 6a, the normalized integrated pulse energy

$$P = \frac{(1-r)}{\eta\Gamma} \int |\hat{a}(\nu)|^2 d\nu \quad (66)$$

is plotted as a function of the pass number through the wiggler. It may be noted that if $P = 1$, the energy lost on reflection at the mirror is equal to the energy extraction from the electron beam assuming all the electrons are trapped in the ponderomotive potential well formed by the combined field of the pulse and wiggler. In practice, $P < 1$ since all the electrons are not trapped and additional sinks for energy loss may occur (for example, if the pulse is subjected to frequency discrimination; see the next section).

The pulse energy P increases exponentially at small pulse amplitudes. After nonlinear saturation of pulse growth occurs, the pulse energy P oscillates in a limit cycle about a finite mean.

The pulse shape at saturation is displayed in Figure 6b. The part of the pulse extending from $v = 0$ to $v = 1$ interacts with the electron beam in the wiggler. With positive phase advance $\beta > 0$, the pulse is shifted to the left on each successive pass. The front part of the pulse ($v < 0$) shifted out of the wiggler no longer "sees" the electron beam and is damped by reflection energy losses at the mirrors. Note that only the front of the pulse is amplified.

The Fourier transform of the pulse amplitude $a(v)$

$$A_{\kappa} = \int e^{i\kappa v} \hat{a}(v) dv \quad (67)$$

is plotted as a function of κ in Figure 6c. For a particular value of κ , the corresponding frequency ω of the laboratory frame is

$$\frac{\omega}{\omega_s} = 1 + \frac{\kappa}{k_w L_w} \left(1 + \frac{k_w}{k_s} \right) \frac{v}{c} \quad (68)$$

The location of the electrons in phase space

$$\hat{\gamma} - \int_{v_1}^v \Gamma dv, \quad \psi \quad (69)$$

is plotted in Figure 6d at different positions v in the wiggler. The electron energy is plotted as a function of the phase angle modulo 2π . If the electrons are freely accelerated,

$$\hat{\gamma} - \int_{v_1}^{v_1} \Gamma dv = \hat{\gamma}_0 \quad (70)$$

where $\hat{\gamma}_0$ is the initial value of $\hat{\gamma}$, and is set to zero for these simulations. If the electrons are trapped at the front of the wiggler and remain trapped throughout

the length of the wiggler, $\hat{\gamma} = \hat{\gamma}_0$, and

$$\hat{\gamma} - \int_{v_1}^v \Gamma dv = \hat{\gamma}_0 - \int_{v_1}^v \Gamma dv \quad . \quad (71)$$

As may be noted from Figure 6d, the electrons are not effectively trapped throughout the length of the wiggler and the energy transferred to the pulse at saturation is small, $P \approx 0.024$.

The same final state was obtained by starting the simulation run with an initial square wave pulse of finite amplitude large enough to trap the beam electrons (see Figure 7). The back of the pulse erodes away, and sideband frequencies $\kappa \sim 60$ below the main pulse frequency (that is, zero frequency in Figure 7) grow in magnitude and finally dominate the spectrum. The sideband frequencies are of the order of the electron bounce frequency $\sim |\hat{a}|^{1/2} \sim 78$ in the ponderomotive potential well. The growth of sidebands leads to a loss of coherence, and the beam electrons are not effectively trapped throughout the length of the wiggler. The amplitude of the back of the pulse falls to a low level compared to the peak amplitude at the front.

This suggests that any tendency of the pulse to broaden towards the back during growth from noise will be hindered by the growth of sideband frequencies. Such

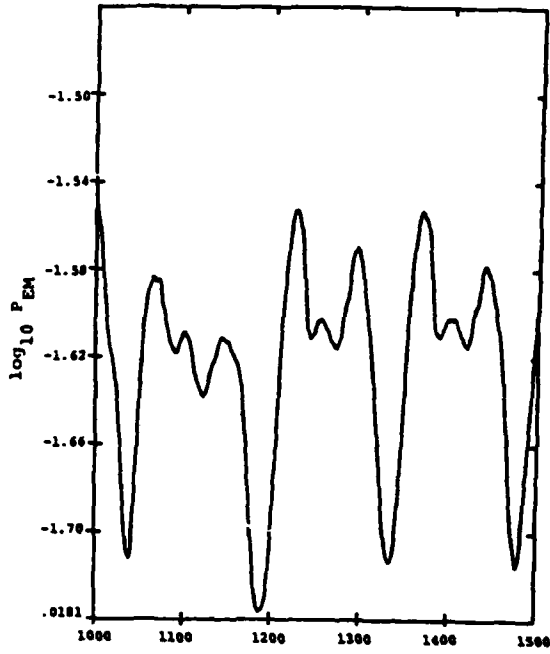


Figure 7a. Pulse Energy vs. Pass Number

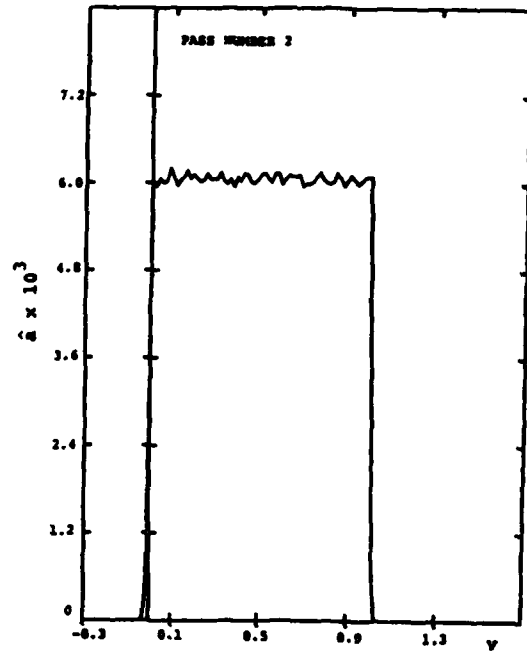


Figure 7b. Amplitude \hat{a} vs. v

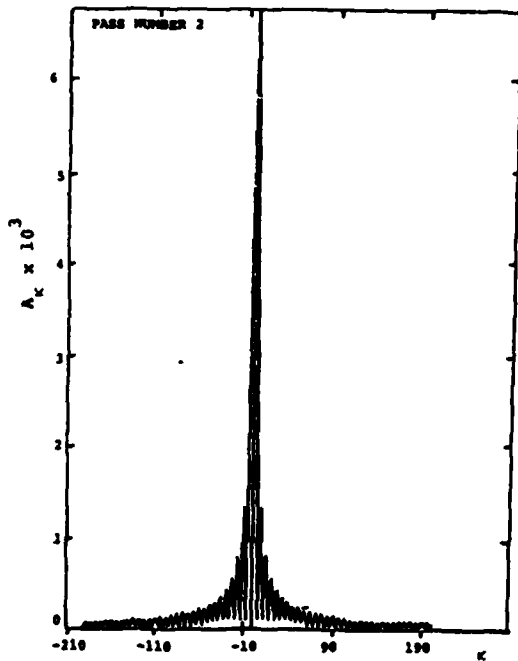


Figure 7c. Complex Amplitude vs. Frequency κ

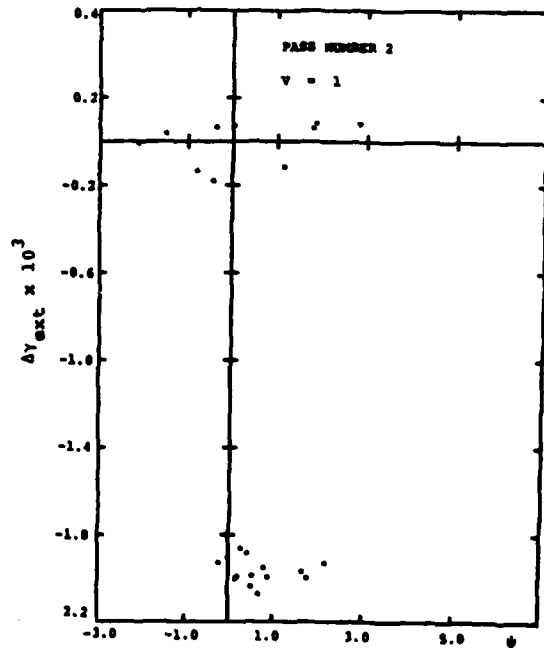


Figure 7d. Energy Extracted vs. Phase ψ

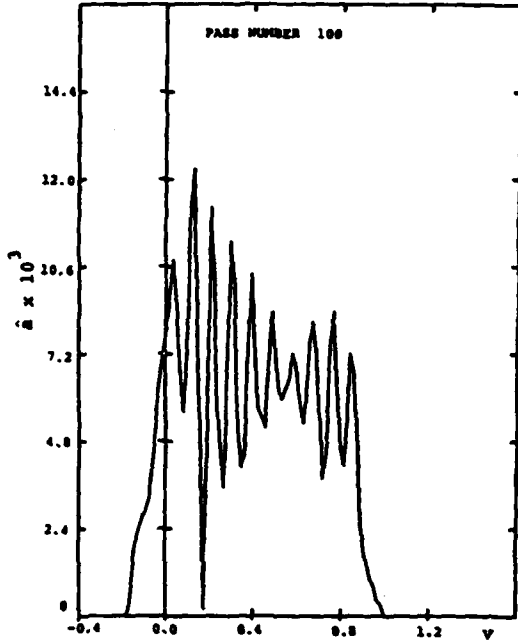


Figure 7e. Amplitude vs. v

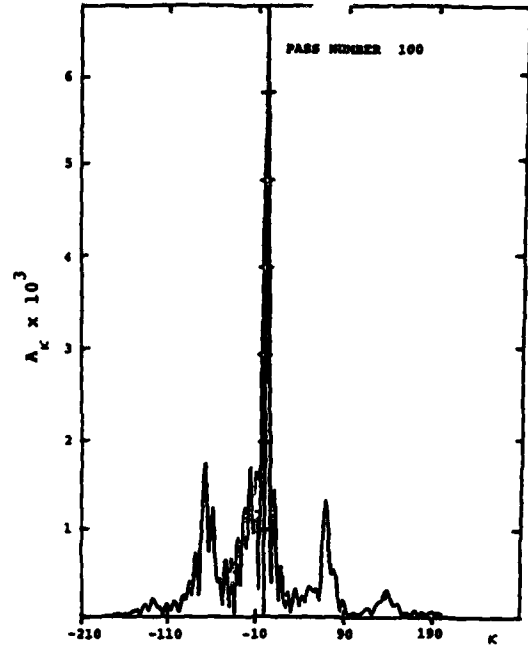


Figure 7f. Complex Amplitude vs. Frequency κ

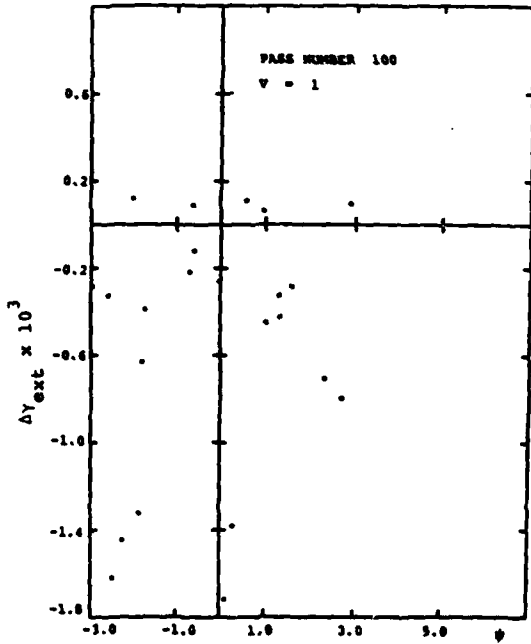


Figure 7g. Energy Extracted vs. Phase ψ

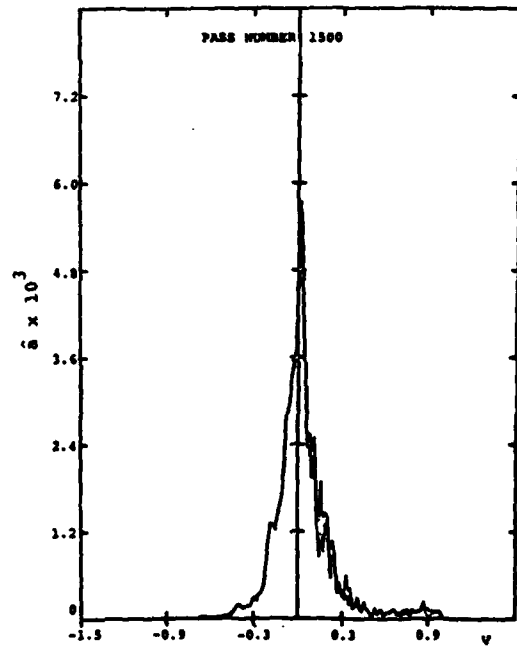


Figure 7h. Amplitude vs. v

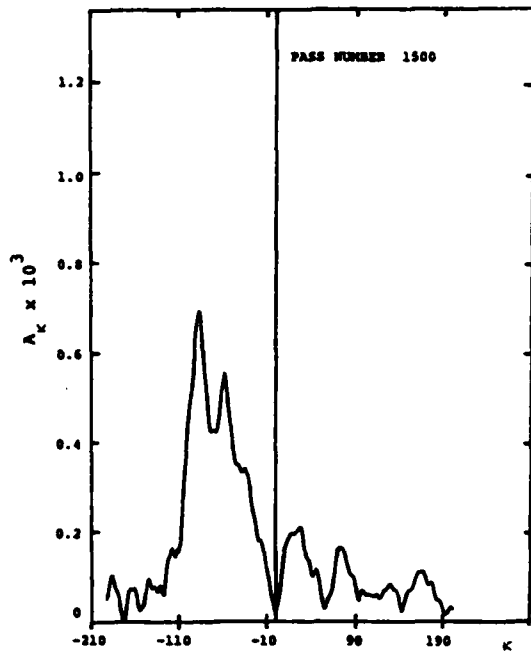


Figure 7i. Complex Amplitude vs. Frequency

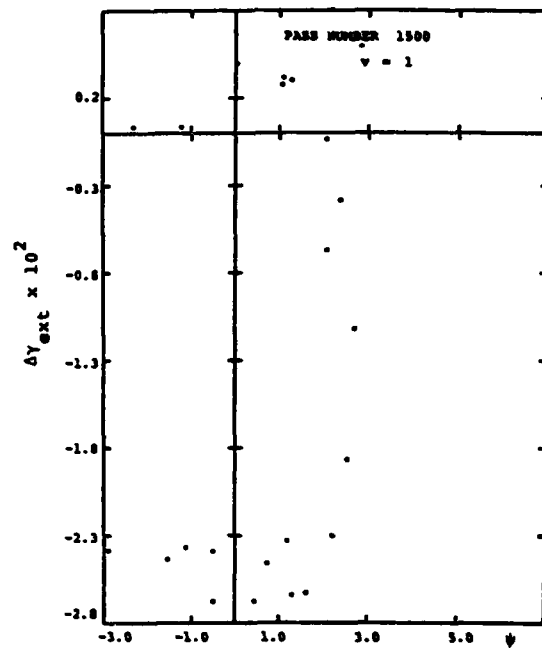


Figure 7j. Energy Extracted vs. Phase ψ

sidebands have been predicted to be unstable by Kroll, et al.²

As we will see in the next section, the suppression of sideband growth by passing the pulse through a band pass filter results in a considerable improvement in the pulse shape and the total pulse energy at saturation.

2. Frequency Discrimination

In FELs with frequency discrimination where the EM pulse is passed through a band pass filter in order to attenuate undesirable sideband frequencies, the band width ν of the filter appears as an additional parameter. Frequency discrimination by a band pass filter has an effect proportional to $1/\nu$ which tends to retard the pulse advance, that is, it tends to reduce the effective pulse advance produced by a finite positive value of β . To avoid the EM pulse running either ahead of or lagging behind the electron beamlets, it is indicated that a choice of $\nu = 1/\beta$ is desirable. This was confirmed by the numerical simulations. A small value of ν is desirable to suppress the sidebands; however, linear gain is reduced if $\nu < 1/\beta$ (see Table 1).

TABLE 1

Variation of linear gain $\text{Re } \delta$ with ν .

$r = 0.99$	$\eta = 600$	$\Gamma = 2000$				
$\beta = 0.01$	$\nu_1 = 0.015$	$\bar{\gamma} = 0$	$\hat{\gamma}_{th} = 0$			
ν	160	140	120	$100 = 1/\beta$	90	80
$\text{Re } \delta$.017	.0294	.0367	.0287	.0143	-0.01

In the simulations we discuss hereafter, we will consider only the case of $\nu = 1/\beta$.

With $\nu = 1/\beta$, the linear gain per pass for a very long constant parameter wiggler ($\beta/\eta^{1/2} \rightarrow 0$) is given by⁵

$$\text{Re } \delta_2 \equiv \left[\text{Re} \frac{2(1-r+\delta)}{(\eta\beta^2)^{1/2}} \right] \approx 2^{1/2} \quad (72)$$

where $\hat{\gamma}_{th} = 0$ and $\bar{\gamma} = 0$. If the beam and wiggler parameters are kept constant, $\text{Re} \left[\beta \delta_2 / \eta^{1/2} \right]$ increases from zero with increasing β , reaches a maximum $\text{Re} \left[\beta \delta_2 / \eta^{1/2} \right] = .012$ at $\beta / \eta^{1/2} = .042$, and finally decreases to zero at $\beta / \eta^{1/2} = 0.118$. The theoretical linear gain curve is plotted as a solid line in Figure 8 while the linear gain obtained in the simulations is represented by the circled points. The agreement between theory and simulation improves as β is made smaller.

If the wiggler is made variable ($\Gamma \neq 0$), the linear gain remains close to that of the constant parameter wiggler when $\beta^2 \Gamma^2 / \eta \ll 1$. As the magnitude of the variation increases, $\text{Re} \delta_2$ decreases and asymptotes to zero. The theoretical linear gain curve⁵ for a very long variable wiggler ($\beta / \eta^{1/2} \ll 1$, $\Gamma \ll 1$) is plotted in Figure 9 as a solid line indicating the variation of δ as a function of $\beta \Gamma / \eta^{1/2}$. The results of the simulation are represented as circled points for values of $\beta / \eta^{1/2} = 5.8 \times 10^{-4}$, .01. The differences between the observed linear gain and the theoretical linear gain curve for $\beta / \eta^{1/2} = .01$ are due to finite length effects not included in the theory.

The reduction of linear gain due to a finite energy spread of the beam becomes significant when

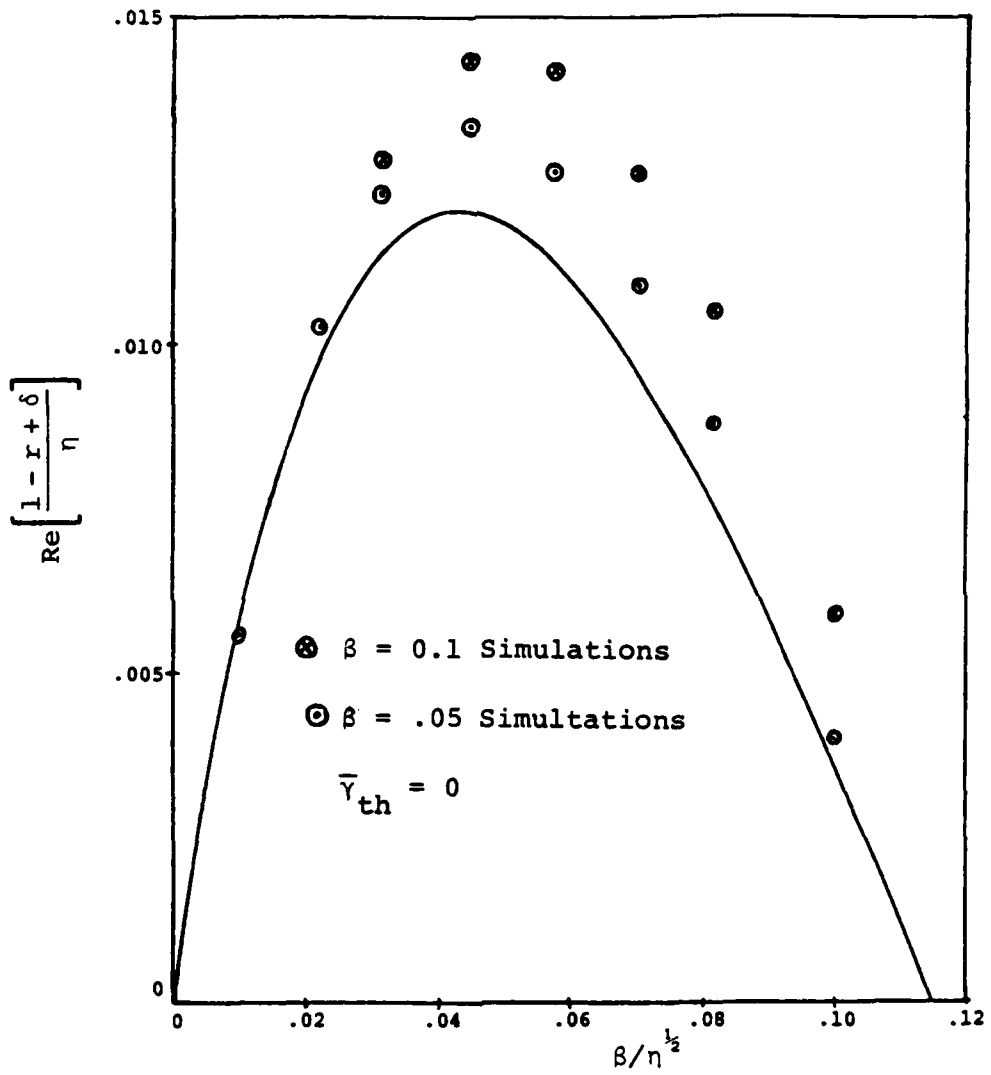


Figure 8. Linear Gain-Constant Parameter Wiggler with Frequency Discrimination

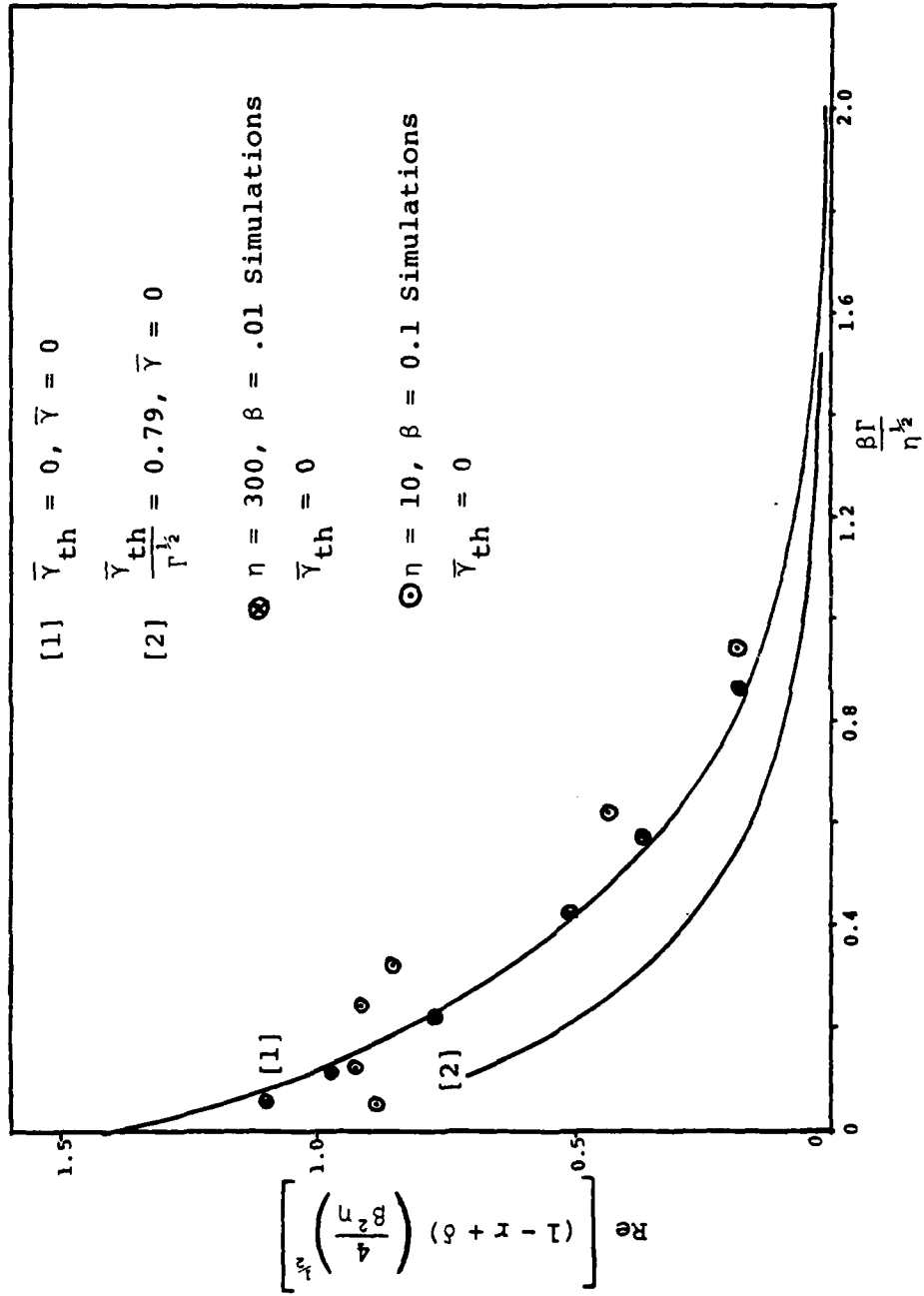


Figure 9. Linear Gain - Variable Parameter Wiggler with Frequency Discrimination

$\bar{\gamma}_{th}/\Gamma^{1/2} \geq 1$. This may be seen from Figure 10 where $\text{Re } \delta_2$ is plotted as a function of $\bar{\gamma}_{th}/\Gamma^{1/2}$ for four values of $\beta\Gamma/\eta^{1/2}$. The energy spread of the beam was modeled by a Lorentzian distribution function.

The early phase of the evolution of the EM pulse growing from noise levels is similar to that discussed in the previous section.

For a variable parameter wiggler, the linear eigenmode grows in amplitude, the peak amplitude moves from the back to the front of the pulse, and the peak amplitude at the front continues to increase to levels where electron trapping in the ponderomotive potential occurs ($\hat{a} \sim \Gamma$). Thereafter, the pulse width broadens towards the back in addition to increasing in amplitude. The final phase of the evolution depends critically on the band width ν of the filter. If ν is small, the pulse broadens into a square pulse (approximately) of width $\nu = 1$ and the electrons trapped in the ponderomotive potential well remain trapped during its passage through the wiggler.

The results of a simulation run for the same parameters previously shown without frequency discrimination, showing the evolution of the pulse energy, pulse shape, and pulse spectrum are presented in Figure 11. The FEL parameters are

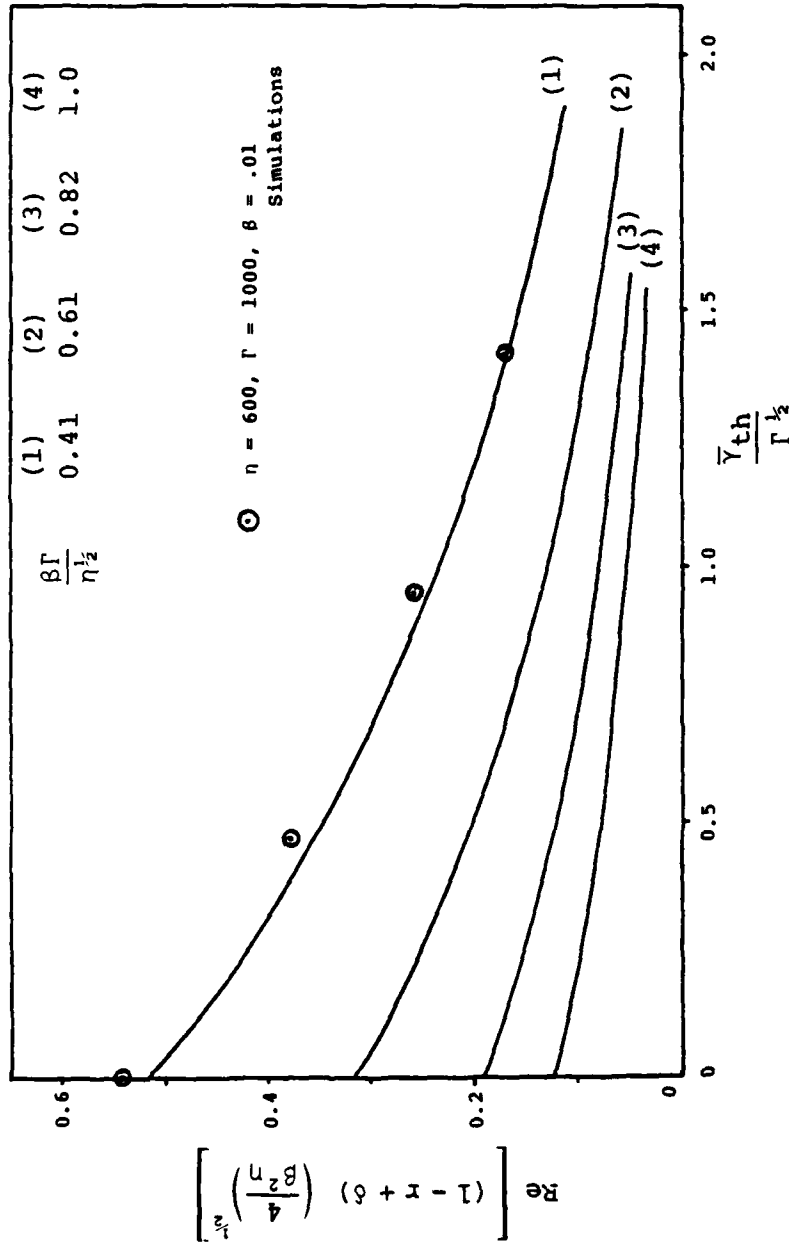


Figure 10. Linear Gain - Variable Parameter Wiggler Without Frequency Discrimination

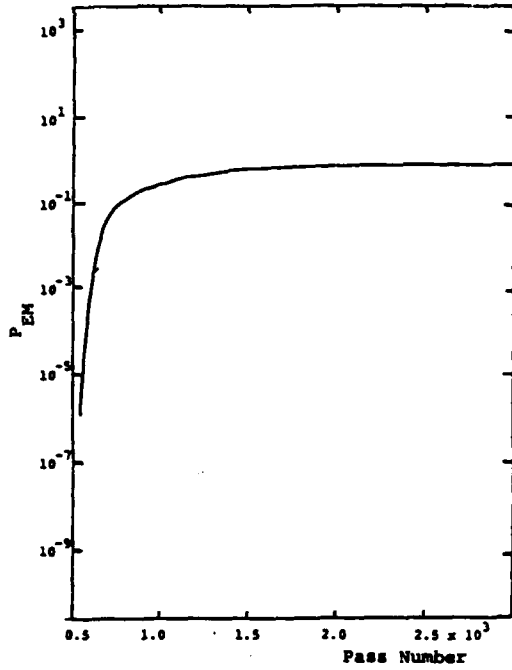


Figure 11a. Pulse Energy vs. Pass Number

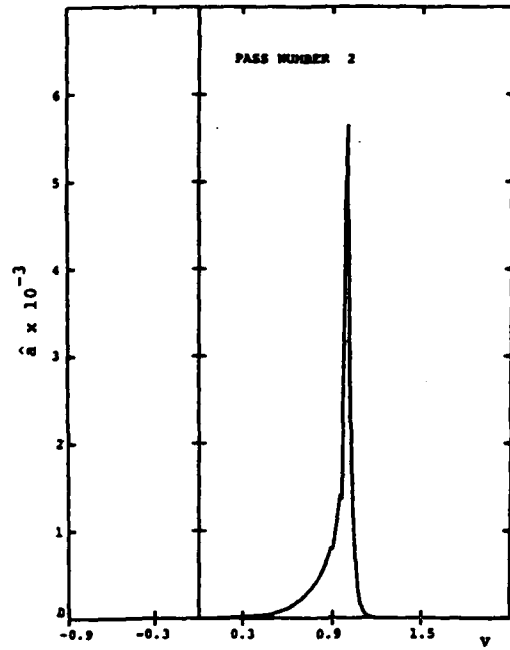


Figure 11b. Amplitude vs. v

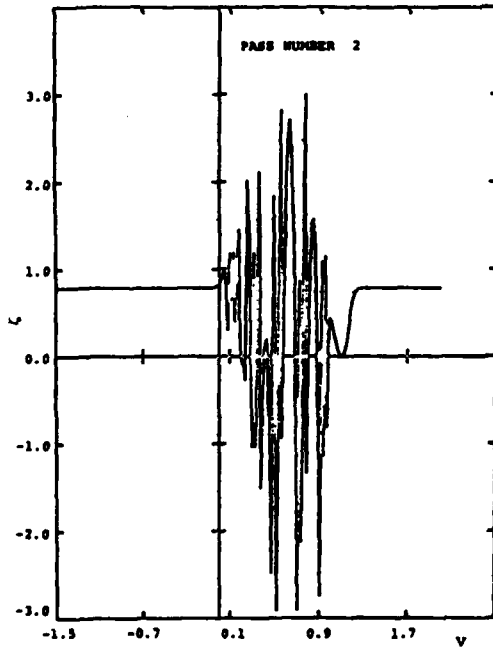


Figure 11c. EM Pulse Phase vs. v

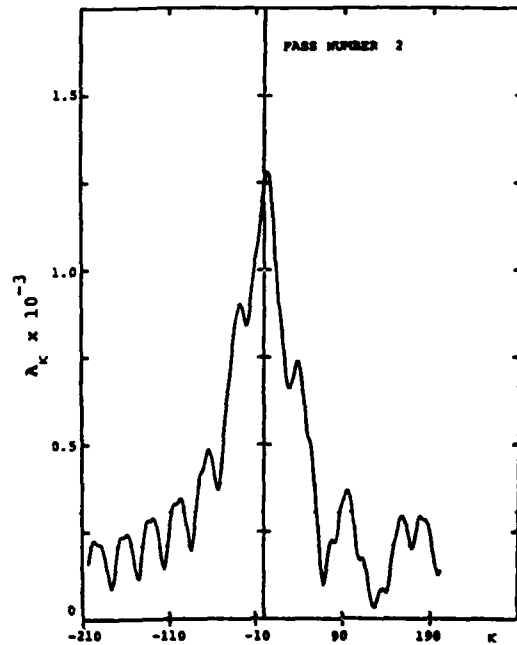


Figure 11d. Complex Amplitude vs. Frequency κ

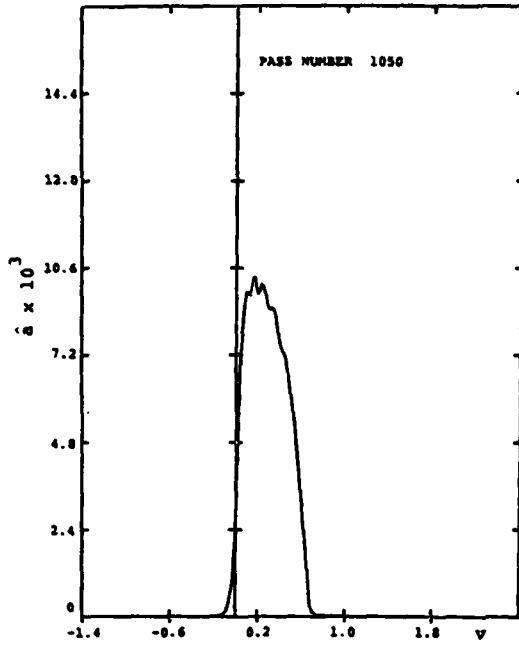


Figure 11e. Amplitude vs. v

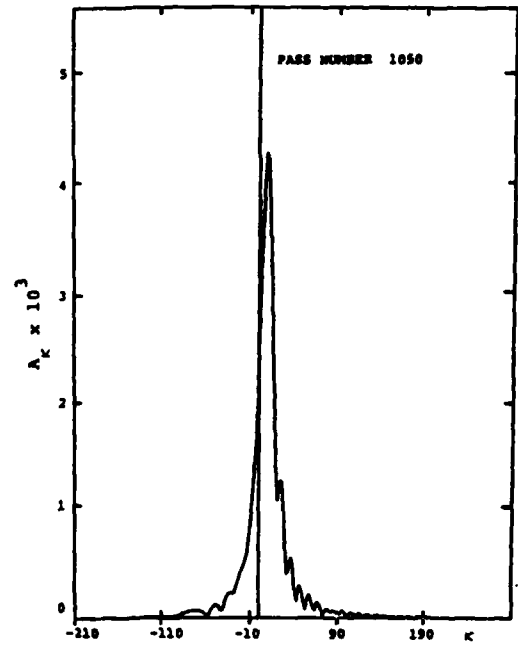


Figure 11f. Complex Amplitude vs. Frequency κ

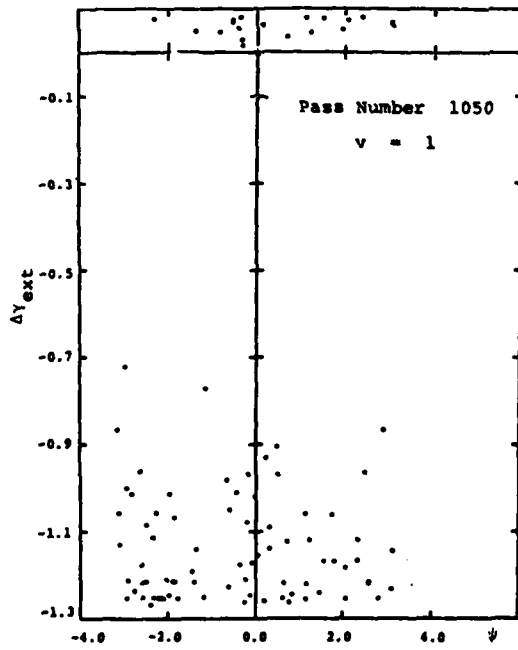


Figure 11g. Energy Extracted vs. Phase ψ

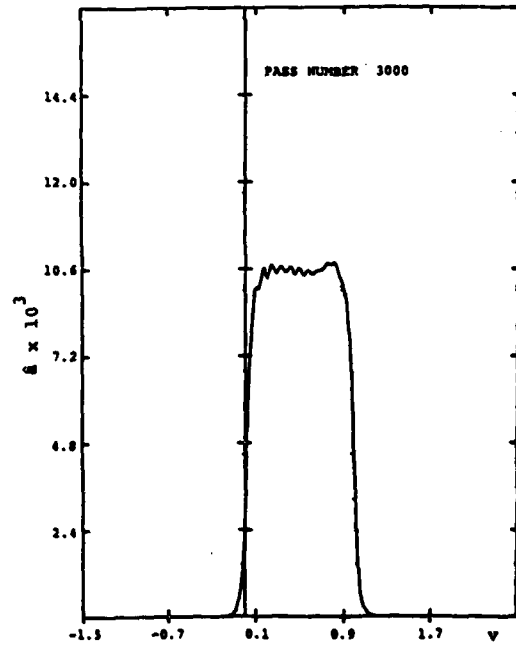


Figure 11h. Amplitude vs. v

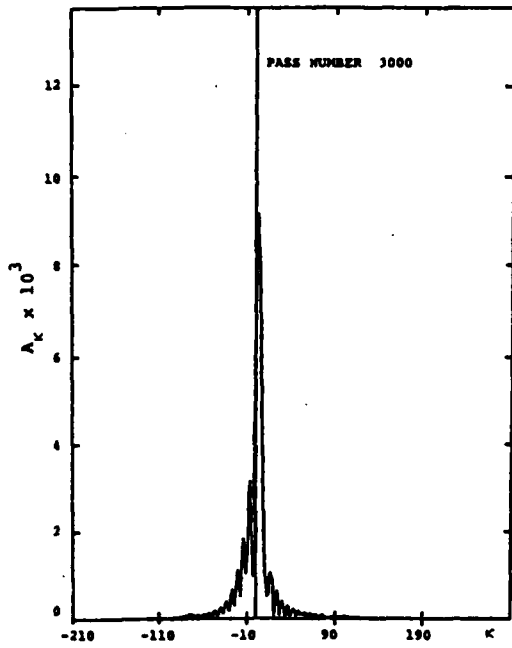


Figure 11i. Complex vs. Frequency κ

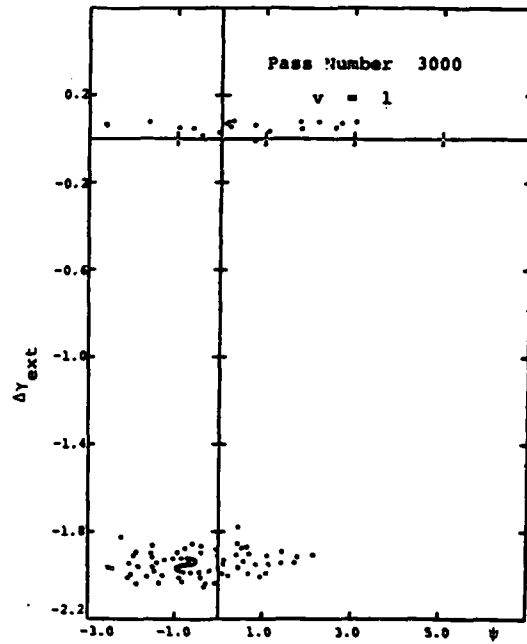


Figure 11j. Energy Extracted vs. Phase ψ

$$\begin{aligned}
r &= 0.99 \\
\eta &= 600 \\
\beta &= .007 \\
\Gamma &= 2000 \\
v_1 &= .015 \\
v &= 1/.007 \\
\bar{\gamma}_{th} &= 0.
\end{aligned}$$

In contrast to the simulation results of the previous section, the pulse spectrum remains narrow with a large peak at zero frequency. Sidebands have been suppressed and the large amplitude saturated pulse propagates coherently. Electron trapping is very efficient. From Figure 11j, it may be seen that ~20% of the electrons on exit from the wiggler have $\hat{\gamma} - \int \Gamma dv \sim 0$ and therefore these electrons have been freely accelerated through the wiggler. The remaining ~80% of the electrons have $\hat{\gamma} - \int \Gamma dv \sim -2000$, which implies that these have been trapped throughout the length of the wiggler.

The energy extracted is about 80% of the maximum possible in contrast with 2% for the same parameters without frequency discrimination. About 14% of the energy extracted from the beam is lost in the frequency discriminators.

Results for pulse energy and the fraction of electrons trapped at saturation are presented in Table 2.

TABLE 2

$$r = .99$$

$$v = 1/\beta$$

β	Γ	η	v_1	P	$\left[\frac{\beta^4 \Gamma \eta}{(1-r)^3} \right]^{1/2}$	f_t
.032	1000.	300.	.022	.49	561.	.7
.02	1000.	300.	.022	.57	219.	.75
.01	1000.	300.	.022	.68	54.8	.79
.005	1000.	300.	.022	.06	13.7	---
.022	2000.	600.	.015	.54	530.	.67
.007	2000.	600.	.015	.69	53.7	.80
.005	2000.	600.	.015	.06	27.4	---

The total pulse energy is increased by increasing the electron current η . The efficiency of energy transfer is improved by increasing Γ .

Further increase in total pulse energy may be obtained by increasing the band width $v = 1/\beta$ up to some critical value v_{crit} .

As v is increased above the critical value v_{crit} , the pulse shape at saturation exhibits a

progressive depression in the amplitude at the back of the pulse. Figure 12 displays the results of a simulation run with FEL parameters similar to Figure 11 but with ν increased slightly to $\nu = 1/\beta = 1/.005$. The electrons are no longer effectively trapped throughout the whole length of its passage through the wiggler, and the energy transfer from beam electrons to the pulse is less efficient. At the same time, the spectrum is no longer narrow. Sideband frequencies of the order of the electron bounce frequency begin to appear and eventually dominate the spectrum.

The deterioration of the pulse is attributable to the growth of the sidebands. When $\nu < \nu_{\text{crit}}$, the filter is narrow enough to suppress the growth of the unstable sidebands and the saturated pulse propagates coherently as a finite amplitude square pulse. We discuss the implications in Section 4 below.

Linear gain can be enhanced significantly, particularly for large β , by adding a constant parameter section to the front of the variable parameter wiggler. The constant parameter section however cannot be too long since electron trapping may be adversely affected. The linear growth phase in the constant parameter section will tend to saturate at $(\hat{a})^{1/2} \nu_1 \approx \pi$, and this amplitude

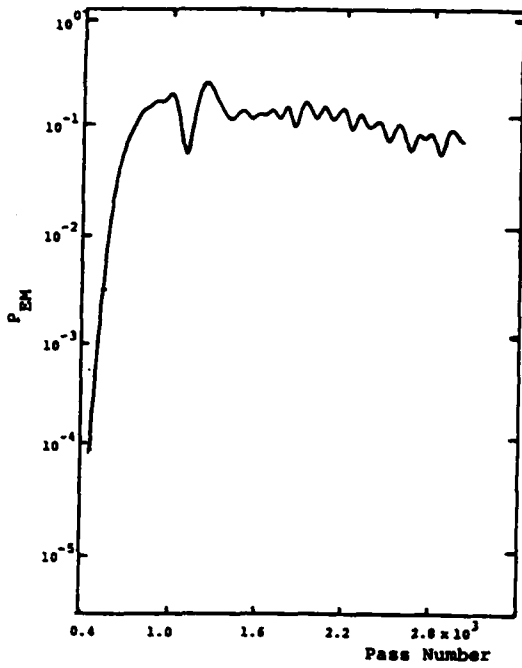


Figure 12a. Pulse Energy vs. Pass Number

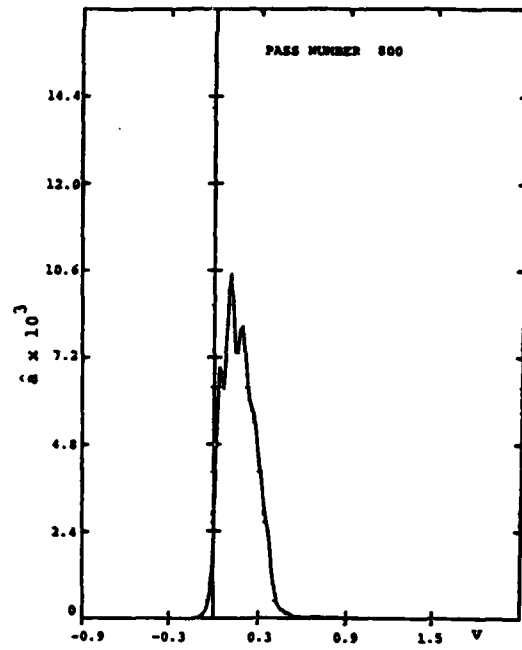


Figure 12b. Amplitude vs. v

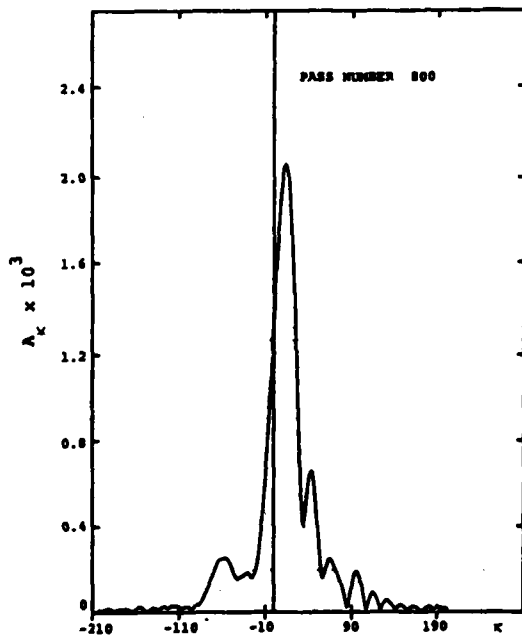


Figure 12c. Complex Amplitude vs. Frequency κ

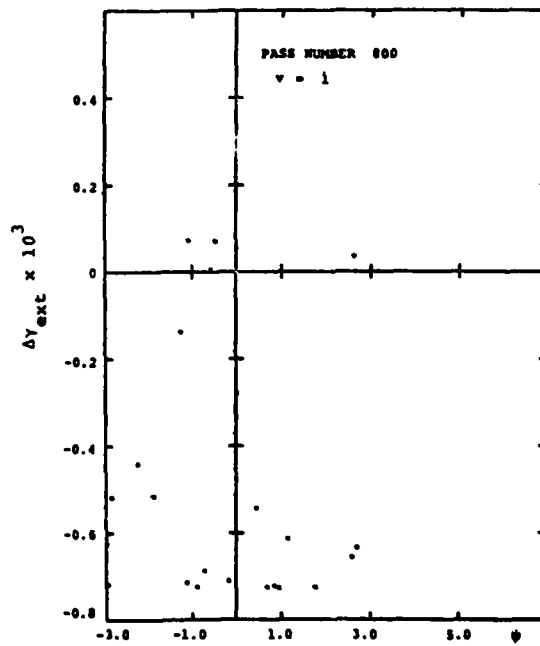


Figure 12d. Energy Extracted vs. Phase ψ

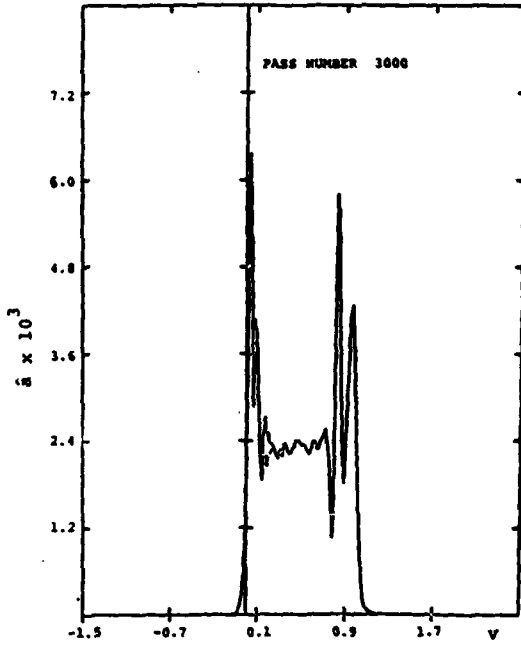


Figure 12e. Amplitude vs. v

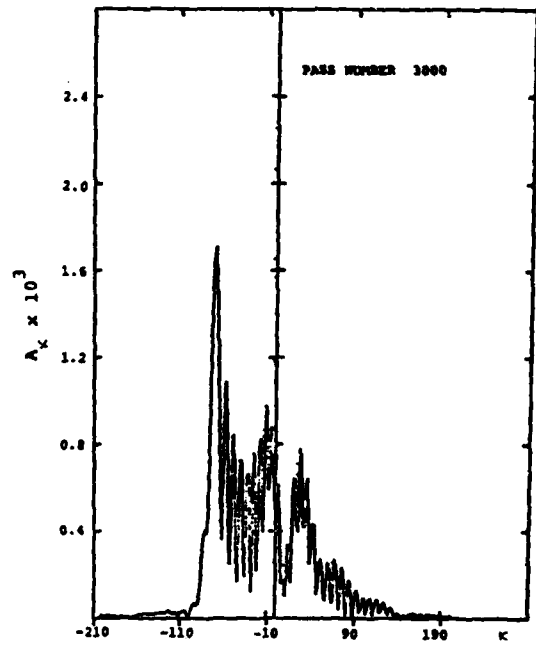


Figure 12f. Complex Amplitude vs. Frequency κ

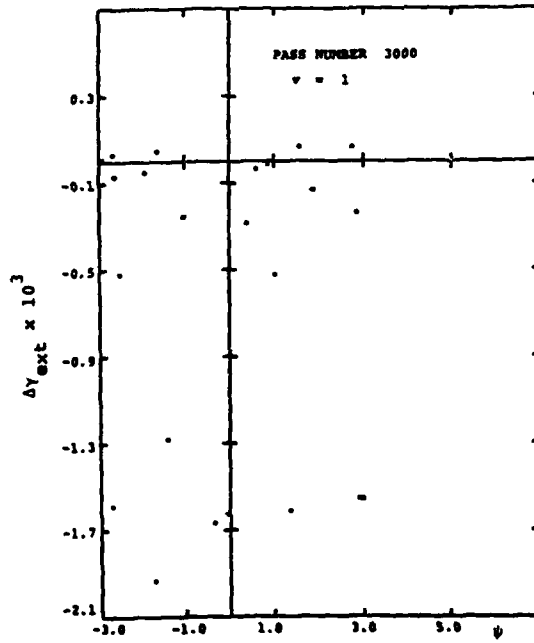


Figure 12g. Energy Extracted vs. Phase ψ

$(a)^{1/2} \sim \pi/v_1$ may not be large enough to begin to trap the beam electrons.

In Table 3, we present the results of a series of runs in which the effect of varying the fractional length of the constant parameter wiggler is investigated. It appears that the length of the constant parameter wiggler should be limited by $\Gamma^{1/2} v_1 \lesssim 1$ to ensure effective electron trapping. The enhancement of gain is not sufficient to alter our previous conclusions.

TABLE 3

$r = .99$ $\eta = 60.$ $\Gamma = 200.$ $\beta = .05$

$\Gamma^{1/2} v_1$	δ	P
0.	.006	.37
.283	.01	.38
.566	.02	.38
.85	.023	.37
1.13	.031	.02
1.41	.034	.01

3. Thermal Effects

The presence of a finite thermal energy spread $\bar{\gamma}_{th}$ in the electron beam affects not only the linear gain, but also the fraction of electrons trapped at saturation.

As may be seen from Figure 10, the linear gain is significantly reduced if $\bar{\gamma}_{th}/\Gamma^{1/2} > 1$.

In order to trap a large fraction of electrons, $\bar{\gamma}_{th}^2/2$ should be less than the well depth of the ponderomotive potential well. The effective well depth at saturation, estimated from energy conservation, is $\hat{a}_0 \sim [f_t \eta \Gamma / (1-r)]^{1/2}$, and thus the limit on energy spread is

$$\frac{\bar{\gamma}_{th}}{\Gamma^{1/2}} < \frac{\hat{a}_0^{1/2}}{\Gamma^{1/2}} \sim \left[\frac{f_t \eta}{(1-r)\Gamma} \right]^{1/4} \quad (73)$$

If the smallest values of $\eta/(1-r)\Gamma$, as determined by Equation (80) in the next section, is substituted in Equation (73), the limitation on energy spread may be written

$$\frac{\bar{\gamma}_{th}}{\Gamma^{1/2}} < 2 \quad (74)$$

Good linear gain therefore restricts the energy spread to about half that which would be deduced from looking at the requirement for effective electron trapping.

Figure 13 summarizes the results of a simulation using an electron beam with $\bar{\gamma}_{th} = 25$. The other FEL parameters are identical to that of the simulation presented in Figure 11.

The linear gain was reduced by a factor of 3 from $\text{Re } \delta = 0.029$ ($\bar{\gamma}_{th} = 0$) to $\text{Re } \delta \approx 0.01$ ($\bar{\gamma}_{th} = 25.0$). Note that in these runs a constant parameter section of length $v = 0.015$ was included to enhance the linear gain.

The fraction of electrons trapped was reduced from $f_t = 0.8$ ($\bar{\gamma}_{th} = 0$) to $f_t \sim 0.6$ ($\bar{\gamma}_{th} = 25$), while the integrated pulse energy was reduced by 75% from $P = 0.69$ ($\bar{\gamma}_{th} = 0$) to $P = 0.52$ ($\bar{\gamma}_{th} = 25$).

These results support the conclusion that the limitation on beam energy spread will probably be determined more by the need for linear gain than by that for effective electron trapping.

4. Discussion

We may interpret the results of Section 2 ($\bar{\gamma}_{th}=0$) in terms of the theory of sideband instabilities,² which indicates that modes of frequency ω , $0.2 \omega_b < \omega_s - \omega < \omega_b$,

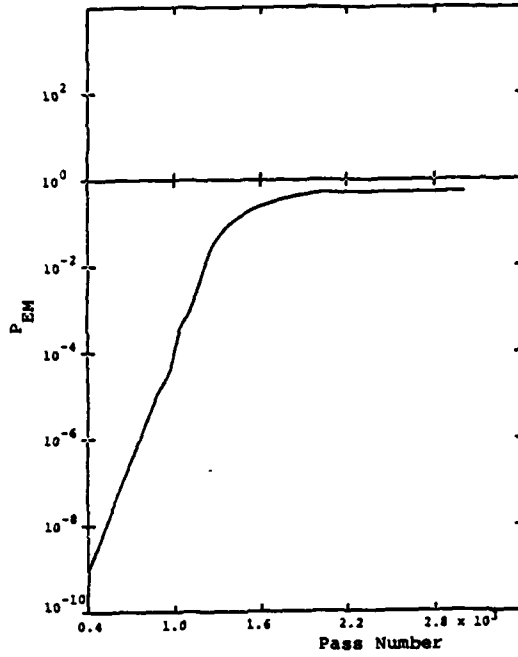


Figure 13a. Pulse Energy vs. Pass Number

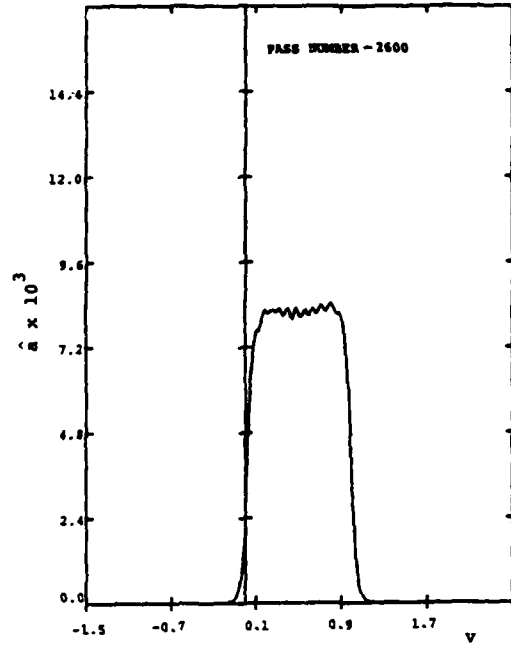


Figure 13b. Amplitude vs. v

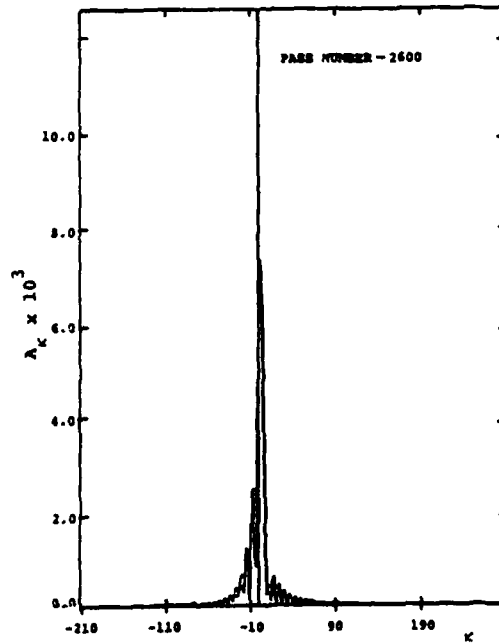


Figure 13c. Complex Amplitude vs. κ

where $\omega_b \propto \hat{a}^{1/2}$ is the bounce frequency, should be unstable with gains several times the signal gain, leading to detrapping.

To suppress sideband frequencies $\Delta\omega$ of the order of a quarter of the electron bounce frequency $\frac{1}{4}|\hat{a}|^{1/2}$, the reduction in the pulse energy due to filtering, i.e.,

$$|\hat{a}_{\Delta\omega}|^2 \left[1 - \frac{1}{1 + \left(\frac{\Delta\omega}{v}\right)^2} \right]$$

[see Equation (32)] should exceed the relative gain due to sideband instabilities. Thus

$$\frac{\hat{a}}{16v^2} > 2(1-r)(\bar{G}-1) \quad (75)$$

where \bar{G} is the ratio of gain of sideband instability to the gain of the pulse amplitude. Substituting for the amplitude at saturation $\hat{a}^2 \sim \eta\Gamma f_t/(1-r)$ and taking $v = 1/\beta$:

$$\beta^2 \left[\frac{\Gamma\eta}{(1-r)^3} \right]^{1/2} > \frac{32(\bar{G}-1)}{f_t^{1/2}} \quad (76)$$

Theoretical estimates indicate $\bar{G} \approx 2$ to 3.

From a survey of the simulation results for a range of FEL parameters, summarized in Table 2, it was estimated that for stable propagation,

$$\beta^2 \left[\frac{\Gamma \eta}{(1-r)^3} \right]^{1/2} \approx 50 \quad (77)$$

where the numerical coefficient is approximate.

This appears in good agreement with the above theory.

It may be noted that large β (that is narrow band width) is desirable for stable propagation in the presence of the sideband instability. However, linear gain becomes small if β is too large (see Figure 7). From the linear eigenmode analysis of a very long variable parameter wiggler, the linear gain $\text{Re } \delta_2$ is a known function of the dimensionless parameter $\beta \Gamma / \eta^{1/2}$, $\text{Re } \delta = f(\beta \Gamma / \eta^{1/2})$. Thus, to obtain linear gain, it is required that

$$\frac{(1-r)\Gamma}{\eta} < \left(\frac{\beta \Gamma}{\eta^{1/2}} \right) f \left(\frac{\beta \Gamma}{\eta^{1/2}} \right) \quad (78)$$

Equation (77) may be rewritten as

$$\frac{(1-r)\Gamma}{\eta} < \left(\frac{\beta \Gamma}{7\eta^{1/2}} \right)^{4/3} \quad (79)$$

By equating the right-hand sides of Equations (78) and (79), which may be done graphically, we determine that the inequalities can only be satisfied if:

$$\frac{(1-r)\Gamma}{\eta} < 0.06 \quad (80)$$

to ensure that a value of frequency discrimination may be chosen which allows both for linear gain and stable propagation.

From the definitions of Γ and η (Equation 27 and Equation 28), it may be seen that the above inequality imposes the following lower limit on the electron beam current

$$\langle I \rangle > \frac{1.42 \times 10^5}{k_w^2 r_0^2} \frac{(1-r) \Delta \gamma_r}{\gamma_r^2} \text{ amps} \quad (81)$$

where $\langle I \rangle$ is the beam current averaged over the slippage distance ($u_0 = 1$), the wiggler length $L_w = k_s r_0^2$ is set equal to the "diffraction" distance, and $\Omega^2/k_w^2 c^2 = 1$. If the beam radius is restricted to $k_w r_0 \leq \frac{1}{3}$ so that the transverse variation of the pulse amplitude across the beam is small, the minimum current criterion is

$$\langle I \rangle > 1.28 \times 10^6 (1-r) \frac{\Delta\gamma_r}{\gamma_r^2} \text{ amps} \quad (82)$$

This minimum current implies a minimum circulating power P_{\min} of

$$P_{\min} = 654 f_t \left(\frac{\Delta\gamma_r}{\gamma_r} \right)^2 \text{ GW} \quad (83)$$

In the case of the simulations presented in Figure 11,

$$P_{\min} = 84 \text{ GW} .$$

This value of P_{\min} is about two times the estimate of minimum circulating power calculated by Kroll, et al.² for $\Delta\gamma_r/\gamma_r = 0.4$. Their calculation takes account of the constraints imposed on pulse amplitude variations transverse to ($k_w r_0 = 1/3$) and along ($L_w = k_s r_0^2$) the direction of propagation, but does not include the need for good linear gain and suppression of unstable sideband frequencies.

5. Summary

We have developed a 1-D code for the simulation of FELs following the self-consistent interaction of electrons and the EM wave in a wiggler, while reflecting and optically filtering the EM pulse for multiple passes through the system. In this way, both pulse formation and the steady state may be studied. We have included provisions for both constant and variable wigglers and for thermal energy spread in the entering electron pulse. In this paper we concentrate on the results obtained with electron pulses of zero length (δ -function) which reduces the simulation time required. This should be a good representation for pulses such that $\Gamma^{1/2} u_0 < 1$.

Our principal results are:

(1) We have verified analytic results previously obtained for linear pass to pass growth of the pulse at low amplitude.

(2) We find that for high saturation systems optical discrimination is required in order to prevent nonlinear signal breakup. Qualitative agreement with the theory of sideband instabilities is obtained for the width of the required frequency filter.

(3) The further requirement that the linear phase of growth saturate at a high enough level to ensure trapping seems to be satisfied except for systems which

seek to enhance linear gain by use of a long constant parameter section.

(4) With proper choice of frequency discrimination (and for an ultrashort electron pulse) we have demonstrated very high extraction systems (30% efficiency at 1μ) which grows from noise to a stable steady state. We derive and numerically verify a criterion

$$\langle I \rangle > 1.28 \times 10^6 \frac{(1-r) \Delta \gamma_r}{\gamma_r^2} \text{ Amps}$$

for the minimum current required for such a system.

(5) The limitation on beam thermal energy spread $\bar{\gamma}_{th}$ is determined more by the need for good linear gain ($\bar{\gamma}_{th}/\Gamma^{1/2} < 1$) than by that for effective electron trapping, ($\bar{\gamma}_{th}/\Gamma^{1/2} < 2$).

ACKNOWLEDGEMENTS

The authors would like to acknowledge useful suggestions made by Norman Kroll regarding formulation of the FEL problem.

This work was supported by the Defense Advanced Research Projects Agency through the Air Force Office of Scientific Research under Contract No. F49620-81-C-0077.

REFERENCES

1. L. R. Elias, W. M. Fairbank, J. M. J. Madey, H. A. Schwettman, and T. I. Smith, Phys. Rev. Lett. 35, pp. 717-720 (1976).
2. N. M. Kroll, P. Morton and M. N. Rosenbluth, "Free Electron Lasers with Variable Parameter Wigglers," IEEE Journal of Quantum Electronics, Vol QE-17, pp. 1436-1468 (1981).
3. W. B. Colson and S. K. Ride, "The Free-Electron Laser: Maxwell's Equations Driven by Single-Particle Currents," Physics of Quantum Electronics, Vol. 7, Free Electron Generators of Coherent Radiation, Addison-Wesley, Reading, MA., pp. 377-414 (1980).
4. W. B. Colson, Physics of Quantum Electronics, Vol. 8, p. 457 (Addison-Wesley, 1982).
5. M. N. Rosenbluth and H. Vernon Wong, "Theory of Linear Gain: Free Electron Lasers Operated in Oscillator Mode," ARA Report No. I-ARA-82-U-73, July, 1982.
6. John C. Goldstein and W. B. Colson, "Pulse Propagation in Free Electron Lasers with a Tapered Undulator," Los Alamos Preprint.